NATIONAL INSTITUTE FOR HIGHER EDUCATION, DUBLIN

School of Electronic Engineering.

Control Technology Research Unit.

Thesis Submitted for the Degree of

Master of Engineering.

High Dynamic Performance Controller for an Induction Motor.

by:

Seamus M. O' Driscoll BE

for:

Dr. Charles Mc Corkell.

Dr. Frank Devitt.

September 1988.

I declare that the research herein was completed
by the undersigned.

Signed Seamus O'Driscoll Date 9th Sept. 1988.

ACKNOWLEDGEMENT

Sincere thanks to both my supervisors, Dr. Charles M^{c} Corkell and Dr. Frank Devitt for their continued guidance and support during this work. Thanks to all the Electronic Engineering staff at the N.I.H.E. Dublin, especially John Whelan for his invaluable assistance. The encouragement and help from the members of the Control Technology Research Unit, in particular Niall Walsh is greatly appreciated. Thanks to Breda M^{c} Manus who expertly typed this thesis.

ABSTRACT

HIGH DYNAMIC PERFORMANCE CONTROLLER FOR THE INDUCTION MOTOR.

By: Seamus O'Driscoll.

The rugged and relatively inexpensive Induction Motor is becoming increasingly important for use in high performance servo motor systems. This thesis describes the complete design and implementation of an all digital Field Oriented Controller for a 1.5 KW Squirrel Cage Induction Motor. The classical steady state motor model and dynamic models in both D.Q. and Space Vector format are presented. A specific controller structure is selected, and tuned using Discrete-time design techniques. The Field Weakening technique is analytically investigated. Methods for rotor air-gap flux vector determination are reviewed. The sensitivity of the controller forward path to variations in the rotor time constant is studied. Equations for the corresponding errors in the torque and in the machine excitation level are derived. Simulation results, predicting the overall performance of the controller on the full, non-linear and cross-coupled D.Q. model of the motor are given. The influences of Rotor Time Constant variations and P.W.M. amplifier non-linearities on the Stall Torque dynamics are experimentally evaluated. Steady state oscillations are found to exist in the developed Stall Torque. It is shown that these are caused by the Cross Over Delays introduced by the P.W.M. amplifier and represent the key problem in the use of Induction Motor based servo systems in Low Speed and Position Control applications. Further, it is proven that these non-linear effects have major implications on the stability of Field Oriented Controllers with the Voltage Source Inverter Fed Induction Motor.

TABLE OF CONTENTS.

INTRODUCTION

1.1 Introduction.

The Induction or Asynchronous motor, which was invented by Nikola Tesla in 1887, is one of the simplest and most reliable of all electric motor types. The three phase Squirrel Cage Induction Motor is a very common practical drive and is ideal for non-critical fixed speed or even variable speed applications. This motor is, however, very difficult to control accurately, and so for high performance servo motor systems the Permanent Magnet (PM) Brush DC motor or the PM Synchronous motor is more often used. Recently, because of advances in semiconductor technology which make the implementation of complex control algorithms more feasible, considerable attention is being devoted to the design of high dynamic performance controllers for the Induction motor. This motor looks set to become the basis of many reliable and inexpensive servo motor systems.

1.2. Features of Induction Motor based Servo Systems.

Induction motors have various inherent advantages over both Permanent Magnet Synchronous motors and Brush DC motors, which make their use in certain servo applications desirable. Leissmeier et al.,[1], provides a comprehensive assessment of the relative merits of different types of ac motors for use in servo drives. Brown, [2], reviews both DC and AC servo motors and contrasts the features of these motors against those of the Induction motor. Some brief comparisons between the different motor systems are presented here in order to indicate the applications which might be best served by Induction motors.

Both Synchronous machines and Brush DC machines usually have permanent magnets

made with rare earths such as semarium and cobalt. In the case of Synchronous machines these magnets are generally bonded to the rotor. In contrast most Squirrel Cage rotors are cast from aluminium, a much cheaper material. The stators of both Induction and Synchronous motors can be identical and are of equal complexity as the armature winding on a Brush DC motor. For machines of comparable power output ratings, therefore, the Induction motor is considerably less expensive.

The Power Inverter and PWM amplifier stages for both Synchronous and Induction motors are similar and are marginally more expensive than the power electronic drives needed for a Brush DC motor. The controller needed for the Induction machine is considerably more complicated since as a control plant the Induction motor can be modelled as a sixth order, non-linear, multivariable and cross-coupled system. There are also problems with parameter variations. Controllers for Synchronous machines (or Brushless DC motor systems) are less complicated and for Brush DC motors they are more complicated again. Recently, the availability of high speed Digital Signal Processors and Floating Point Coprocessors is acting in favour of the Induction motor system, enabling the implementation of elaborate and possibly adaptive digital control algorithms.

Absolute position feedback is necessary for the operation of Synchronous servos while a rotor velocity signal only, is required for an Induction motor servo. Resolvers, being brushless, reliable and having low inertia are usually used in both types of systems, but must be specially aligned when being mounted on the Synchronous motors. DC motors, having brushes and commutators do not require position feedback devices, although they may sometimes be used in closed loop position control applications.

Electronic commutation in both types af AC drives enables their use in hazardous environments where the sparking of the brushes and commutator in a DC motor might be a limitation. The absence of moving contacts other than bearings makes the AC

machines virtually maintenance free.

For motors of similar torque ratings, the Induction motor rotor tends to have a larger diameter-length ratio, giving it a higher rotor inertia than that of the Synchronous machine which has a smaller rotor due to the high power magnets' capability of establishing a sufficient field. The Brush DC motor usually has a wound rotor which has typically a similar inertia to that of the Induction motor. This is not a factor in applications where the load inertia dominates but in low inertial load situations considerably better acceleration rates will be achieved with the Synchronous motor.

The formulation of the Field Oriented Control technique (Blaschke [3]) was a major impetus to the use of Induction motors in high dynamic performance applications. Until this theory was proposed most controllers for the Induction motor were based on its steady state model and so the possibility of servo performance was excluded. Now, however, instantaneous control over torque (neglecting leakage lags) is theoretically obtainable with all three types of motors. Indeed Leissmeier et al.,[1], contrasts the speed reversal times of an Induction motor and a Synchronous motor system, both 1.5 KW. They are found to be almost identical, taking roughly 15 msec to change from +1800 rpm to -1800 rpm.

The Induction Motor has a poor power factor especially with light load which means increased losses in both the power inverter and in the windings. Apart from this effect, there are considerable RI^2 losses in the cage of an induction motor which further reduces its efficiency. However for high powers, the Induction motor has the advantage that higher flux densities are achievable, resulting in a higher torque / q-axis amp. The higher excitation level means that a higher bus voltage would be possible with Induction motors, especially with the advent of higher voltage semiconductor devices. This would further reduce the cost of the Induction motor system.

Field weakening is easily implementable with the Induction motor. When the voltage

saturates at base speed the machine excitation level is decreased so that the speed may be further increased. Speeds far above the base speed of the machine are easily achievable. The corresponding technique with Synchronous motor control involves the variation of the torque angle but is not as easy to achieve. At all speeds the Induction motor needs a magnetising current which means increased sizing of the motor due to increased losses. Even when the motor is in stand-by mode significant currents must flow. The synchronous machine does not normally need an excitation current but for operation above base speed negative "magnetising currents" are required. So if the machine is to be rated for high speed operation its sizing must also be increased. In servo systems, therefore, the constant magnetising current needed by the Induction motor does not present a significant disadvantage. There is a lag in varying the field due to the main rotor time constant which gives lower dynamic performance with operation above base speeds.

From this discussion it is clear that the Induction motor servo system could be a very cost effective option in the larger power areas where the savings in the motor cost more than outweigh the increased controller cost. High Dynamic Performances are achievable but with reduced efficiency and torque-size ratios.

1.3 Theoretical Overview of Induction Motors and Controllers.

The three phase steady-state operational characteristics of the Squirrel Cage Induction motor are reviewed briefly here. Supply voltages and currents are assumed to be perfectly balanced and sinusoidal and the machine is assumed to be two pole.

The stator is wound with three identical, symmetrically placed, phase windings. Each phase winding is distributed so as to produce an approximately sinusoidal distribution of MMF (Magneto Motive Force) around the air-gap. The rotor, although a cast cylindrical cage, can be thought of and modelled as a similar set of windings symmetically placed around the rotor.

A balanced set of sinusoidal currents will establish a rotating MMF of constant magnitude and at synchronous speed, (Slemon et al., [4]). At an arbitrary angle, $\in$, around the stator periphery, this is described by:

$$Fs\ (\ \alpha, t\ ) = \frac{3}{4}\ Nse\ Is\ Cos\ (\ w_0 t + \gamma_S - \alpha\ ) \qquad \ldots\ldots\ (\ 1.1.)$$

Is = magnitude of stator current

w_0 = stator supply frequency

γ_S = arbitrary phase angle

$\propto$ = Angle around stator periphery

Nse = Number of turns of phase winding, adjusted to relate the amplitude of the fundamental in the MMF to the amplitude that would occur with an ideally sinusoidally distributed winding.

By transformer action currents are induced in the rotor windings which establish a rotor MMF. This MMF will lag the stator MMF due to the rotor lag and the instantaneous mechanical angle of rotation of the rotor. This MMF referred to the stator is given by:

$$Fr\ (\ \alpha,\epsilon,t\ ) = \frac{3}{4}\ Nre\ Ir\ Cos\ (\ w_r t + \gamma_r - \alpha + \epsilon\ ) \qquad \ldots\ldots\ (\ 1.2.)$$

w_r = frequency of rotor currents

ϵ = mechanical angle of rotation

These MMFs may be considered to be Space Vectors and the resultant MMF is given by the superposition of these two MMFs. These MMFs cause a rotating air-gap flux vector.

$$F\ (\ \alpha,\epsilon,t\ ) = Fs\ (\ \alpha,t\ ) + Fr\ (\ \alpha,\epsilon,t\ ) \qquad \ldots\ldots\ (\ 1.3.)$$

Torque production results from the interaction of the two MMFs and is given by:

$$T_e = K\ Fs\ Fr\ Sin(\ \delta\ ).\quad (N.m) \qquad \ldots\ldots\ (\ 1.4.)$$

δ is the angle between the MMF Space Vectors.

T_e = Developed Electrical Torque

There are two main techniques for getting an expression for the developed torque in terms of applied voltages or current. Slemon et al.,[4], considers the motor on a per phase basis by using a transformer model with a rotating secondary and computes the power which crosses the air-gap. This power minus rotor resistive losses represents the per-phase mechanical power developed in the machine.

Leonhard, [5,] retains the Space Vector approach throughout. Flux Density Vectors are derived from the MMF vectors by taking global permeability and leakage factors. By integration over the winding areas and taking the distribution of the windings into account, corresponding flux linkage vectors are obtained. These can then be related to current space vectors which in turn are driven by voltage vectors. Using this technique a set of differential equations relating voltage space vectors to current vectors are derived and an expression for steady-state torque is obtained.

$$Te\ (\ S.S.\ ) = \frac{3\ (\ 1 - \sigma\ )\ Us^2}{\sigma\ w_0^2\ Ls\ [\ S/Sp + Sp/S\ ]} \qquad \ldots\ldots\ (\ 1.5.\ )$$

$$\text{Normalised Slip } S = \frac{w_0 - w_m}{w_0} \qquad \ldots\ldots\ (\ 1.6.\ )$$

$$\text{Pull Out Slip } Sp = \frac{Rr}{\sigma\ w_0\ Lr} \qquad \ldots\ldots\ (\ 1.7.\ )$$

σ is a general leakage factor.

$$\sigma = 1 - \frac{1}{[\ 1 + \sigma_r\ ][\ 1 + \sigma_s\ ]}$$

..... (1.8.)

σ_s, σ_r = Stator and rotor Leakage Factors

For the Squirrel Cage motor σ_r is assumed equal σ_s and so Lr equals Ls and leakage is neglected. Under normal operating conditions the slip approaches zero (rated slip for motor used in this work equals 0.06) and so the above relationship may be simplified to become

$$Te\ (\ S.S.\ ) = \frac{3\ Us^2\ S}{w_0\ Rr}$$

..... (1.9.)

Slemon et al., [4], gives the ideal efficiency of the motor as

$$\eta_{\ IDEAL} = 1\text{-}S$$

..... (1.10.)

Many controllers were based on the above steady-state expression for torque production. Variable frequency, variable voltage or current power electronic stages were used to amplify sinusoidal reference values from the controller. The controllers

had closed loop speed control but usually relied on open loop flux control by varying the applied voltage in proportion to the frequency. These methods were very sensitive to parameter variations. Bose, [6], provides a good general overview of classical control schemes. Some controllers were based on the dynamic model but these usually utilised flux sensing coils or Hall Devices to produce a measure of air gap flux.

For lower power systems, PWM inverters incorporating either Bipolar transistors or Mosfets are now used.

These are basically voltage source inverters but may incorporate Analog current control loops, to be regarded as current source inverters. They give good performance because of the high switching frequencies used but may introduce harmonics due to over modulation and cross-over delay effects. At higher powers, thyristors are usually used to form current source inverters. These ideally give instantaneous control over each phase voltage or current and so are used with dynamic performance controllers.

1.4 The Field Oriented Control Strategy.

The Field Oriented Control principle (Blaschke et al, [7]) is used to achieve high dynamic performance from rotating-field machines, particularly Induction motors. With a separately excited DC machine there is virtually instantaneous control over torque by varying the armature current which is perpendicular to the field flux linkage. With the Field Oriented control strategy the controller coordinate reference frame is rotating with the field so that components of stator current both parallel to and orthogonal to the field may be impressed. The component parallel to the field or the d component establishes the field (with a time lag). The orthogonal or q component current will be torque producing and may be considered analogous to the armature current of the DC machine. With the control strategy the main objective is to achieve independent

or decoupled control over the field producing or torque producing components.

The stator current could be oriented with respect to either the stator, air-gap or rotor field. Sathiakumar et al, [8] discusses the different orientations and concludes that orientation with respect to either the stator or the air-gap fields will yield to instantaneous control after torque but will not give decoupled control over the flux. Bayer et al, [9] show that stability problems could occur under large loading conditions if orientation is not done with respect to the rotor flux. Throughout this work orientation with respect to the rotor flux only is considered.

Leonhard [5] uses the diagram of fig (1.1) to explain the control principle. $i_{mr}(t)$ is a space vector which represents the rotor flux magnetising current. A stator current vector, $i_s(t)$ will have two components with respect to this vector, $i_{sd}(t)$ and isq(t). isd(t) establishes the field, while isq(t) is the torque producing component.

With a transformation to a coordinate system aligned along the rotor flux (at angle ρ), the induction motor operation can be described by the following equations:

$$Te = k\ imr.\ isq \tag{1.11}$$

$$Tr \frac{d\ imr}{dt} \tag{1.12}$$

$$\frac{d\rho}{dt} = \omega + \frac{isq}{Tr\ imr} \tag{1.13}$$

Te is the developed electrical torque.

ω = angular velocity of rotor shaft.

Eqn (1.12) shows that imr lags i_{sd} according to the main rotor (field) time constant T_r). isd is controlled to be constant so that imr and the corresponding field flux will be constant in the steady state. isq can, theoretically, be instantaneously controlled by varying the stator current frequency in accordance with eqn. (1.13).

Perfect operation of the controller will occur if Tr is accurately known. If it is not eqn. (1.13) shows that the required slip frequency will differ from the actual slip frequency.

For impressed stator voltage operation the required d and q currents are evaluated and a knowledge of the stator voltage equations enables calculation of d and q voltages to give decoupled control over field and torque respectively. Because of leakage inductances there will be a small lag in the control of torque.

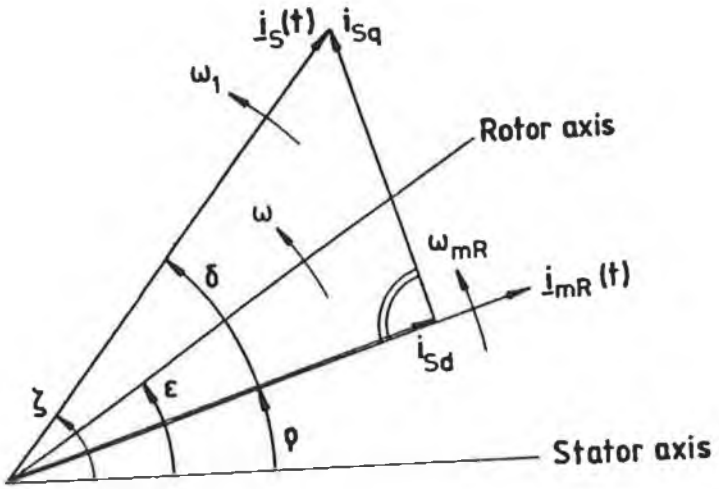

Fig. (1.1) Angular Relationships of Vectors.

ϵ = Mechanical Angle of Rotation.

$w = \dfrac{d\,\epsilon}{dt}$ = Angular Velocity of rotor shaft.

ζ = Instantaneous phase angle of the stator

ρ = Instantaneous angle of the rotor flux.

MODELLING

2.1 Introduction

Models in both the d-q representation and the space vector representation for the Induction motor are presented here. These models account for the full electrical dynamics of the Induction motor. All the models assume linear magnetics by assuming a smooth air-gap, neglecting hysteresis and magnetic saturation. All the models use lumped parameter representation.

The d-q model is presented for both rotating and stationary reference frames. Transformation equations between the coordinate frames are given.

The model in space vector format is given, using similar notation to the d-q model so that there is an exact correspondence between this model and the d-q model when the space vectors are resolved into d and q components.

Again using similar notation, a steady state model is given so that parameter values for the Squirrel Cage motor used in this work can be ascertained from both rating plate information and Locked rotor / No Load tests. Nominal parameter values are derived.

2.2 The D-Q model

D-Q theory can be applied to any machine. Depending on the type of machine a set of transformations are used to transform the currents in the actual phase windings to a set of currents in mutually perpendicular d axis and q axis coils in the "Primitive Machine", (Adkins and Harley [10]). These d and q axis currents establish equivalent MMFs which result in flux linkages and induced voltages (both by rotation through a flux and by transformer action). For any machine therefore, a set of equations

relating d and q axis voltages to d and q axis currents can be derived. This is then a complete electrical model of the machine. Fig (2.1) shows the "Primitive Machine".

The transformed axes move with a particular coordinate reference frame. Referring to fig. (2.1) the reference frame is stationary if the D and d coils are coincident. Alternatively these coils may rotate relative to each other to form a rotating reference frame. Usually a reference frame which rotates synchronously is selected. This could be attached to any of the stator airgap or rotor field. All d-q currents and voltages will therefore be DC under steady state, giving stator and rotor MMFs which are fixed relative to each other. D and Q coils are "pseudo-stationary", in that they can have induced rotational voltages, but currents in these coils produce stationary MMFs.

In nearly all d-q machines as in Park's model of the Induction motor the rotor represents the stator of the actual machine, (Adkins et al, [10]). Only in Kron's equations of the Induction motor is the reference frame attached to the primary member, with the D coil coinciding with stator phase A.

To derive the transformations for the currents two approaches are possible and lead to identical transformations.

- Assume the same currents in the 2 phase and 3 phase coils but different numbers of turns so that the resultant MMFs are the same. This is the approach taken by Hindmarsh, [11].

- Assume the same number of turns in d q axes coils as in the actual machine but a changed base value of current so that the same MMFs occur. This method is adopted by Adkins and Harley, [10].

Both methods arrive at the same transformation, with Hindmarsh, [11] neglecting zero sequence components.

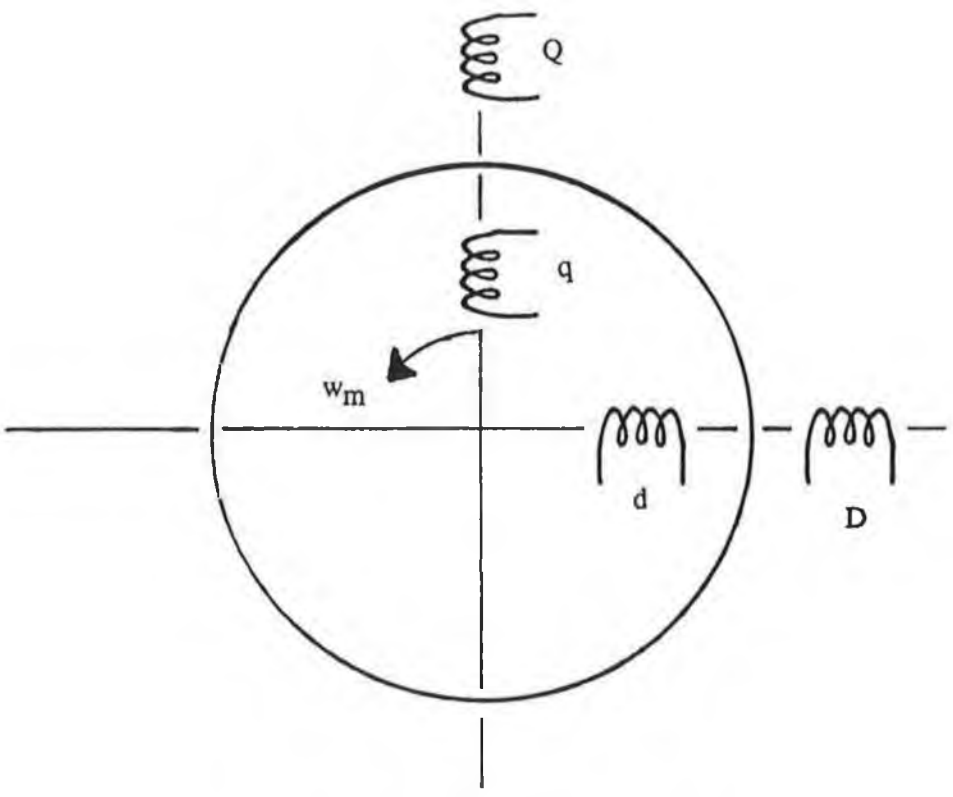

Fig. (2.1.) The " Primitive Machine ".

Similar transformations hold for voltages. The transformation do not change the total power so that the developed torque predicted by the d-q equations corresponds to the actual torque developed by the machine.

Figure (2.2) shows how the transformations from three phase stationary to two phase stationary, α-β arise. The α-β currents can then be easily transformed to two phase rotating, d-q. Using these transformations and the condition for balanced three phase currents, $i_{s1} + i_{s2} + i_{s3} = 0$ yields the following transformation and inverse transformation equations, between the reference frames:

$$i_\alpha = \frac{1}{\sqrt{2}} i_{s1} \qquad \ldots\ldots (2.1)$$

$$i_\beta = \frac{1}{\sqrt{2}\sqrt{3}} [\, i_{s2} - i_{s3} \,] \qquad \ldots\ldots (2.2)$$

$$i_{des} = i_\alpha \cos\theta + i_\beta \sin\theta \qquad \ldots\ldots (2.3)$$

$$i_{qes} = i_\beta \cos\theta - i_\alpha \sin\theta \qquad \ldots\ldots (2.4)$$

e Signifies the rotating reference frame, S refers to stator.

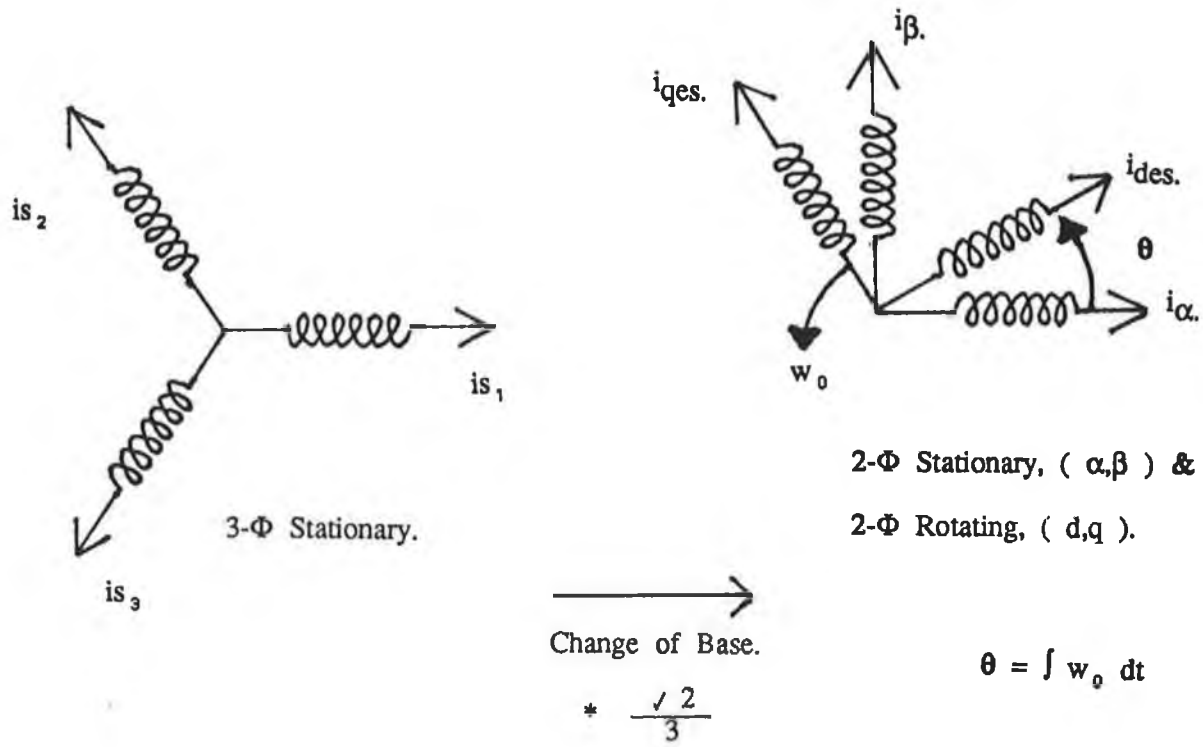

Fig. (2.2.) Transformations between the Coordinate Reference Frames.

$$i_\beta = i_{des} \sin\theta + i_{qes} \cos\theta$$

..... (2.5)

$$i_\alpha = i_{des} \cos\theta - i_{qes} \sin\theta$$

..... (2.6)

$$i_{s1} = i_\alpha \sqrt{2}$$

..... (2.7)

$$i_{s2} = \frac{i_\beta \sqrt{2}\sqrt{3} - i_{s1}}{2}$$

..... (2.8)

$$i_{s3} = - i_{s1} - i_{s2}$$

..... (2.9)

Kron's equations for the Induction motor are generally used (Ohnishi et al, [12] for motors with single cage rotor windings. The d-q axes are fixed to the stator windings and so the model corresponds more closely to the physical construction of the motor. The stationary reference frame representation is as follows:

$$\begin{vmatrix} V_{ds} \\ V_{qs} \\ V_{dr} \\ V_{qr} \end{vmatrix} = \begin{vmatrix} Rs + LsS & & LmS & \\ & Rs + LsS & & LmS \\ LmS & Lm\,\omega_m & Rr + LrS & Lr\,\omega_m \\ -Lm\,\omega_m & LmS & -Lr\,\omega_m & Rr + LrS \end{vmatrix} \begin{vmatrix} i_{ds} \\ i_{qs} \\ i_{dr} \\ i_{qr} \end{vmatrix}$$

..... (2.10)

If the reference frame is rotating with supply frequency w_o as is most often selected, (Ohnishi et al., [13]) the following d-q model describes the induction motor. "e" denotes synchronous rotation of the axes.

$$\begin{vmatrix} V_{des} \\ V_{qes} \\ 0 \\ 0 \end{vmatrix} = \begin{vmatrix} Rs + LsS & -\omega_0 Ls & LmS & -\omega_0 Lm \\ \omega_0 Ls & Rs + LsS & \omega_0 Lm & LmS \\ LmS & -(\omega_0-\omega_m)Lm & Rr + LrS & -(\omega_0-\omega_m)Lr \\ (\omega_0-\omega_m)Lm & LmS & (\omega_0-\omega_m)Lr & Rr + LrS \end{vmatrix} \begin{vmatrix} i_{des} \\ i_{qes} \\ i_{der} \\ i_{qer} \end{vmatrix}$$

..... (2.11)

The electrical torque is given by:
$Te = 3\ M\ [\ i_{qs}\ i_{dr} - i_{ds}\ i_{qr}\ ]$.

The rotor windings are shorted so that V_{der} and V_{qer} equal zero. With the reference axes now rotating rotational voltage terms can now be observed in all four voltage equations.

Equation set (2.11) has been put in block diagram form to show the full model of the induction motor in d-q coordinates Ohnishi et al, [13]. This model is shown in fig. (2.3) and has been used in this work for simulating motor operation. The notation has been adapted to correspond to the notation used in the steady state models and the space vector representation.

2.3 The Dynamic Model in Space Vector Format

The states are quantified by space vectors, which vary with both spacial displacement and time. This theory is very easy to grasp intuitively because all the usual electromagnetic relations can be applied to the space vectors, once they are defined properly. For example, the stator voltage vector is related to the stator current vector and flux linkage vector by $\underline{Vs}(t) = Rs\ \underline{is}(t) + {}^{d}/_{dt}\ \underline{\Psi s}(t)$.

There is no difficulty in transforming between different reference frames; a phase shift is simply applied to the space vector. This theory is particularly suitable for

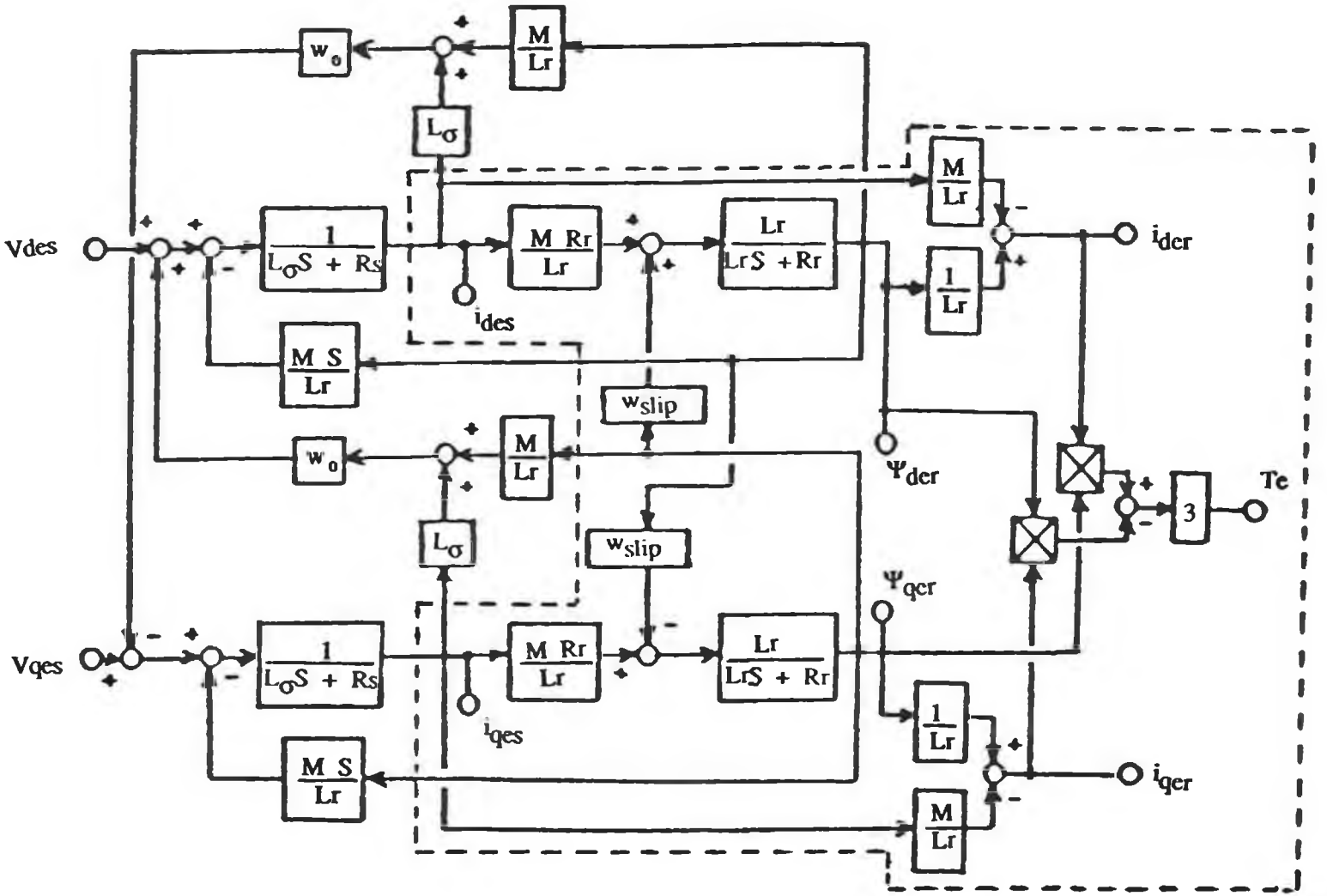

Fig. (2.3.) Induction Motor Model in Synchronously Rotating d - q Reference Frame.

analysing the Squirrel Cage Induction machine because of its symmetry. Leonhard, [5] makes extensive use of this theory and to derive the space vector models which are presented here he makes the following assumptions:

- Both Stator and Rotor have infinite permeability.
- Linear magnetics (no saturation or hysteresis).
- Iron losses neglected.
- No saliencies in the machine.
- Winding and slot effects are neglected.

Leonhard, [5] derives the complete mathematical model of the machine and inertial load as;

$$Rs\ \underline{is} + Ls\ \frac{d\ \underline{is}}{dt} + Lm\ \frac{d\ [\ \underline{ir}\ e^{j\epsilon}\ ]}{dt} = \underline{us}(t)$$

..... (2.12)

$$Rr\ \underline{ir} + Lr\ \frac{d\ \underline{ir}}{dt} + Lm\ \frac{d\ [\ \underline{is}e^{-j\epsilon}\ ]}{dt} = 0$$

..... (2.13)

$$J\ \frac{d\ \omega_m}{dt} = \frac{3}{2}\ Lm\ Im\ \left|\ \underline{is}\ [\ (\underline{ir}\ e^{j\epsilon})^*\ ]\ \right| - T_l(\epsilon, \omega_m, t)$$

..... (2.14)

$$\frac{d\ \epsilon}{dt} = \omega_m$$

..... (2.15)

J = Load Inertia.

T_l = Load Torque.

ϵ is the mechanical angle of rotation of the rotor shaft and transforms the rotor current vector to the stator frame in (2.12). In (2.13) ϵ is used to phase shift the stator current vector to the rotor reference frame to form part of the rotor voltage equation.

$$L_m\ (-1+\sigma_S) = L_S \qquad (2.16)$$

$$L_m\ (1+\sigma_R) = L_R \qquad (2.17)$$

The above model is sixth order comprising six real differential equations when the vectors are resolved into orthogonal components.

These equations are transformed to a synchronously rotating reference frame and the vectors are resolved into orthogonal components to give a model which corresponds to the d-q model. All quantities are referred to the rotating stator voltage vector.

$$T's\ \frac{d\ x_S}{dt} = -x_S + T's\ \omega_0\ y_S + \frac{1}{1+\sigma_r}\ x_r + c_1\ us(t) \qquad \ldots\ldots\ (2.18)$$

$$T's\ \frac{d\ y_S}{dt} = -T's\ \omega_0\ x_S - y_S + \frac{1}{1+\sigma_r}\ y_r \qquad \ldots\ldots\ (2.19)$$

$$T'r \frac{d x_r}{dt} = \frac{1}{1 + \sigma_s} x_s - x_r + T'r (\omega_0 - \omega_m) y_r$$

..... (2.20)

$$T'r \frac{d y_r}{dt} = \frac{1}{1 + \sigma_s} y_s - T'r (\omega_0 - \omega_m) x_r - y_r$$

..... (2.21)

And the mechanical model:

$$Te = 2 [1 + \sigma_s][y_s x_r - x_s y_r] - T_l(\omega, \epsilon, t)$$

..... (2.22)

$$\omega_m = \frac{d \epsilon}{dt}$$

..... (2.23)

The leakage time constants are derived as:

$$T's = \frac{\sigma\, Ls}{Rs} \quad ; \quad T'r = \frac{\sigma\, Lr}{Rr}$$

$$\text{The leakage Factor, } \sigma = 1 - \frac{1}{[\,1 + \sigma_s\,][\,1 + \sigma_r\,]}$$

The stator and rotor flux linkage vectors are resolved into components parallel to and orthogonal to the voltage vector.

$$\underline{\Psi s}(t) = c\,[\,x_s(t) + jy_s(t)\,]$$

$$\underline{\Psi r}(t) = c\,[\,x_r(t) + jy_r(t)\,]$$

The constant c normalises the flux linkage to that at rated voltage and frequency.

Applying balanced sinusoidal currents to the model results in the single phase steady state equivalent circuit of the Induction motor. This is as shown in fig (2.4).

2.4 Determination of Parameters

Squirrel cage motors are divided into four classes: A,B,C,D, (Slemon et al, [4]). The characteristics of each are specified by the electrical manufacturers associations NEMA and CEMA. The Squirrel Cage motor used for this work is a class B type motor which has a deep bar type rotor to tailor the steady state torque versus slip curve. This motor has a very low rated slip (0.06) and is therefore very efficient. This particular rotor construction also provides a combination of high starting torques and low starting currents. A problem with this type of motor is that the rotor leakage inductance and rotor resistance parameters cannot be easily evaluated from tests, (Slemon et al, [4]). The reason is that if the locked rotor test is performed at line frequency the rotor resistance is substantially increased over its DC value and the leakage inductance is somewhat reduced. Under normal load conditions the rotor

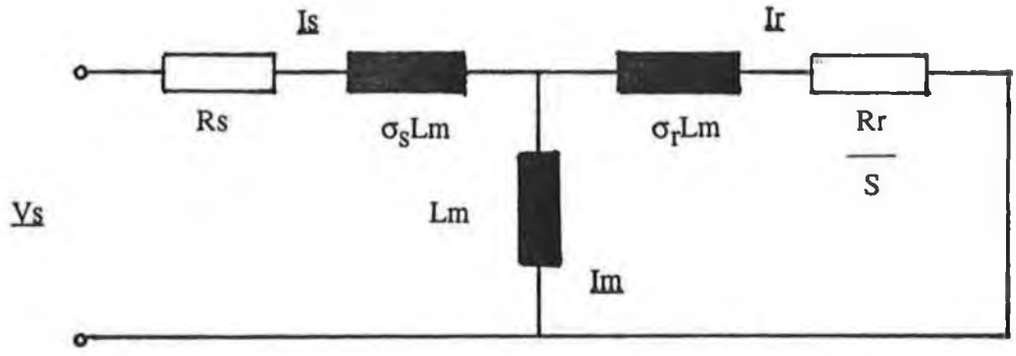

Fig. (2.4.) Single Phase, Steady State Equivalent Circuit of the Induction Motor.

frequency will be very low, typically being three Hz (rated slip x rated line frequency). A combination of tests and rating plate data were used to determine nominal values for parameters.

The stator windings were connected in the delta configuration so that the motor's rated voltage could be achieved with the three phase inverter operating from a three hundred volt DC bus. The rating plate specifications are as follows:

1.5 Kw.

2 Ps.

220 Volts (line - line rms.)

1410 rpm.

6.2 Amps.

Rated Power Factor Cos γ_r = 0.82.

Since for every delta representation there is an equivalent star representation the motor was assumed to be star wound with the above specifications. No Load and Locked Rotor tests were conducted to give the following results.

NO LOAD TEST:

$V_{LINE - EARTH}$ set at 127 V_{rms} (= 220 $V_{LINE - LINE\ rms}$)

I_{LINE} measured to be 6.4 amps peak = 4.5 A_{rms}.

Current was found to lag voltage by 71°.

LOCKED ROTOR TEST:

I_{LINE} set at 7 A_{rms} = 10 A_{peak}.

$V_{LINE - EARTH}$ measured to be 30 v_{rms}.

Current was found to lag voltage by 30°.

With the windings warm after conducting the locked rotor test the average line to line resistance was measured.

$R_{\Phi-\Phi} = 4.0\ \Omega.$

This gives $R_{\Phi} = 2.0\ \Omega.$

The no load test (Slemon, [4]) gives the magnetising current as:

$$Im = I_{NL} * \text{Sin } \theta = 4.5 * \text{Sin } 71^{0} = 4.25 \text{ Amps.}$$

The magnetising reactance is then found:

$$Xm = (V_{\Phi} / Im) - Rs = 28 \ \Omega.$$

Slemon et al. [4] gives the magnetising inductance as:

$$Lm = (k * Xm) / w_{0}.$$

Where $k = 1 / (1 + \sigma_{S})$.

The stator leakage factor is assumed to equal the rotor leakage factor (symmetry of the leakage flux), and is determined from the global leakage factor which can be computed from the rated power factor, as shown by Leonhard [5]:

$$\text{Cos } \gamma_{r} = 0.82 = (1 - \sigma) / (1 + \sigma) = 0.1$$

$$\Rightarrow \quad \sigma_{S} = \sigma_{r} = 0.05.$$

$$k = 0.9.$$

$$Lm = 0.08 \text{ Henries.}$$

The Pull - out slip is related to the rated slip (Leonhard [5]) by:

$$Sr / Sp = \sqrt{\sigma}.$$

$$Sr = (1500 - 1410) / 1500.$$

$$\Rightarrow \quad Sp = 0.19.$$

Ls = Lr (Symmetry of leakage fluxes assumed) = 1.05 * Lm = 0.084 H.

The Rotor Time Constant is determined from rating plate information (Leonhard [5]) by:

$$Tr = 1 / (Sp * \sigma * w_0) = 0.167 \text{ sec.}$$

Rr (referred rotor resistance) = Lr / Tr = 0.5 Ω.

CONTROLLER DESIGN

3.1 Introduction

The Field Oriented control strategy essentially resolves the motor model into two Single Input, Single Output Linear Time Invariant systems. Control methods, therefore, tend to be based on closed loop PI structures. The salient features of the controller topology selected for implementation in an induction motor based servo system, are presented here. A full analysis of the field weakening method is given. Discrete time controller design techniques using Z-transforms are used to tune the controllers.

3.2 Controller Design.

TheField Oriented control method enables the achievement of high dynamic performance with the Induction motor. The stator current is regarded as a space vector quantity with independently controllable excitation and torque components. Blaschke [3] formulated this control strategy for use when a direct measurement of the rotor flux vector was available. The so called slip frequency control method, is a variation used when the motor angular velocity is fed back. The controller designed for this work is based on this method. Because the Field Oriented control strategy essentially resolves the motor into two Linear Time Invariant systems, one for torque generation and one for field generation, most field oriented controllers will be of similar structure with differences being mainly dictated by hardware considerations. The Field Oriented controller presented here is again similar to most vector controllers surveyed but its salient features are discussed.

Use of a Voltage Source Inverter was decided upon:

- A Pulse Width Modulated Voltage Source Transistor Inverter has a negligible delay due to the high switching frequencies used and has a high bandwidth.

- High power Current Source Inverters employing thyristors or GTOs have a low bandwidth.

- At lower power ratings local analog current loops are often placed around PWM Voltage Source Inverters so that current source inverter type operation is achieved. These closed loops have a residual lag and the design of the analog PI controllers is never optimal because an RL representation, only of the motor, neglecting the back emf, is used. Also, the currents to be controlled are sinusoidal so that inevitable phase shifts will occur.

- Transistor Inverters are now available over a wide range of power ratings so that an all digital Field Oriented controller for a VSI fed motor could be used with motors from a fraction of a kilowatt to tens of kilowatts with software changes, to parameter values only needed. Field oriented controllers with Induction motors could therefore be suited to large servomotor applications.

- With a VSI fed machine current loops can be digital and in d-q coordinates. The quantities being controlled will be DC in steady state. The loops can be designed to be optimal and will not be affected by the back EMF.

- Software values for the voltages will be available and so eliminate the need for sensing voltages. Isolated sensing of the fundamental components of Inverter output voltages is difficult. These software voltage values are available for implementation of a field weakening scheme or could be used with the stator voltage equations and sensed currents for a rotor time constant estimation scheme.

- With a Voltage Source Inverter additional voltage decoupling equations will be

needed in the controller algorithm but the parameters used in these equations are not so subject to drift as the rotor parameters. Advances in microprocessors, coprocessors and digital signal processors mean that this addition to the control algorithm is not a serious limitation.

- The Field Oriented controller combined with a VSI fed motor is much less sensitive to rotor parameter variation effects than the controller and CSI fed motor combination. Harashima et al, [29] explain how V-type control is more robust to rotor time constant variations than I-type control. The reasoning behind this is given in 6.2.

The controller topology selected is shown in fig (3.1). The rotor shaft velocity as opposed to a shaft position signal, is fed back. Either signal could be used by the controller but since the slip frequency is determined and an integral is needed anyway to calculate the instantaneous slip, the velocity signal, which is easier to measure, is fed back.

Closed loops for d-q torque and flux current components incorporating PI controllers are used. Variations in parameters in the stator voltage equations are therefore accounted for. The phase currents are easily and accurately measurable states. Only one of the controllers surveyed dispensed with current loops and relied on open loop control of torque and flux current components (Harashima et al, [29]). PI controllers for speed and flux are also used. The output of the speed controller, the torque demand, is limited to prevent saturation of the torque current PI controller. This limiting is a function of the actual d-rotor flux linkage which governs the achievable torque. Given that the field reference is constant the need for PI control over the field is only needed where extended periods of operation in the field weakening region are expected. This controller can be designed by accounting for the dynamics of the field generation loop to achieve specific control performances for changes in the field reference.

The overall structure of the controller is designed so that a hierarchy of execution times of the different control loops could be achieved. The inner current loops could be controlled with very fast sampling times to achieve a high bandwidth. The outer speed and flux loops need not be executed so often - especially if the load dynamics dominate over the machine dynamics. The possibility, therefore, exists of synchronous operation of the inner loops with the inverter switching signals thereby reducing noise.

A feature that should be included in an actual implementation of the controller is torque reference limiting at start up. Before the field has established a large torque demand would result in a large slip frequency and a field would not be established.

In nearly all controllers surveyed control over the slip frequency was open loop. Sathiakumar et al, [15], however describes a closed loop scheme whereby voltages, reference currents, speed and a PI controller are used to derive a signal for the incremental stator current vector position. With open loop schemes either of the following two equations can be used to compute the required slip frequency, for decoupled control:

$$\omega_{slip} = \frac{R_R \, iqes}{L_R \, ides} \qquad (3.1)$$

or

$$\omega_{slip} = \frac{R_R \, M \, iqes}{L_R \, \Psi der} \qquad (3.2)$$

Since Ψder equals M.Ides in the steady state (3.1), necessitating one less multiplication, has been used here.

Another very important issue is the use of reference values or measured values of the currents in eqn (3.1). Ψder_{ref} or a value estimated from the d measured current can be used in equation (3.2). There is no general concensus as to whether measured states or reference state should be used. Nabae et al, [16] shows that with using reference values to determine the slip frequency with Open loop control methods gives a stable control system even if parameter errors occur. In Chapter six where effects due to parameter mistmatch occur, it is shown that even if measures states are used and there are parameter deviations a stable control system will result, with error envelopes decaying subject to the actual rotor time constant.

Most controllers employing adaptive control schemes or observers with predictive error correction use reference values for the current components when computing the required slip frequency. Kumamoto et al, [17] utilise this method. Some, despite using adaptive control methods, use the measured states. Koyama et al, [18] derive an identification function for the rotor time constant and use measured states for computing the required slip. Use of reference values in cases where adaption techniques are employed possibly makes the control system less sensitive to noise in measured states.

In cases where controllers are not adaptive the measured values for the states have been used. Leonhard, [19] details control designs where the measured current component values are used to compute the slip frequency. In the controller in fig (3.1) measured values of the current components are used in view of the high quality of the current measurements available with hall effect devices.

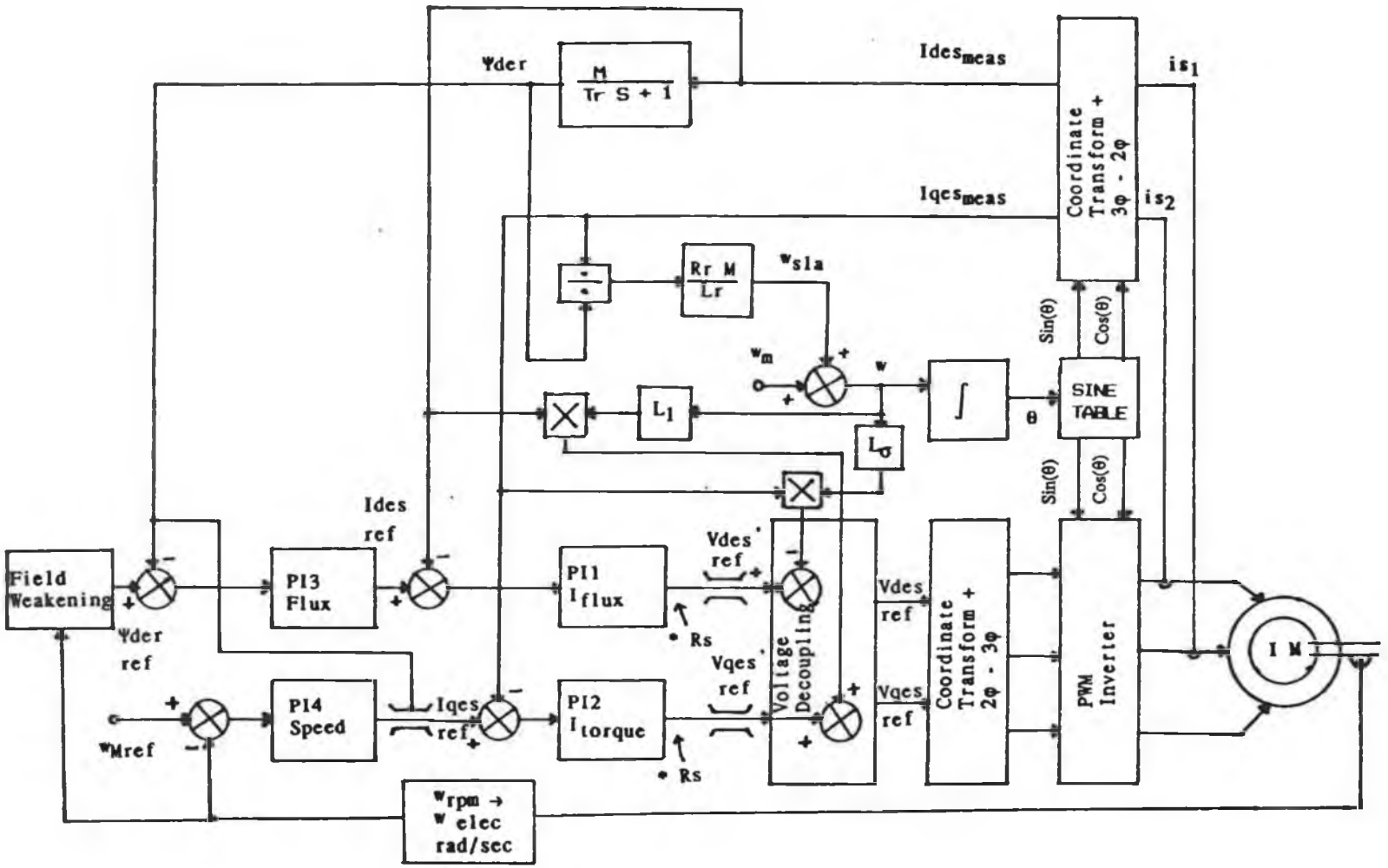

Fig. (3.1.) Field Oriented Controller for a Voltage Source Inverter Fed Induction Motor.

3.3. Field Weakening Analysis.

Over the normal speed range the field is maintained constant. At higher speeds the field is reduced to further raise the speed at reduced loads. As the speed is increased the magnitude of the stator voltages increases. At a speed referred to as " Base Speed ", the ceiling voltage of the invertor is reached (voltage source saturated) and a further increase in speed is not possible without a reduction in the field. The technique can be thought of as a reduction in the d voltage component so that the q or torque producing voltage component can be increased, since it is the magnitude of the voltage vector that is limited. Alternatively, it can be regarded as a reduction of the " Back Emf ", thereby leaving a greater voltage for a speed increase.

A variety of techniques for implementing Field Weakening have been used in the Field Oriented Controllers surveyed.

In nearly all cases where the motor is CSI fed or where a VSI with local analog current loops are used, a nonlinear function generator is used to derive the field reference. The velocity measurement (which is normalised to the stator frequency) is used as the input. Above Base Speed an inverse square function decrements the field reference. This method is also done with controllers for VSI fed motors if transient excursions into the Field Weakening region only, are anticipated. Sugimoto et al. ([20]) describe a controller which uses this method.

With controllers for VSI fed motors the software voltage reference values are available. These give a measure of the stator voltages and avoids the difficult measurement of the PWM / Inverter output voltage fundamental components. Lessmeier et al. ([1]) in their controller show a method whereby the product of the rotor magnetising current and the speed are used to give a measure of the voltage vector magnitude. This is subtracted from the maximum voltage value to give an

error signal for a P controller, which generates the field reference.

A variation on this scheme can be used (Leonhard, [19]) whereby the magnitude of the voltage vector is obtained from the d and q voltage reference values. This is then compared with the maximum possible value to form an error signal for a P I controller which generates the field reference. This method has the advantage that the field is always weakened by just the correct amount for maximum utilisation of the inverter. The disadvantage of the method is that two multiplications and a square root must be obtained.

The following are the stator voltage equations in d - q coordinates (Leonhard, [19]).

$$I_{des} = \frac{V_{des}}{Rs} + \sigma\, Ts\, w_{mr}\, I_{qes} \qquad \ldots\ldots (3.1.)$$

$$I_{qes} = \frac{V_{qes}}{Rs} - (1 - \sigma)\, Ts\, w_{mr}\, I_{mr} - \sigma\, Ts\, w_{mr}\, I_{des} \qquad \ldots\ldots (3.2.)$$

Where:

σ is an overall leakage factor.

I_{mr} represents a rotor air - gap magnetising current vector.

w_{mr} is the angular velocity of this vector.

Ts equals Ls / Rs.

In the steady state:

$$w_{mr} = w_0, \qquad \ldots\ldots (3.3.)$$

$$\Psi_{der} = M\, I_{mr} = M\, I_{des}.$$

..... (3.4.)

So that:

$$\Psi_{der}\ (S.S.) = \frac{M}{1 + \sigma \frac{Ls^2\, w_0^2}{Rs^2}} \left[\frac{V_{des}}{Rs} + \frac{\sigma\, Ls\, w_0}{Rs^2}\, V_{qes} \right]$$

..... (3.5.)

Over the normal speed range Ψder_{ref} is kept constant and at a value close to the machine's maximum operating flux density. At Base Speed the magnitude of the voltage vector has reached its maximum, limited by the DC bus voltage of the inverter. The field must be weakened to extend the speed range. A reduction in Ψder_{ref} means a reduction in V_{des} which will allow a reduction in V_{qes}.

$$\sqrt{V_{des}^2 + V_{qes}^2} \leqslant V_{max}$$

..... (3.6.)

In steady state equations (3.1.) and (3.2.) give the following:

$$V_{qes} = Rs \left[I_{qes} + Ts\, w_0\, I_{des} \right]$$

..... (3.7.)

$$V_{des} = Rs \left[I_{des} - \sigma\, Ts\, w_0\, I_{qes} \right]$$

..... (3.8.)

V_{des} is always very small, even for large negative torques. At w_0 equals 300 rad.sec^{-1} σ Ts w_0 equals 1.26 for the motor used in the prototype system, so that from eqn. (3.5.) V_{des} would rarely exceed 25 volts.

Inserting the motor parameter values gives:

$$\Psi_{der}\ (\ S.S.) = \frac{0.042}{1 + 1.7 * 10^{-4} w_0^2} \left| V_{des} + 4.2 * 10^{-3} w_0 V_{qes} \right| \quad \ldots\ldots\ (\ 3.9.)$$

At high frequencies ($w_0 > 200$ rad.sec^{-1}):

$$\Psi_{der}\ (\ S.S.) \approx \frac{245}{w_0^2} V_{des} + \frac{1}{w_0} V_{qes}. \quad \ldots\ldots\ (\ 3.10.)$$

From (3.10.) it is seen that Field Weakening will be more than adequately accomplished if the field reference is reduced by the square of the difference between the stator frequency and the base speed frequency.

3.4. Discrete Design of Current Loop.

Discrete design of the digital controllers was done by utilising Root Locus techniques. It was assumed that the controller parameters were accurate so that perfect decoupling of the Flux and Torque loops was achieved. P I controllers were incorporated in each loop. The simplest discrete P I controller algorithm, obtained by using the Backward Difference approximation for the derivative, was used. This was justified by the use of the relatively small sample times needed for servo performance. S - domain closed loop transfer functions (in the d - q reference frame) are first presented for each loop. By Partial Fraction Expansion and by modelling A / D convertion as Zero Order Hold, transfer functions in the Z - domain were obtained. These transfer functions resemble those of standard second order systems so that well known methods for pole location in the Z - plane, by controller Gain and Integral Time constant selection, were used.

Design of Torque Current Loop.

It is assumed that perfect decoupling of the voltage equations has been achieved by the controller so that V_{qes} and V_{des} give independent control over torque and flux respectively. Referring to the full motor model in the d - q rotating reference frame, it is assumed that Ψ_{qer} is always equal to zero. Accounting for the fact that $Vqes_{ref}$ equals Rs * $Iqes_{ref}$, the complete torque current loop with controller in d - q coordinates can be modelled as shown in fig. (3.2.).

$$G(s) = \frac{1}{1 + T_\ell S}$$

..... (3.11.)

Where $T_\ell = L_\sigma / Rs = 7.8 * 10^{3} / 2 = 0.0039$.

For this system surrounded by an A / D and a D / A the corresponding Z transform is given by;

$$G(z) = (1 - z^{-1}) \left[\left[\frac{1}{S(1 + T_\ell S)} \right] \right]$$

..... (3.12.)

$$G(z) = (1 - z^{-1}) \left[\frac{z}{z + 1} - \frac{z}{z - e^{-T/T\ell}} \right]$$

..... (3.13.)

$$G(z) = \left[\frac{1 - a}{z - a} \right]$$

..... (3.14.)

Where $a = e^{-T/T\ell}$.

The transfer function for the P I controller, where E (z) is the input (error) signal is given by:

$$\frac{O(z)}{E(z)} = \frac{K_c (z - 1) + K_c T / T_i}{(z - 1)} = D(z)$$

..... (3.15.)

$$D(z)G(z) = \frac{K_c[z - (1 - T/T_i)](1 - a)}{(z - a)(z - 1)}$$

..... (3.16.)

Closed loop transfer function for the torque current loop:

$$\frac{D(z)G(z)}{1 + D(z)G(z)} =$$

$$\frac{(K_c - K_c a)z - (K_c - K_c a)(1 - T/T_i)}{z^2 + (K_c - K_c a - a - 1)z - (K_c - K_c a)(1 - T/T_i) + a}$$

..... (3.17.)

The design parameters are Kc and T_i.

The sampling time,T equals 0.003.

Initially T_i was set equal to infinity so that the maximum gain, K_c, to give a stable system was found to be 0.75. The integral time constant was then varied from 0.0015 to 0.004 to give a locus of poles varying from 0.56 ± j 0.7 to 0.56 ± j 0.25 as shown in plot (3.1.)

Design of Flux Current Loop

Accounting for the fact that the derivative of Ψ_{der} does not always equal zero, the flux loop can be modelled in the S domain as shown in fig. (3.3.). The Laplace transfer function for the continuous time field generation system is:

$$G(s) = \frac{M^2 s}{(T_r T_L Lr) s^2 + (T_L Lr + T_r Lr + M^2) s + Lr} \quad \ldots\ldots (3.18.)$$

Where: $T_\ell = L_\sigma / Rs$, $T_r = Lr / Rr$.

$T_\ell = 0.0039$, $T_r = 0.168$.

$$G(s) = \frac{116.36}{(s + 4.23)(s + 359.36)} \quad \ldots\ldots (3.19.)$$

For this system surrounded by an A / D and D / A the

Z transfer function is:

$$G(z) = (1 - z^{-1}) \left[\left[\frac{G(s)}{s} \right] \right] \quad \ldots\ldots (3.20.)$$

$$G(z) = (1 - z^{-1}) \left[\frac{0.327\ z}{z - e^{-4\ 23\ T}} - \frac{0.327\ z}{z - e^{-359\ 36\ T}} \right] \quad \ldots\ldots (3.21.)$$

For T = 0.003:

$$G(z) = \frac{0.212\,z - 0.212}{z^2 - 1.33\,z + 0.33}$$

..... (3.23.)

Again the P I Controller is given by:

$$D(z) = \frac{K_c\,(z - 1) + K_c\,T / T_i}{(z - 1)}$$

..... (3.24.)

Initially the integral time constant was set equal to infinity to find the maximum value for K_c so that the closed loop system was stable. With K_c equal to 1.5 the roots of the system characteristic equation are 0.99 and 0.017. As T_i was allowed vary from 0.001 to 0.004 the locus of the poles (plot (3.2.)) was found to go from $0.5 \pm j\,0.845$ to $0.5 \pm j\,0.18$, all well within the z - plane unit circle.

Specific pole locations in the Z - plane within the Unit Circle are selected to achieve certain performance specifications. Pole locations for second order systems govern the Overshoot, Rise time and Settling time in a step response.

To achieve a Damping Factor greater than 0.5 poles should be located in the right half of the Unit Circle and close to the real axis. This will result in a small amount of overshoot.

To obtain a fast Rise Time all poles should be located well away from the origin in the S - plane or well into the right half of the Unit Circle (Z - plane) and away from its centre.

To achieve a fast Settling Time poles should be located well away from the Unit Circle centre.

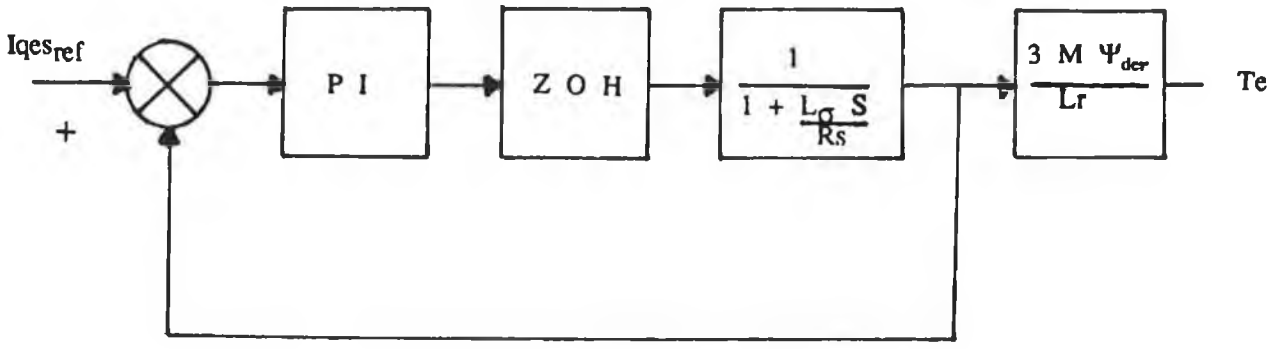

Fig (3.2.) Torque Current Loop in d - q Coordinates

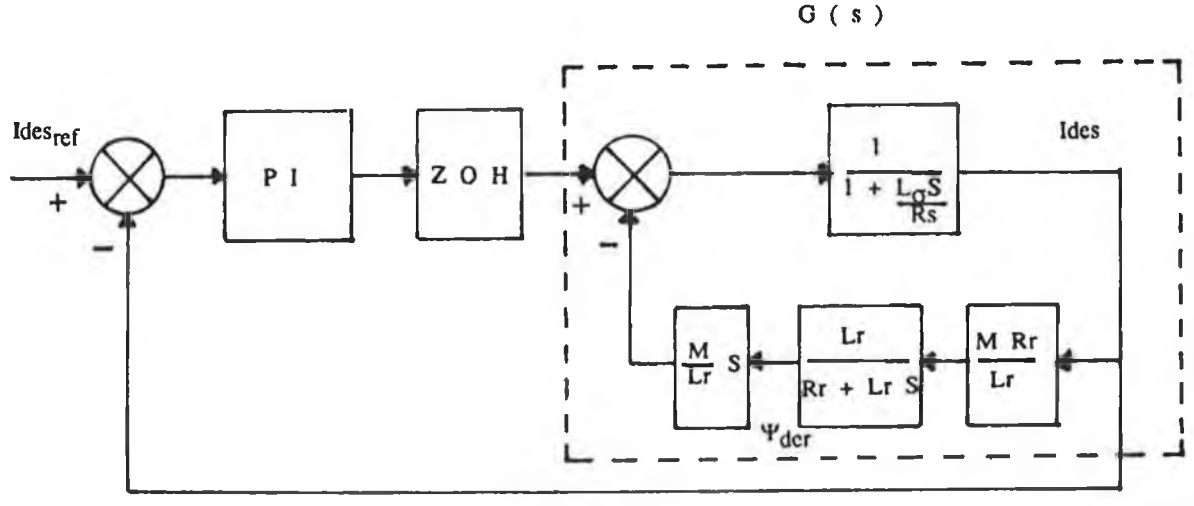

Fig (3.3.) Flux Current Loop in d - q Coordinates.

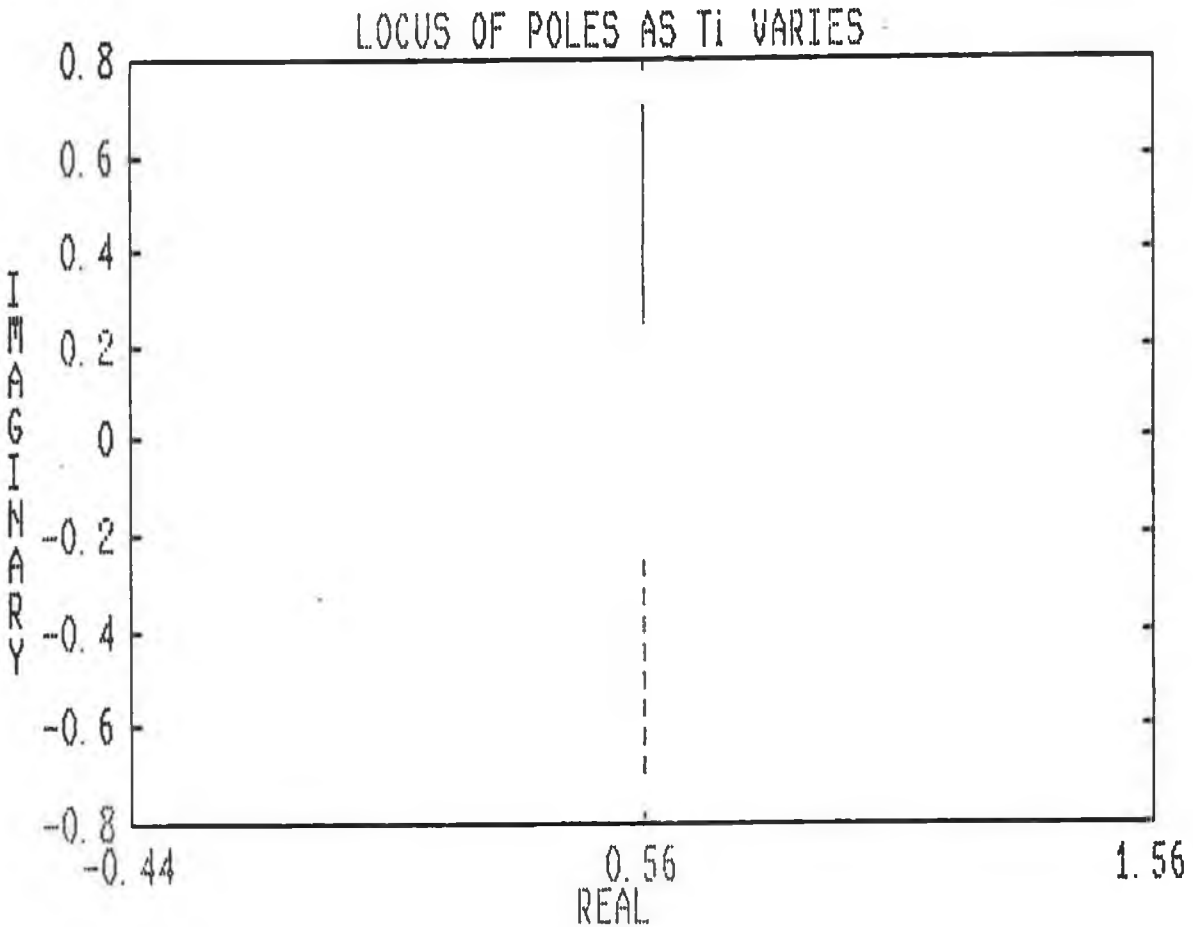

Plot (3.1.) Locus of Poles as T_i varies for the Torque Current Loop.

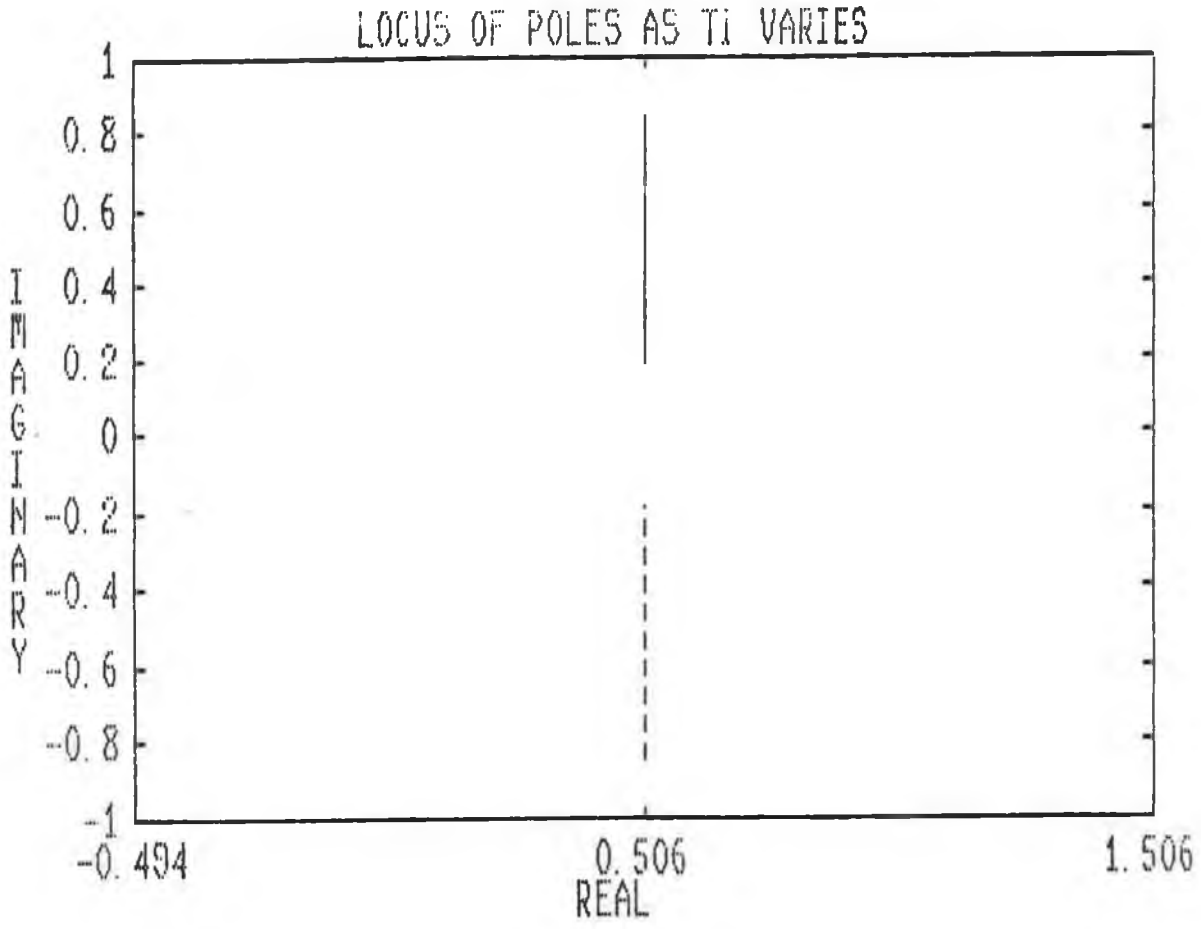

Plot (3.2.) Locus of Poles as T_i varies for the lux Current Loop.

SIMULATION OF DESIGNED SERVO SYSTEM

4.1 Introduction.

The motor model, controller and mechanical load model are discretised to simulate the performance of the designed prototype servo system. The full d-q model of the motor is used. Because of cross coupling in this model the discretised equations are solved algebraicly to derive equations for the internal states after each time interval. Closed loop and open loop, steady state and dynamic performances are predicted, discussed and validated analytically.

4.2 Motor Model Simulation Technique.

The model in the synchronously rotating d-q reference frame was employed for simulating motor behaviour. Transformations to the stationary reference frame are only done for observing the three phase voltages and currents. The d and q stator currents, ides, iqes respectively and the d and q rotor flux linkages, Ψder, Ψqer respectively are regarded as the four main internal states of the model. The d and q stator voltages and the slip frequency (actual frequency - mechanical frequency [electrical rad sec^{-1}]) are regarded as the inputs. Equations for the four internal states are as follows:

$$\Psi_{der} = \frac{Lr}{Lr\ S + Rr} * \left[\frac{M\ Rr}{Lr}\ I_{des} - w_{sla}\ \Psi_{qer} \right]$$

..... (4.1.)

$$\Psi_{qer} = \frac{Lr}{Lr\ S + Rr} * \left[\frac{M\ Rr}{Lr}\ I_{qes} - w_{sla}\ \Psi_{der} \right]$$

..... (4.2.)

$$I_{des} = \frac{1}{L_\sigma\ S + Rs} * \left[e_{des} + w_o \left| \frac{M\ \Psi_{qer}}{Lr} + L_\sigma I_{qes} \right| - \frac{M\ S\ \Psi_{der}}{Lr} \right]$$

..... (4.3.)

$$I_{qes} = \frac{1}{L_\sigma\ S + Rs} * \left[e_{qes} + w_o \left| \frac{M\ \Psi_{der}}{Lr} + L_\sigma I_{des} \right| - \frac{M\ S\ \Psi_{qer}}{Lr} \right]$$

..... (4.4.)

S is the Laplace Operator.

w_{sla} is the actual Slip Frequency.

L_σ is a Leakage Inductance = Ls * σ = Ls - (M^2 / Lr).

Using the Backward Difference to approximate the derivative, these equations were discretised to give the following:

$$a_k = \left[\frac{b_k\ w_o\ L_\sigma\ T}{T_1} + \frac{d_k\ w_o\ M\ T}{Lr\ T_1} - \frac{M\ c_k}{Lr\ T_1} + \frac{M\ c_{k-1}}{Lr\ T_1} + \frac{e\ T}{T_1} + \frac{L_\sigma\ a_{k-1}}{T_1} \right]$$

..... (4.5.)

$$b_k = \left[- \frac{a_k \, w_0 \, L_\sigma \, T}{T_1} - \frac{c_k \, w_0 \, M \, T}{Lr \, T_1} - \frac{M \, d_k}{Lr \, T_1} + \frac{M \, d_{k-1}}{Lr \, T_1} + \frac{f \, T}{T_1} + \frac{L_\sigma \, b_{k-1}}{T_1} \right]$$

..... (4.6.)

$$c_k = \left[\frac{a_k \, M \, Rr \, T}{T_2} + \frac{d_k \, w_{sla} \, T \, Lr}{T_2} + \frac{c_{k-1} \, Lr}{T_2} \right]$$

..... (4.7.)

$$d_k = \left[\frac{b_k \, M \, Rr \, T}{T_2} - \frac{c_k \, w_{sla} \, T \, Lr}{T_2} + \frac{d_{k-1} \, Lr}{T_2} \right]$$

..... (4.8.)

Where :

$a_k = ides_k.$ $\quad e_k = edes_k.$
$b_k = iqes_k.$ $\quad f_k = eqes_k.$
$c_k = \Psi der_k.$ $\quad g_k = ider_k.$
$d_k = \Psi qer_k.$ $\quad h_k = iqer_k.$

$T_1 = L_\sigma + Rs \, T.$ $\quad T_2 = Lr + Rr \, T.$

Initially all the "k-1" states are zero because of the lag between applied voltages and resulting currents. At any time, kT, equation set (4.5) - (4.8) represents a fourth order set of simultaneous algebraic equations, with four unknowns. The "k-1" states will be known, the slip frequency, stator frequency and the voltages are determined by the controller and so are regarded as known inputs. The equation set was solved to give general expressions for the solutions of $ides_k$, $iqes_k$, Ψden_k and Ψqen_k

To simulate the motor operation these expressions (c.f. Appendix A) are evaluated at each iteration time interval to give values for the main internal motor states.

4.3. Discretisation of the Controller.

The complete controller structure, incorporating speed and flux loops, as detailed in chapter three was discretised for the simulations and for deriving the eventual control algorithms. The PWM inverter stage was originally just modelled as being a gain stage, although later the cross-over delay non linearities were modelled in.

For implementing each PI controller the following discrete version of the algorithm was used:

$$u(k) = K\left[e(k) + \frac{T}{Ti}\sum_{i=0}^{k} e(i-1)\right] \qquad \ldots\ldots (4.9.)$$

The integration is done by simple rectangular summations. This version (which is used where the sampling time is small) was chosen to minimise eventual controller algorithm execution time. T represents the control time interval or sample time and is different from the model simulation time interval.

u(k) is the output from the PI block at any time kT.

e(k) is the closed loop error or input to the PI block.

Ti is the integral time constant.

Bounds on the Integral Action were not implemented.

Assuming correct field oriented control, giving proper decoupling of flux and torque components of current, the following equation relating Ψ_{der} to i_{des} holds:

$$\frac{T_R}{M}\frac{d\,\Psi der}{dt} + \frac{\Psi der}{M} = ides \qquad \ldots\ldots (4.10.)$$

Using the Backward Difference Approximation gives:

$$\Psi_{der}(k) = i_{des}(k)\left|\frac{M\,T}{Tr+T}\right| + \left|\frac{Tr}{Tr+T}\right|\Psi_{der}(k-1) \qquad \ldots\ldots (4.11.)$$

In the simulation this equation was used to give a measure for field flux linkage. The motor current as determined by the model was used. In the final controller $ides_{meas}$ (k) was used.

Limits on the current component reference values which would prevent overcurrents and saturation of the PI controllers in the eventual system were implemented in the simulation.

Transformations between the reference frames were not needed because the model is in d-q format but were incorporated in the simulation to show the 3Φ currents and voltages. "C" maths library continuous functions were used instead of sine look-up tables.

For calculating the flux and the required slip frequency, a "controller value" for Rr could be used to simulate Tr mismatch problems. The slip frequency is calculated by

$$w_{slip}(k) = \frac{M\, Rr_{ref}\, i_{qes}(k)}{Lr\, \Psi_{der}(k)} \qquad \ldots\ldots (4.12.)$$

This was limited by $\pm\, w_{omax} - w_m$ where w_{omax} is the maximum stator current frequency obtainable, which is a function of the sampling time. Numerical Overflow problems occur at start-up since the flux is zero. Whenever the flux was detected to be zero the slip frequency was automatically set at 0.1 times its maximum value so that a field would be established.

4.4 Discretisation of the load model

In the simulation the Mechanical Load Equation was again discretised by using the backward difference approximation:

$$J \frac{d\, w_m}{dt} = Te - T_L. \qquad \ldots\ldots (4.13.)$$

$$W_m(k) = \frac{T}{J}[Te - T_L] + w_m(k-1) \quad \ldots\ldots (4.14.)$$

T_L represents a fixed load torque.

The rotor was assumed to be a simple cylinder for the purposes of calculating its inertia. For the motor used, it was taken to be (0.1)m long and (0.04m) in radius. Given the density of iron at 7.9×10^3 Kg m^{-3} the rotor inertia was estimated to be 0.035 N.m.sec^2 rad^{-1}.

4.5. Servo System Performance Predictions.

The discretised versions of the model, controller and load were incorporated into the one simulation to qualitatively predict the performance of the designed controller. A simulation time of 1×10^{-4} seconds was used for the motor model and load, while a sampling time of 3×10^{-3} seconds was used for the controller. A hierarchial order of executing different controller loops is often used but here all control loops are executed every 3×10^{-3} seconds. The simulation was used to assess overall performance, examine the influence of rotor time constant variations and show the influences of PWM introduced non linearities. More performance predictions are presented and discussed. The current loops were tuned with the gains and integral time constants designed using the Z transform design techniques in Chapter three. Arbitrary amounts of integral action were chosen for the speed and flux loops. For the speed loop the amount would depend on specific control requirements, whereas for the flux loop a lot of integral action is desirable, since the field flux linkage is normally kept constant, and a small steady-state error is required.

The controller tuning settings are:

Flux current loop:

$K_{C1} = 1.5$

$T_{ic1} = 0.05$

Torque Current Loop

$K_{C2} = 1.0$

$T_{ic2} = 0.05$

Flux Loop:

$K_{C3} = 3.0$

$T_{ic3} = 0.06$

Speed Loop:

$K_{C4} = 1.0$

$T_{ic4} = 1.0$

(The gain of the flux current loop was lowered in the actual implementation to make the system less sensitive to variations in Tr).

For the tuning values given above, plots (4.1) to (4.4) predict the likely performance with the complete controller described in Chapter three.

Plot (4.1) shows the speed response with no load applied to the motor. The speed reference is set at 40 r.p.m. and the response are given. The rise time is 2.5 x 10^{-3}

seconds and transients are negligible after 35 x 10^{-3} seconds.

Plot (4.2) shows the corresponding torque current component. The step change in speed is commanded at 0.6 seconds at which time the field flux has been established and is constant so that the torque developed, T_e, directly corresponds to iqes.

Plot (4.3) shows $Vqes_{ref}$. This corresponds to i_{qes} but an offset, which arises in the stator voltage decoupling equations, is present. The 3 millisecond sampling time is clearly evident, with a substantial change in the reference with each sampling time. This indicates that sampling times much longer would not give satisfactory operation of the current loops.

Plot (4.4) shows the rotor q-axis flux linkage. This should ideally be zero but rises to 9 mWb. Some of the error is numerical due to the very complex equations (appendix 4) iterated to give the internal motor states. Another reason is that the following assumptions are made for the stator voltage equations decoupling strategy and these may not be strictly correct at the sampling instances.

$$\frac{d\,\Psi_{der}}{dt} = 0$$

$$\Psi_{qer} = 0$$

$$\frac{d\,\Psi_{qer}}{dt} = 0$$

Plots (4.5) and (4.6). Here operation of the current loops is investigated since good independent control of the current loops is essential. The Flux Loop is closed, whereas Foward Path operation of the torque current loop is examined. $Vqes_{ref}$ and the corresponding iqes plots against time are shown.

Plot (4.7) shows ides. The reference value is set at 3 amps, so the steady state error is 0.01 amps. During transient changes in the torque there are variations in ides due

to transient cross coupling effects. Ides at 3 amps gives Ψder = M.ides = 0.24 Wb.

Plot (4.8) shows the q-axis rotor flux linkage and is again very small. This is mainly shown for comparison with the case of controller and motor T_R mismatch.

Plots (4.9) through (4.12) show steady state operation of the controller. At time, t, = 1 second $iqes_{ref}$ = 6 amps is commanded. 0 amps is commanded at t = 3.5 seconds. Plot (4.9) shows the field flux linkage. This is seen to remain constant after the slow build up. This is not properly established until 0.6 seconds due to PI controller action and the large rotor time constant (0.168 seconds).

Plot (4.10) shows the torque developed when $iqes_{ref}$ = 6.0 amps, over the time interval 1.0 - 3.5 seconds. Theoretically:

$$Te = 3 \frac{M^2}{Lr} i_{des} i_{qes} \quad N.m.$$

$$Te = 4.11 \ N.m.$$

The simulation showed this to stabilise at 4.114 Nm.

Plot (4.11) shows i_{s_1} when zero torque is commanded i_{s_1} is a D.C. current. The motor is stalled and so a D.C. current is required to establish a field which is fixed in time and space. During the interval 1.0 seconds to 3.5 seconds i_{s_1} is sinusoidal and at the slip frequency required to produce a torque of 4.11 Nm.

Plot (4.12) shows the corresponding q-axis rotor flux linkage. This can be seen to decay to zero in the steady state.

4.6. Conclusions and Validation of Simulation Predictions.

The motor model is highly complex and non linear. It was therefore not certain that discretisation by the Backward Difference and Simultaneous Algebraic Solution of the resulting Difference Equations would give correct performance. The method has however worked successfully and so the simulation of the servo system is available for performance prediction with any system.

The robustness of any system to various disturbances, non-linearities, parameter variations or sampling times can now be correctly assessed.

- The actual speed reached the reference speed within two sample periods for an unloaded motor and settled at the desired speed with negligible steady state error after 35 milliseconds.

- The controller worked successfully with the tuning values for the current loops designed by Z-transform design techniques in Chapter two.

- The Q-axis rotor flux linkage, ideally zero, never exceeded 10 mWb, even during transients.

- The d-axis flux settled at the reference value with an error of only 0.01 Wb.

- From space vector theory the following formula for steady state error rotor flux was derived and incorporated in the simulation for comparison with the actual simulated rotor flux. The discrepancy never exceeded 5%.

The steady state stator voltage equations were used to derive an expression for ides in terms of Vdes and Vqes. In steady state Ψ_{mr} = M.ides were:

Ψ_{mr} = magnitude rotor air gap flux linkage vector giving:

$$\Psi_{mr} = \frac{M}{1 + \sigma \left[\frac{Ls}{Rs}\right]^2 w_0^2} \left| \frac{V_{des}}{Rs} + \frac{\sigma\, Ls\, w_0\, V_{qes}}{Rs^2} \right|$$

..... (4.15)

σ = overall leakage factor.

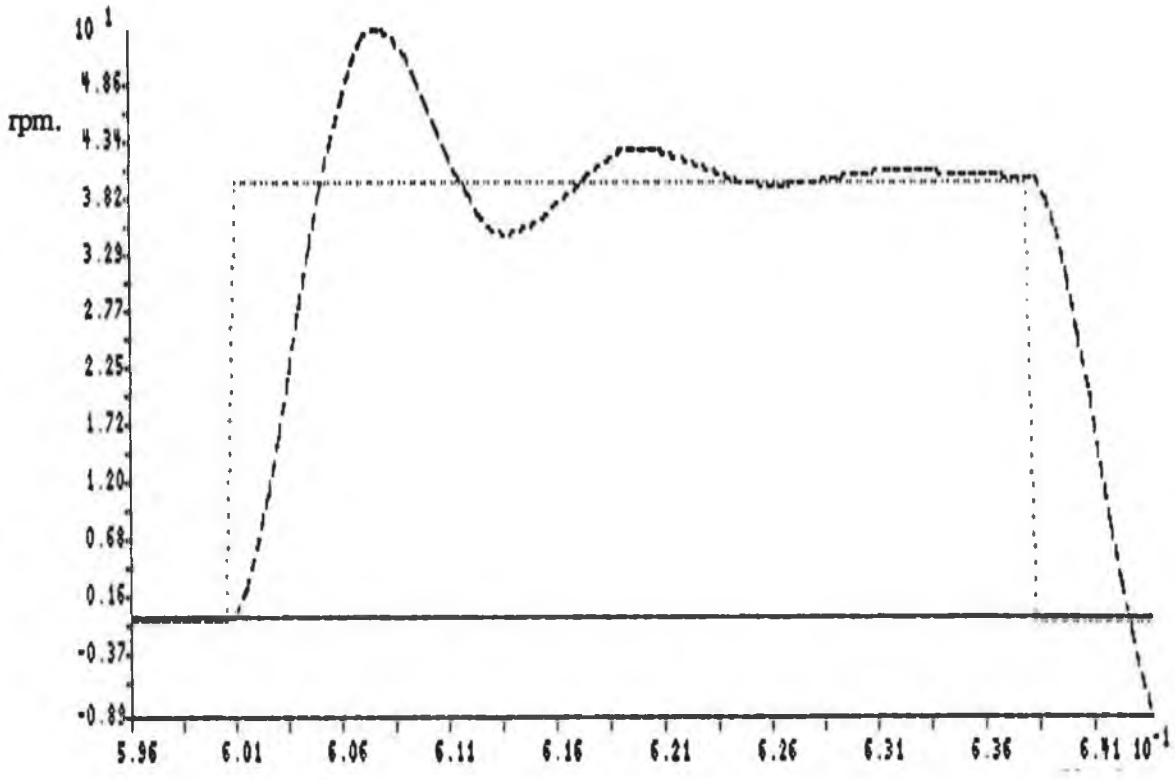

(4.1) Closed Loop Speed Response.

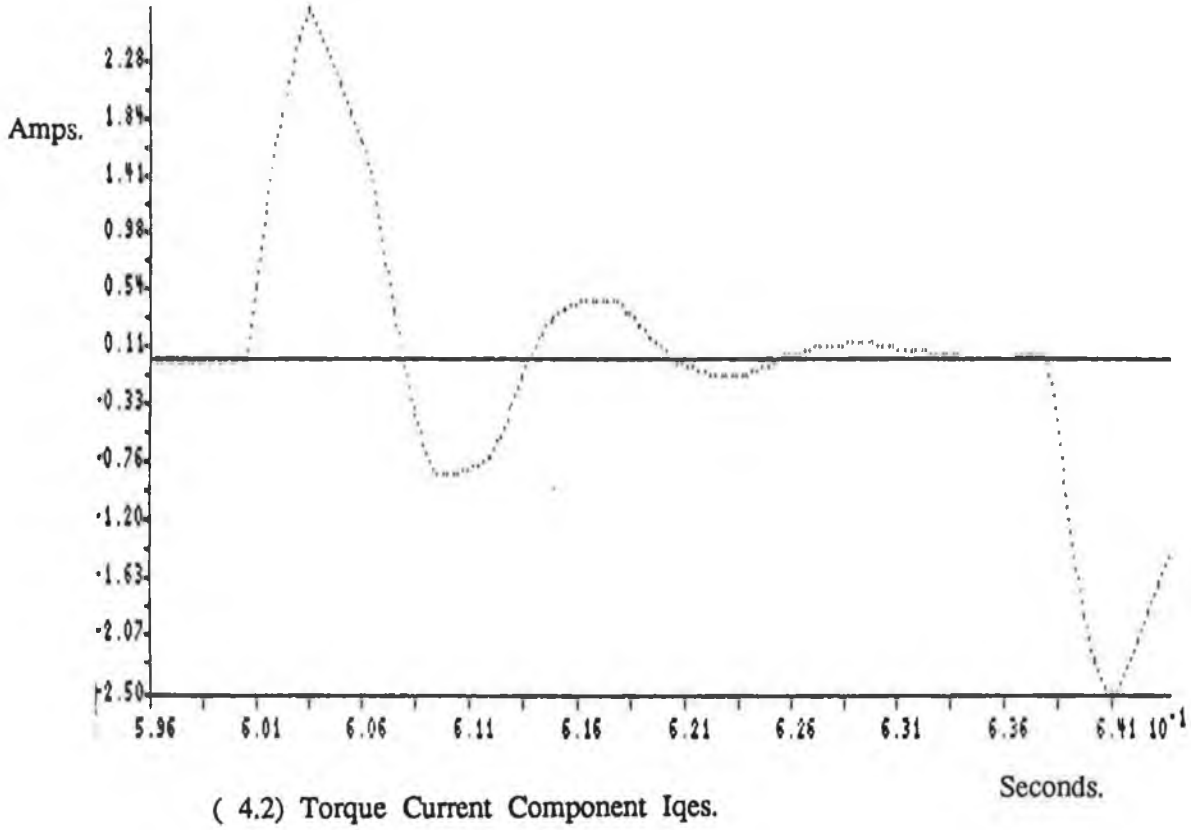

(4.2) Torque Current Component Iqes.

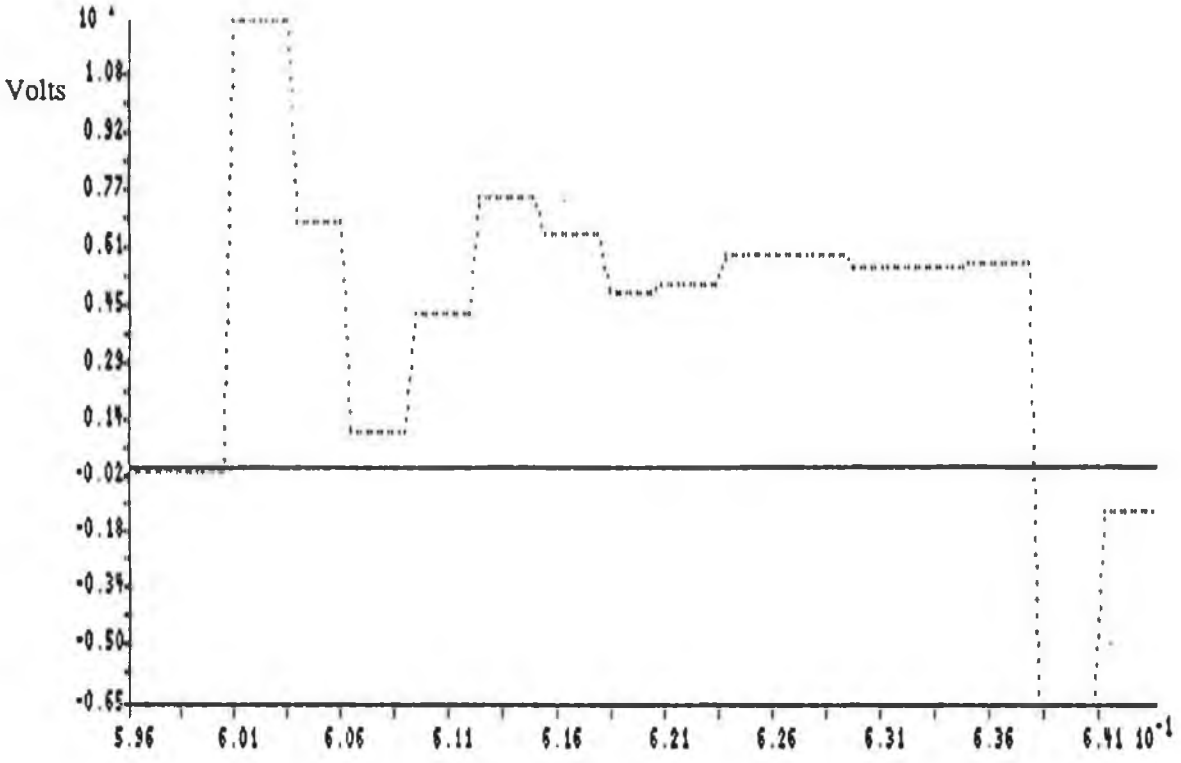

(4.3) $Vqes_{ref}$

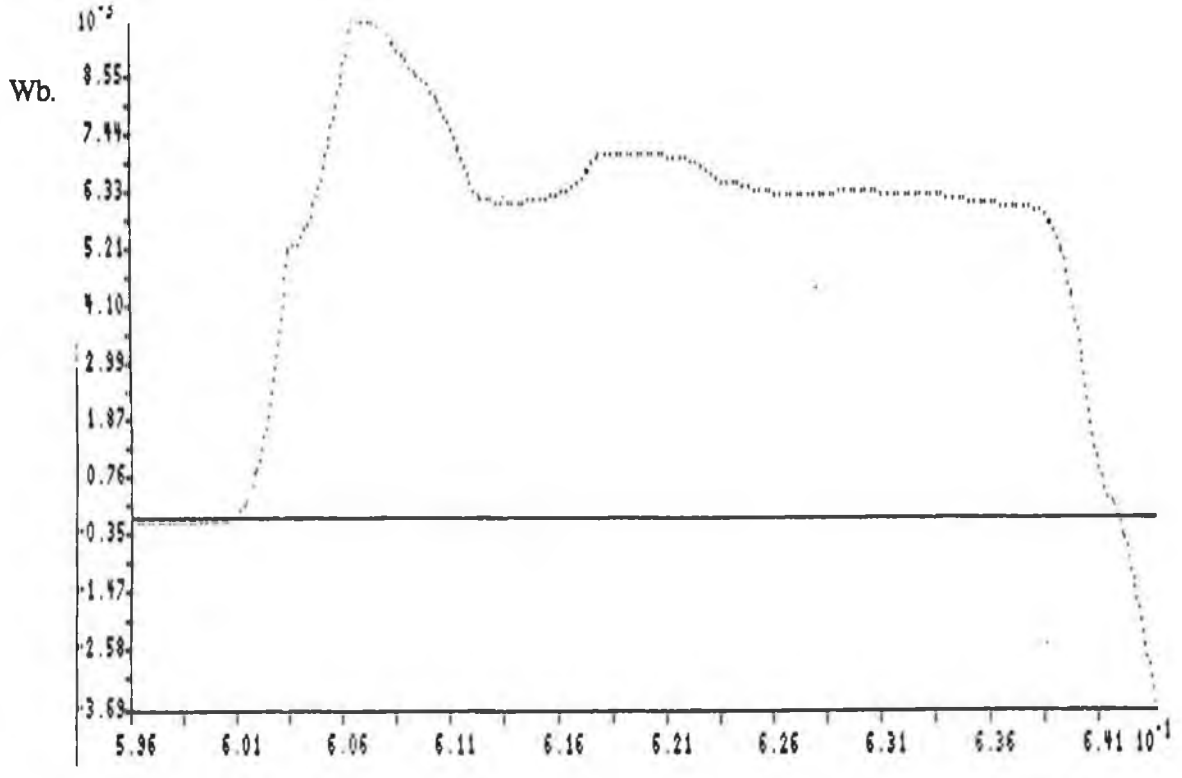

(4.4) Ψqer

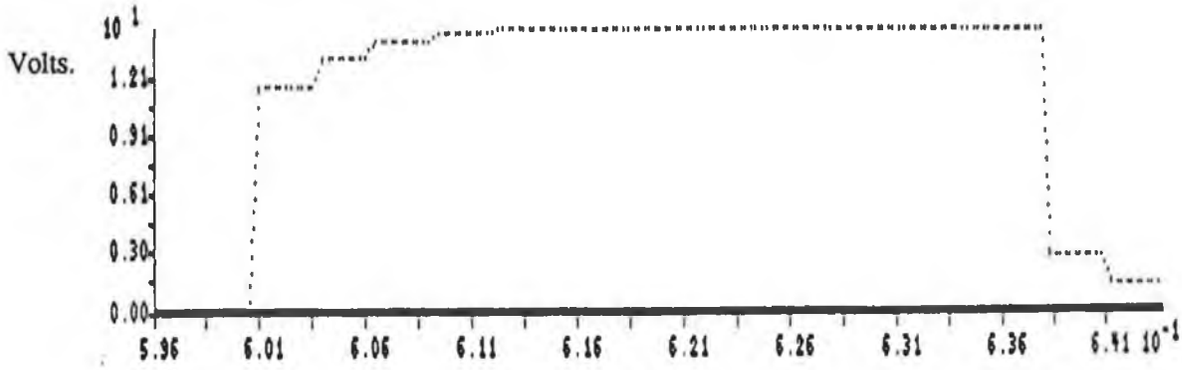

(4.5) $Vqes_{ref.}$ (Open Loop)

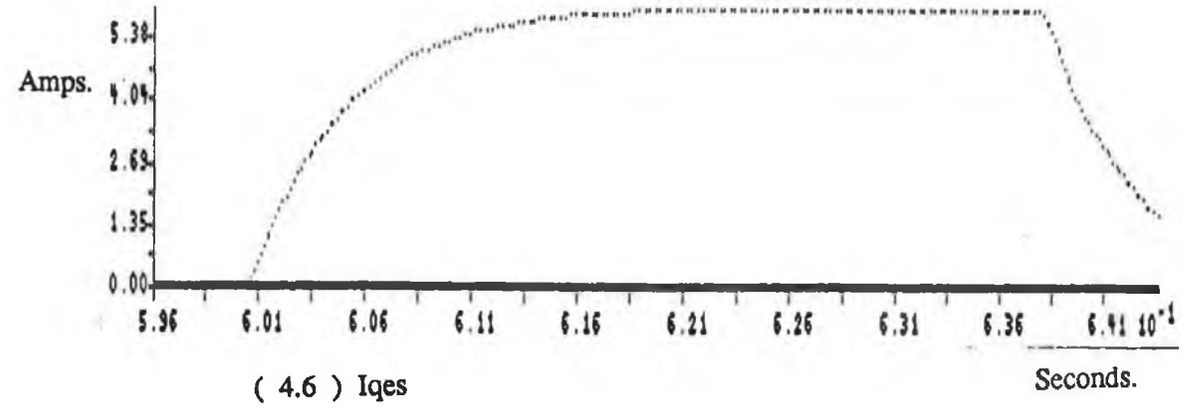

(4.6) Iqes

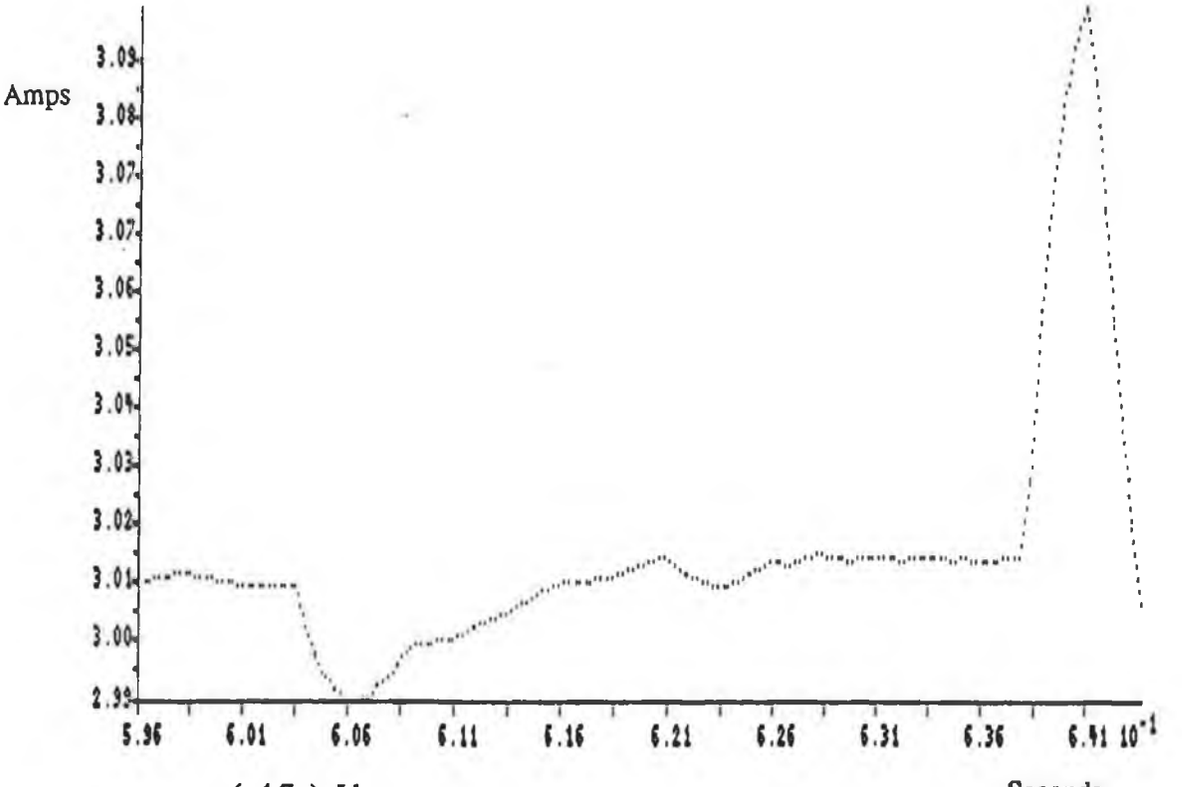

(4.7) Ides.

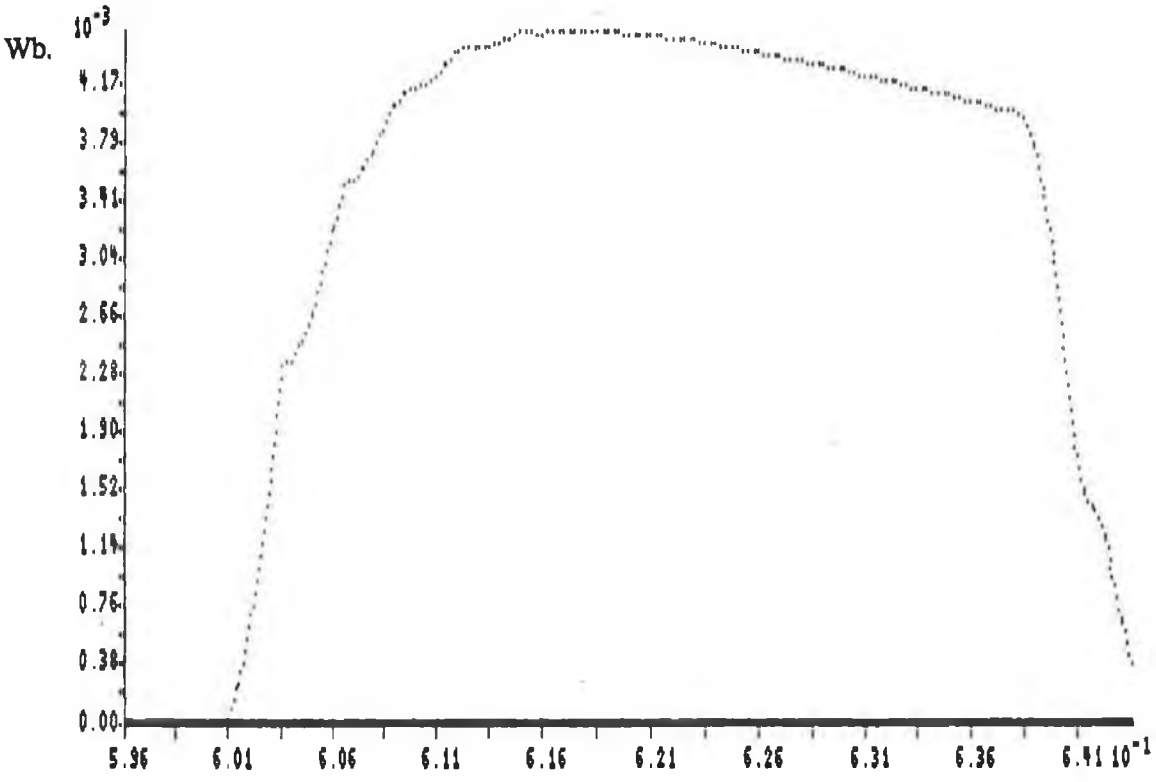

(4.8) Q - axis Rotor Flux Linkage. Ψqer. Seconds.

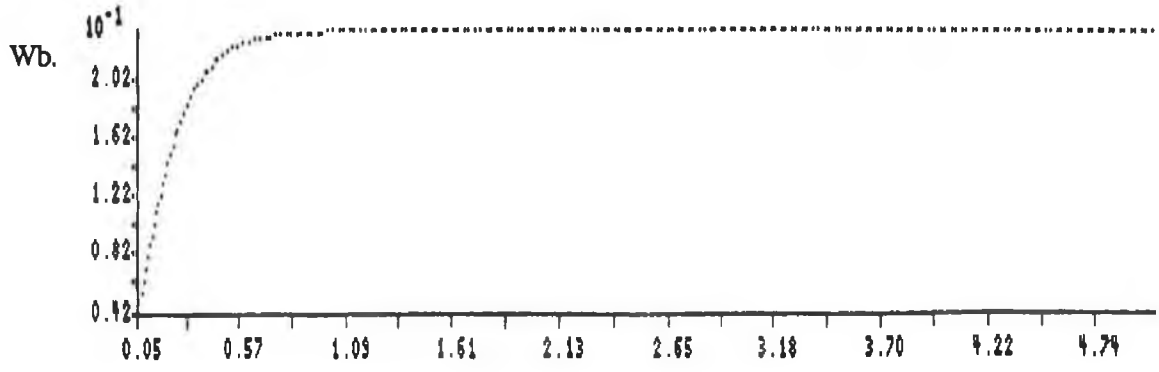

(4.9) Ψder.

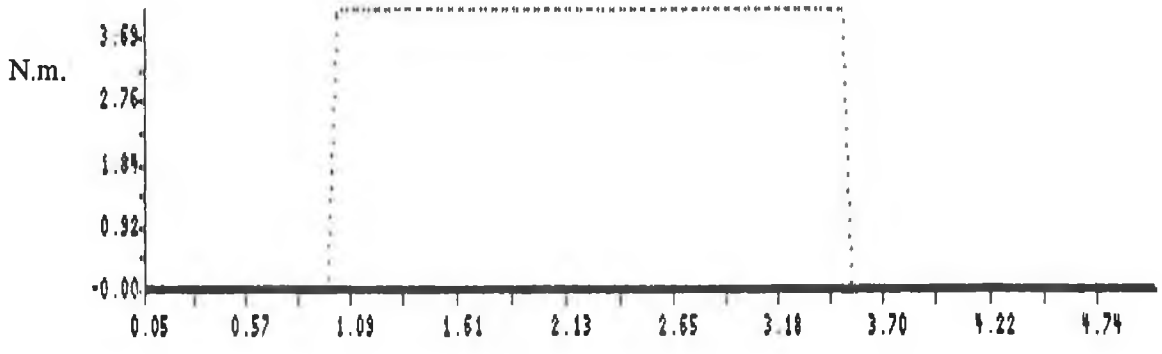

(4.10) Developed Torque, Te.

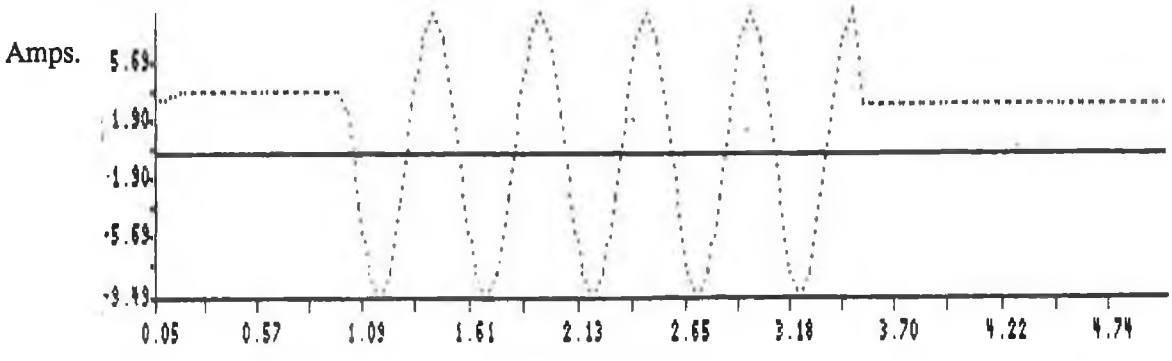

(4.11) Phase 1 Current, is_1

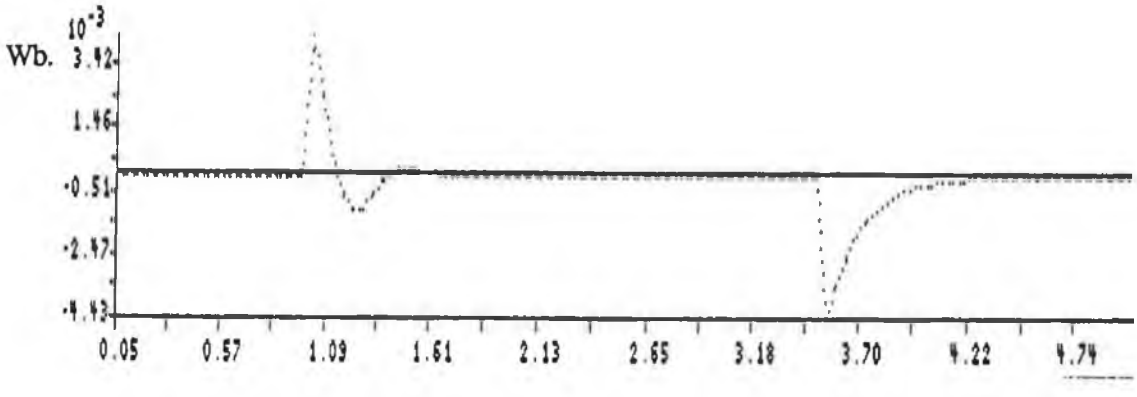

(4.12) Q - axis Flux. Ψqer

PERFORMANCE OF THE PROTOTYPE SERVO SYSTEM

5.1 Introduction

Results to show the overall performance of the prototype servo system are presented here. A brief description of the hardware and the operation of the Controller Algorithm is first given. Initially speed responses were to be measured and fly-wheels of various inertias were milled but satisfactory performance was not obtained so it was decided to begin by concentrating on achieving good, decoupled performance in each of the current loops. Oscillographs showing the operation of the current loops and motor stall torque responses are presented and discussed. Results taken to show Tr variation influences and P.W.M. amplifier distortion effects are analysed in subsequent chapters.

5.2 Hardware Description

An inexpensive 1.5 Kwatt, 3Φ squirrel cage TEFC induction motor, with rated speed at 1410 rpm and a rated power factor, cos γ_r, of 0.82 was used. The stator windings were of the simplest possible type, being single layer, lap wound concentric half coils. The stator was 36 slot whereas the rotor, a cast aluminium cage, had 28 skewed slots. The rotor inertia was calculated to be 0.035 $Nm.sec^2.rad^{-1}$.

The maximum torque rating was taken to be $\omega m_{rated} / P_{max}$ = 10.16 N.m. This was verified by taking the rated line current, changing base, transforming to 2Φ equivalent and using the torque equation.

Current sensing was done with commercially available isolated current sensors. Based on the principle of compensation of the magnetic field, these Hall Effect devices have a peak current rating of 80 amps and a bandwidth extending from DC to over 100 KHz. They were configured to produce a voltage corresponding volt for amp to the

current being measured.

For the power amplification stage a 6 Bipolar Power Transistor Inverter was used. Transistors were rated for 15 amps and had isolated base drives which were optically coupled to the PWM stage. The PWM was implemented by analog circuitry, the technique being double edged modulation with natural sampling, with a 4 kHz carrier. The modulation index was low, giving less higher harmonic heating effects but giving more distortion due to the transistor turn on delays.

A resolver and R-D converter were used to derive a velocity signal. Position information was not used. This analog signal was filtered with a 500 Hz low pass filter.

To measure stall torques dynamically, the rotor was locked with a bar of elastic steel, to which two active foil strain guages were attached. These were connected in Push-Pull arrangement in a bridge amplifier, the output of which was coupled through a 500 Hz low pass filter. The natural response of the bar, rotor arrangement was noted.

5.3 Controller Algorithm Implementation

Dedicated hardware for implementing a digital field oriented controller algorithm would be necessary to achieve high bandwidth performance but it was decided to use an IBM AT compatible which would be adequate for low bandwidth current loop control and investigation of adaptive control algorithms. This machine operates at 13 MHz and utilises an INTEL 80286 microprocessor. An 80287 Floating Point Arithmetic coprocessor was added, since to implement any Field Oriented Controller floating point or some extended form of integer arithmetic is required because of the wide range of constant values used in an algorithm. An analog / digital input / output card was added to the machine. The A / Ds were 12 bit and had a 12 μsec conversion time.

The original simulation controller was cross compiled using a standard "C" compiler. The assembly code was then "hand" optimised to produce a fast executable algorithm. The algorithm is similar to that used in the simulation except that two of the phase currents, the velocity signal and the desired velocity signal (or torque current command signal) are read in. Two of the phase voltage signals are output to analog circuitry which generates the reference values for the PWM stage. The conditions for slip frequency determination when the field is zero which were used in the simulation were not necessary since a certain amount of noise in the current measurements ensured a divide by zero never occurred. The algorithm for current control, incorporating flux calculation, slip frequency determination, field weakening, two PI controllers and transformations between rotating and stationary reference frames involves 34 floating point multiplications, 9 conditional comparison statements and takes 2.8×10^{-3} seconds to execute. Three multiplications are necessary for scaling while fourteen are required for the two phase / three phase transformations.

5.4 Performance Description and Evaluation

In the controller the gain of the flux loop was set at unity to make the system more robust to variations in the rotor time constant. Less integral action was used in the flux and torque current loops to make the system more stable. The controller exhibited stability problems when started with high line voltages so the bus voltage was increased gradually until the field was established. Further variations in the bus voltage during operation were compensated for by the flux controller. This stability problem at high voltage starts was possible due to the fact that the amounts of integral action in the PI controllers were not bounded. All the following results are taken with an inverter bus voltage of seventy volts.

Oscillograph (5.1) shows i_{s_1} and the corresponding torque demand. The field component of current, $ides_{ref}$ is set at 3 amps (corresponding to a phase current of

4.2 amps). The flux current loop is closed, whereas there is forward path control over the torque current. Software scaling means that $iqes_{ref}$ is varying from 4.44 to 12.7 amps. The rotor is locked so that the frequency of i_{s1} is actually the slip frequency or frequency of the rotor currents. The timescale is set at 1 sec cm^{-1} so that the steady state characteristics are shown. With each step increase in torque demand there is a smooth increase in both magnitude and slip frequency of the motor phase current. This is in accordance with that expected from the expression for steady state torque with the rotor locked, approximated by:

$$T_e = \frac{3\ U_S^2\ L_R}{w_0 L_S\ R_R}$$

The controller will try to maintain the ratio V_S/ω_0 constant to retain a constant field and so for torque to increase both Vs (and corresponding phase current magnitude) and the frequency must increase.

Oscillograph (5.2). Here $ides_{ref}$ = 3.0 amps as before to give a field flux linkage, Ψ_{der} = 0.24 Wb. A step increase 0 to 10 amps in $iqes_{ref}$ is commanded (Open Loop). VS_1 ref, the input to the PWM stage is shown with the corresponding measured phase current. The timescale is 10 milliseconds cm^{-1} so it is seen that the transient lag in the current is less than 1 millisecond indicating that there is good decoupling in the control of torque from flux.

Oscillograph (5.3). Shows i_{s1} and the torque demand signal from the signal generator. This is intended to show the lag between the change in motor phase current and the change in the reference signal to the controller. The timescale is 5 milliseconds/Div so the lag is 5.2 milliseconds. 2.7 milliseconds of this lag is accounted for by the controller execution time. The remaining 2.5 milliseconds is caused by delays in the PWM stage (small) and the fact that the demand rising edge

will have occurred a random amount of time before a controller read in, since the signals are not synchronised. However the smooth transition in the phase current occurs less than two controller time intervals after the demand.

Oscillograph (5.4). $ides_{ref}$ = 3 amps. A step change in torque ($iqes_{ref}$ 0, 10 amps) is commanded. is_1 (top trace) is shown with Vs_1 ref, the controller output. The timescale is 10 milliseconds/Div so it is seen that the lag between phase voltage and resulting phase current is small, overall leakage inductance is responsible for some of this lag.

Oscillograph (5.5). The torque demand signal and the actual torque as measured by the strain gauge arrangement are shown. (5.11) shows the natural response of the bar. The timescale is set at 10 milliseconds/Div. After 5 milliseconds the actual torque developed begins to increase and achieves a steady state value after 30 milliseconds.

Oscillograph (5.6). V_{s2ref} and i_{s2} are shown for the above torque demand. The timescale is set at 5 milliseconds/Div. The fast current response can be clearly seen.

Oscillograph (5.7). Shows i_{s1} in steady state for $iqes_{ref}$ demands changing in squarewave fashion from 0 to 12.7 amps. The timescale is at 500 msec/Div. During intervals of zero torque demand a DC current is seen to flow. This current is DC to establish a field in the stalled motor. Its magnitude should be between ±4.27 amps corresponding to $ides_{ref}$ at 3 amps transformed to 3 phase. Its level in any particular winding at any time depends on the instant at which a rotating stator MMF (torque demand) was interruped. Again there is a smooth and never very large transition in the current waveform. The simulation outputs shown show a torque demand with the predicted waveform for i_{s1}. It matches the waveform obtained almost perfectly except for glitches at the zero crossing points and 60° intervals due to cross over delay effects in the PWM section.

Oscillograph (5.8). Here $ides_{ref}$ = 3.0 amps. A ramp increase in $iqes_{ref}$ 0 → 12.7 amps is commanded. i_{s_1} is shown. Since the motor is stalled this is at slip frequency. As $iqes_{ref}$ increases both the magnitude and frequency of is_1 increase. The timescale is set at 500 milliseconds/Div. This result is exactly as expected from the analysis given with oscillograph (5.1). Plots (5.3) and (5.4) show the simulated ramp increase in torque and the corresponding i_{s_1} waveform. The fact that the magnitude and frequency increase linearly indicates that the field remains constant. Note the larger cross over delays at the lower frequencies. This means that at this time the actual fundamental is of lower magnitude. This explains why there is a more pronounced rise in amplitude as $iqes_{ref}$ increases in the simulation plots.

Oscillograph (5.9). Shows a step increase in the torque demand, $iqes_{ref}$ and the measured torque. The steady state characteristics of the developed state torques are to be seen. The timescale is 500 milliseconds/Div. $Iqes_{ref}$ is changed from 0 → 12.7 amps. Significant glitches are to be seen in the torque response but very fast rise and fall times have been achieved (the natural response of the bar (5.11) must be subtracted from the torque response).

Oscillograph (5.10). Shows i_{s_1} with the measured torque. The conditions are the same as those in Oscillograph (5.9). The magnitude and frequency of i_{s_1} stays constant, indicating stable operation and constant field. The glitches in the torque can clearly be seen to be a result of the distortions in the current waveform. Glitches in the current waveform occur at the zero crossings, and at 60° intervals, due to the interaction of the other two phases. With each glitch there is a corresponding change of slope in the measured torque. These glitches in the torque are very significant with open loop control over torque and are approximately 30% of the commanded torque. More studies of this effect are detailed in chapter 7.

Oscillograph (5.11). Shows the natural response of the bar-rotor torque measurement system. Timescale = 500 milliseconds/Div. The rotor was twisted to a torque

approximately equal to 10 Nm and suddenly released. This response can be qualitatively compared with the responses in (5.10) and (5.9) to see that the actual developed torque has very little overshoot or undershoot.

5.5 Conclusions

The hardware was found to be working very satisfactorily, giving good decoupled control over both flux and torque components of current. Any open loop torque commanded was achieved accurately within two sample periods. When no torque was commanded, DC field currents flowed which were exactly equal to $ides_{ref}$ when transformed to rotating two phase. The magnitudes and slip frequencies of the stator currents varied as expected for changing stall torque demands while holding the field flux demand constant. The phase current followed the phase voltage with very little lag (circa 2 msec) indicating good decoupled control of torque from field.

The measured torque lagged the demanded torque by about 30 msec. This was due, however, to the dynamics of the bar-rotor shaft arrangement. When the natural response of the bar was taken, a fall time of approximately 30 msecs was measured for a step change from 10 to 0 Nm.

Actual waveforms for phase current for changing torque demands followed the simulation waveforms almost perfectly. In the current waveforms, distortion effects were observed at 60° intervals, these being most significant at the zero crossing points. These delays were seen to be most significant at lower frequencies (circa 0.5 Hz), corresponding to lower torque demands.

This distortion effect in the current waveforms was observed here to have two main effects. It accounted for the current waveform having a higher amplitude at lower torque demands than those predicted (c.f. oscillograph (5.8), plots(5.3), (5.4). It also

accounted for substantial glitches in the torque developed by forward path (open loop) control.

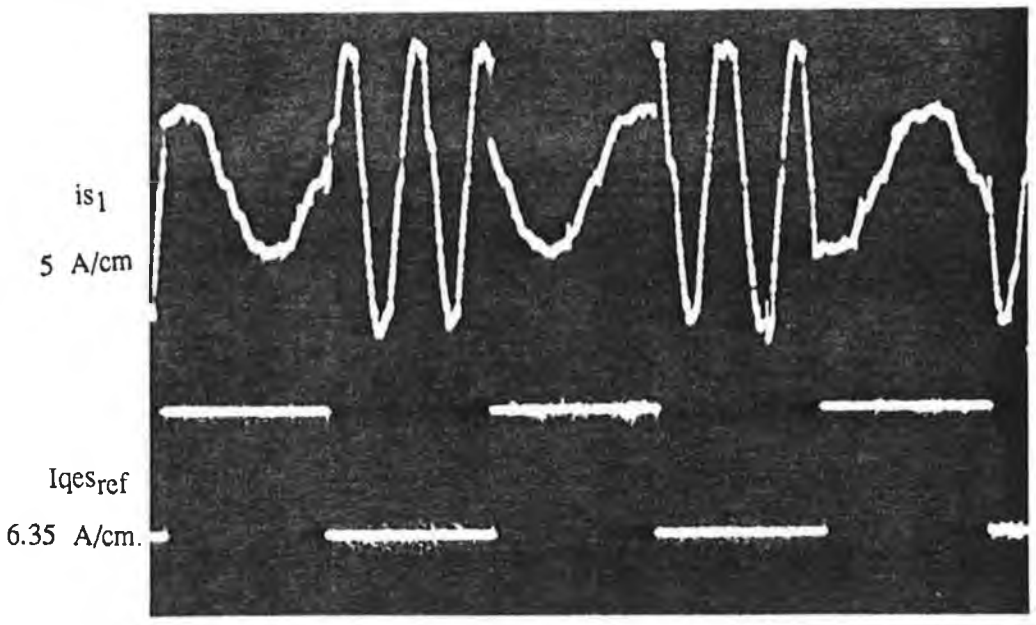

Oscillograph 5.1. 1 sec./div.

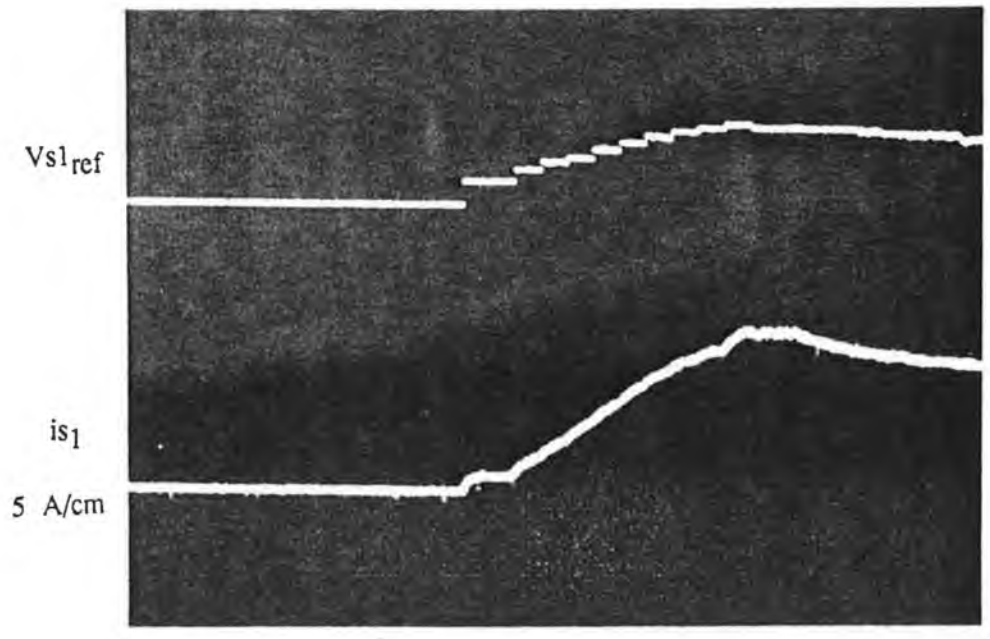

Oscillograph 5.2. 10 millisec./div.

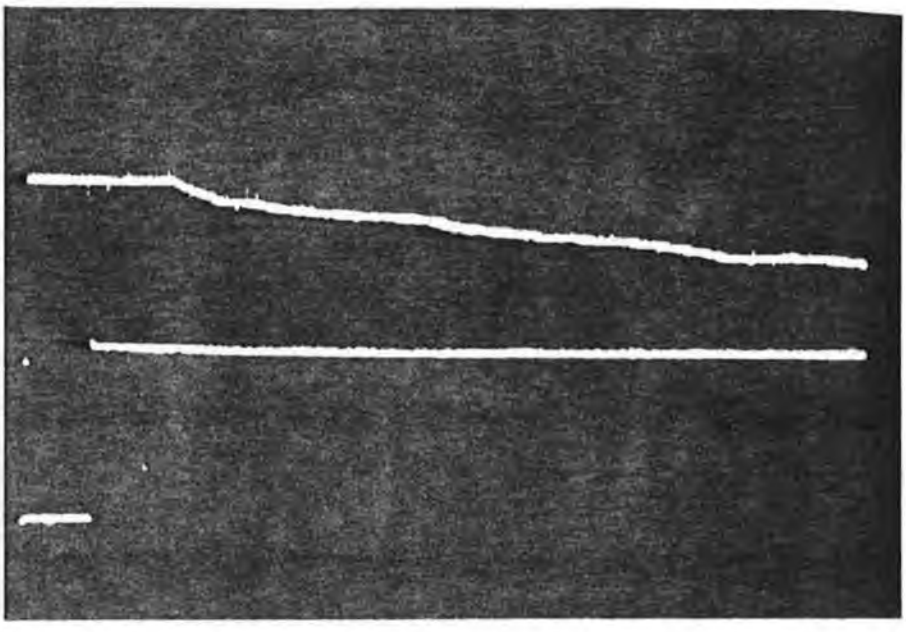

Oscillograph 5.3. 5 millisec./div.

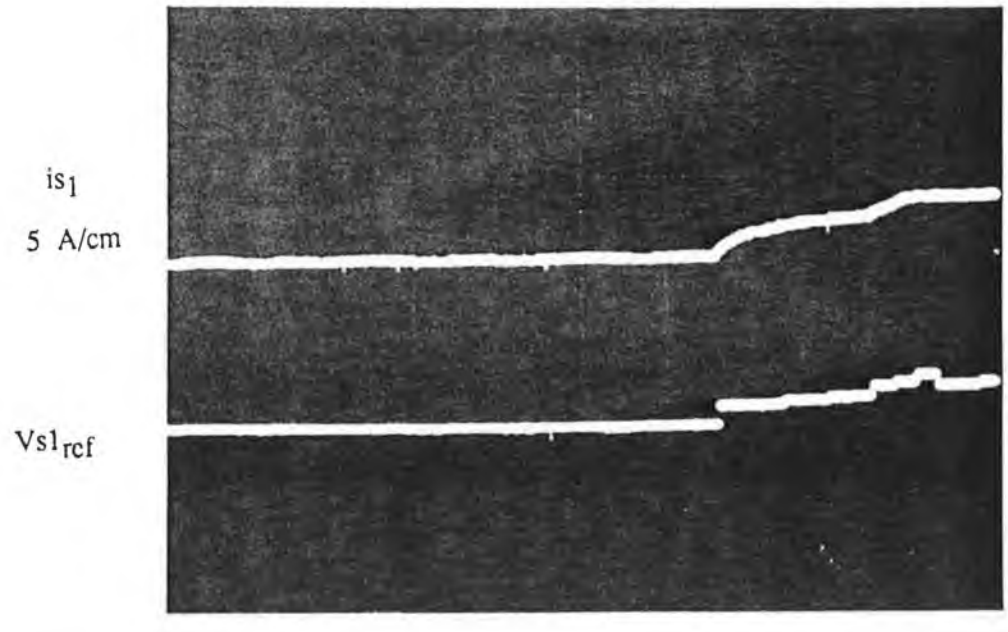

Oscillograph 5.4. 10 millisec./div.

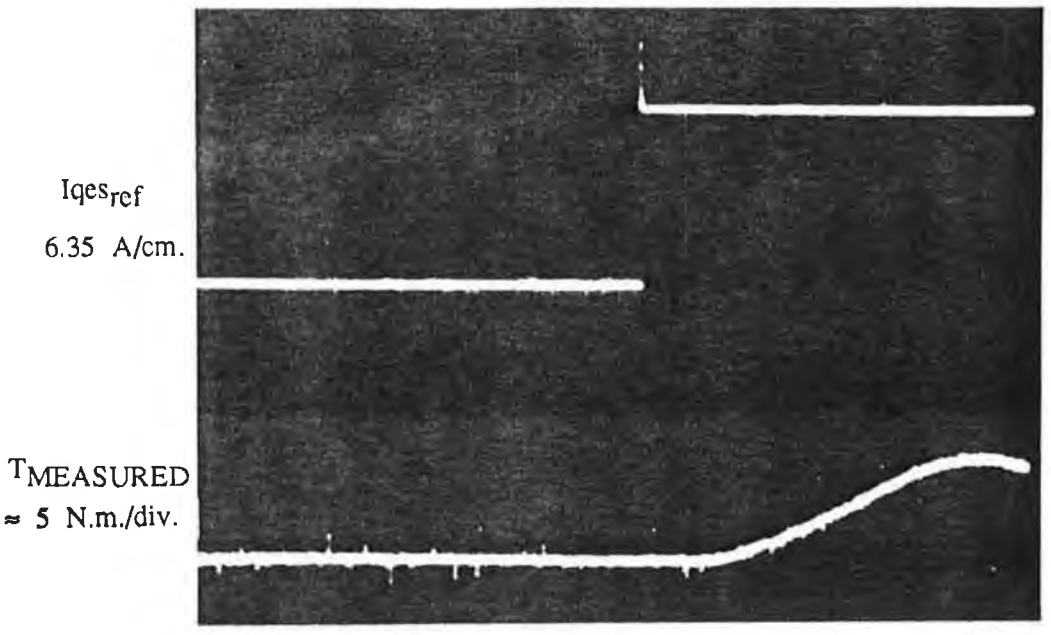

Oscillograph 5.5. 10 millisec./div.

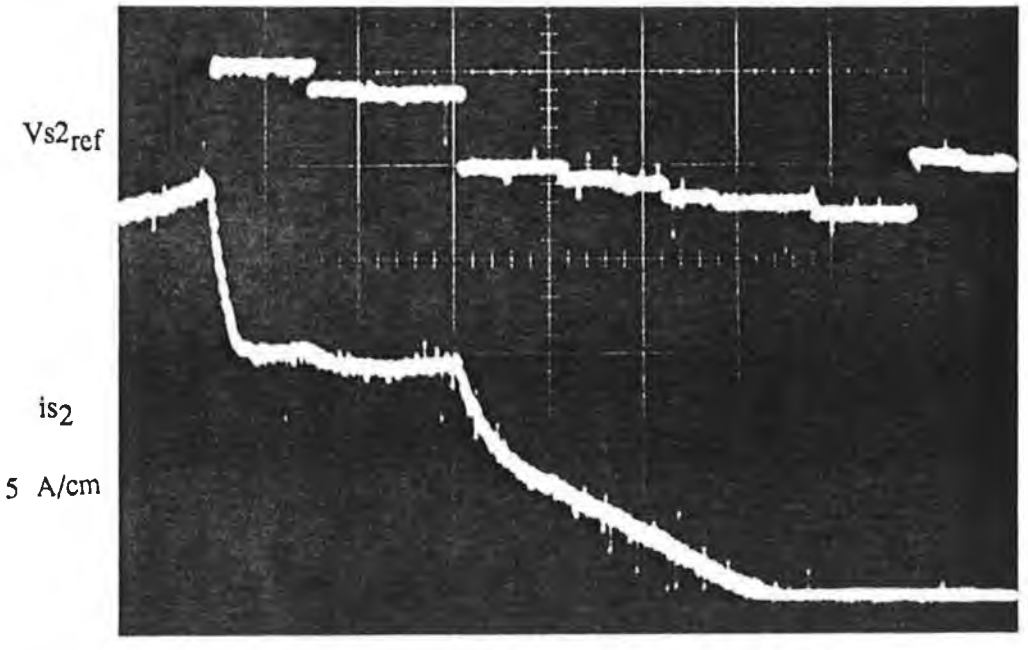

Oscillograph 5.6. 5 millisec./div.

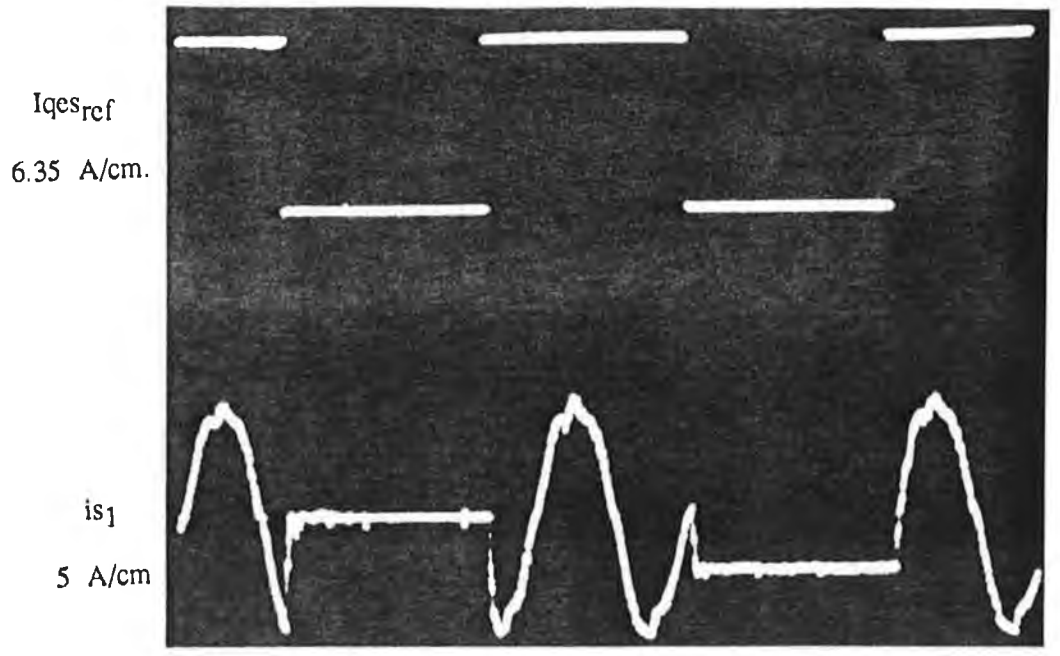

Oscillograph 5.7. 500 millisec./div.

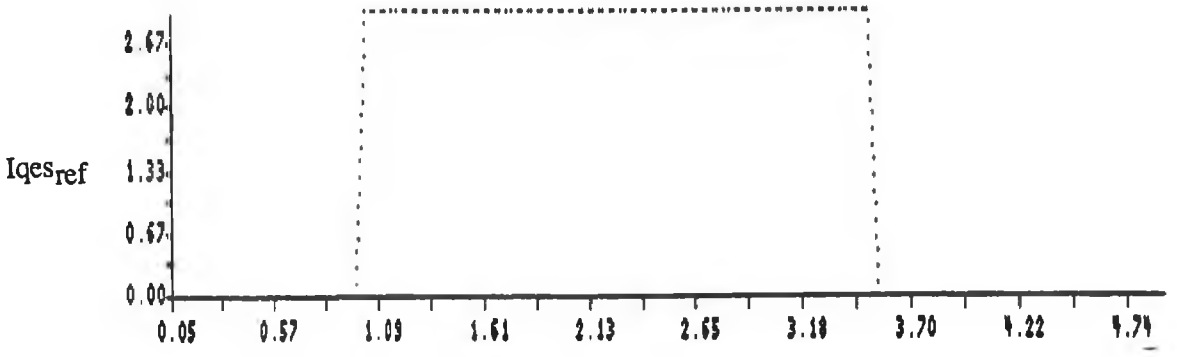

Plot 5.1.

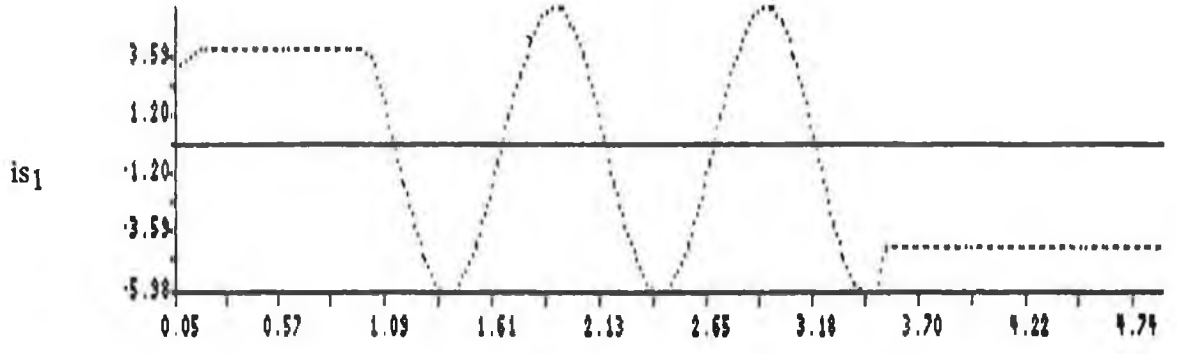

Plot 5.2.

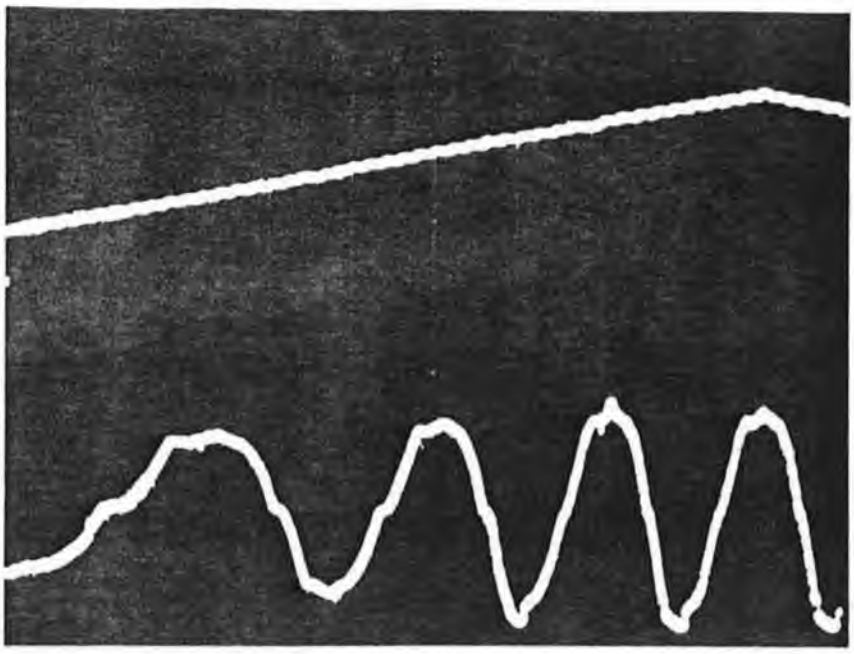

Oscillograph 5.8. 500 millisec./div.

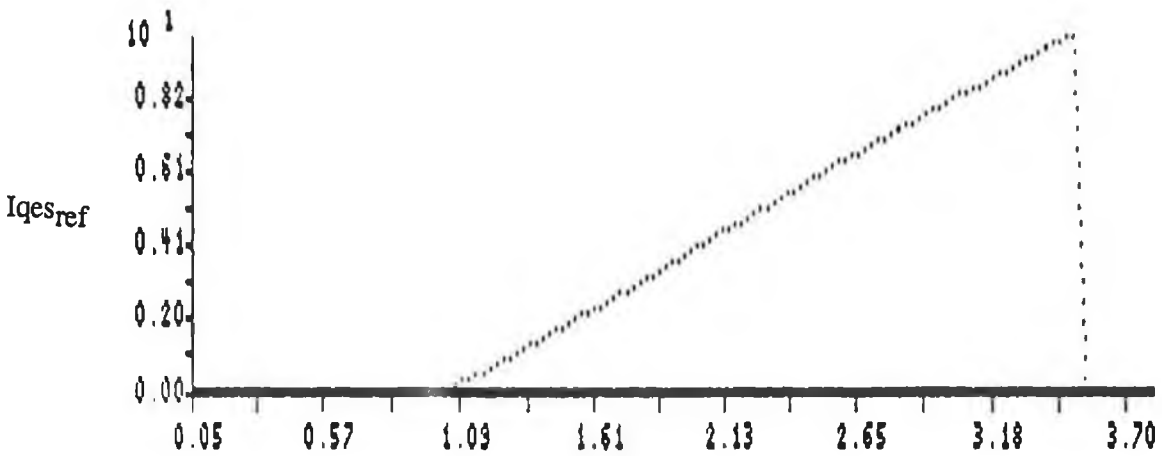

Plot 5.3.

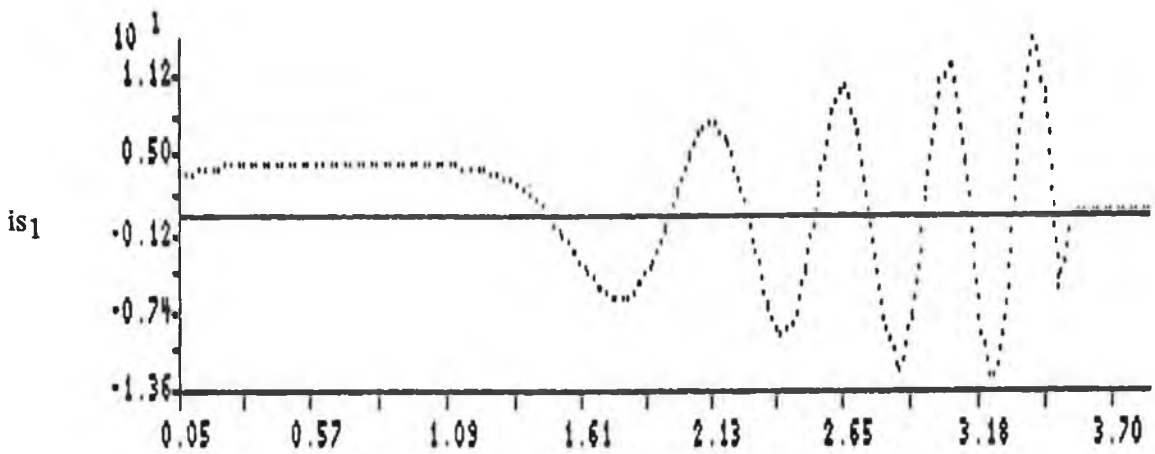

Plot 5.4.

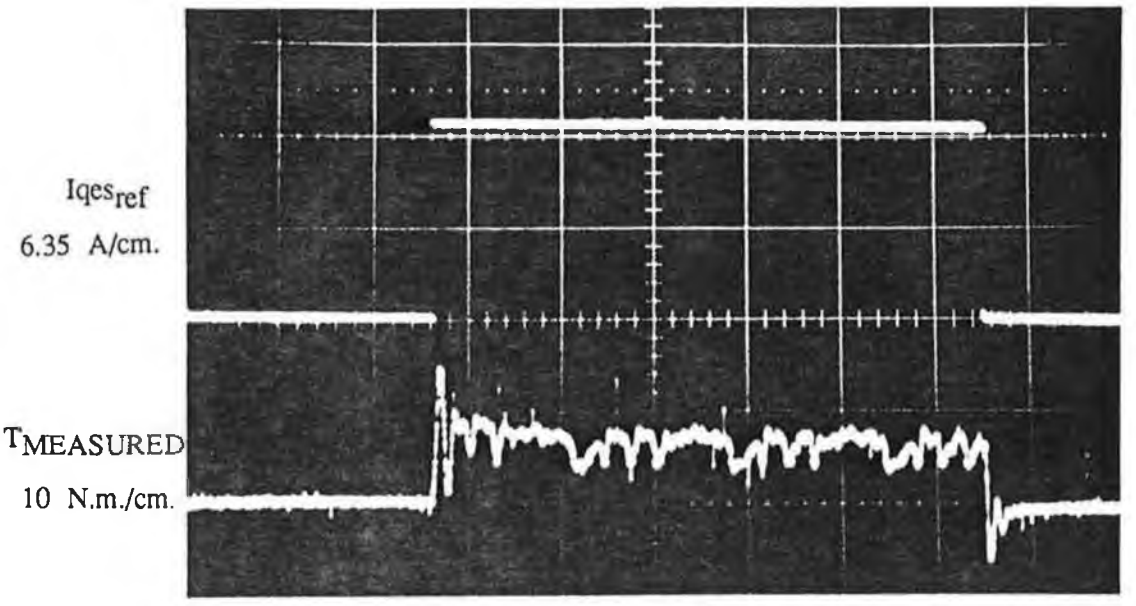

Oscillograph 5.9. 500 millisec./div.

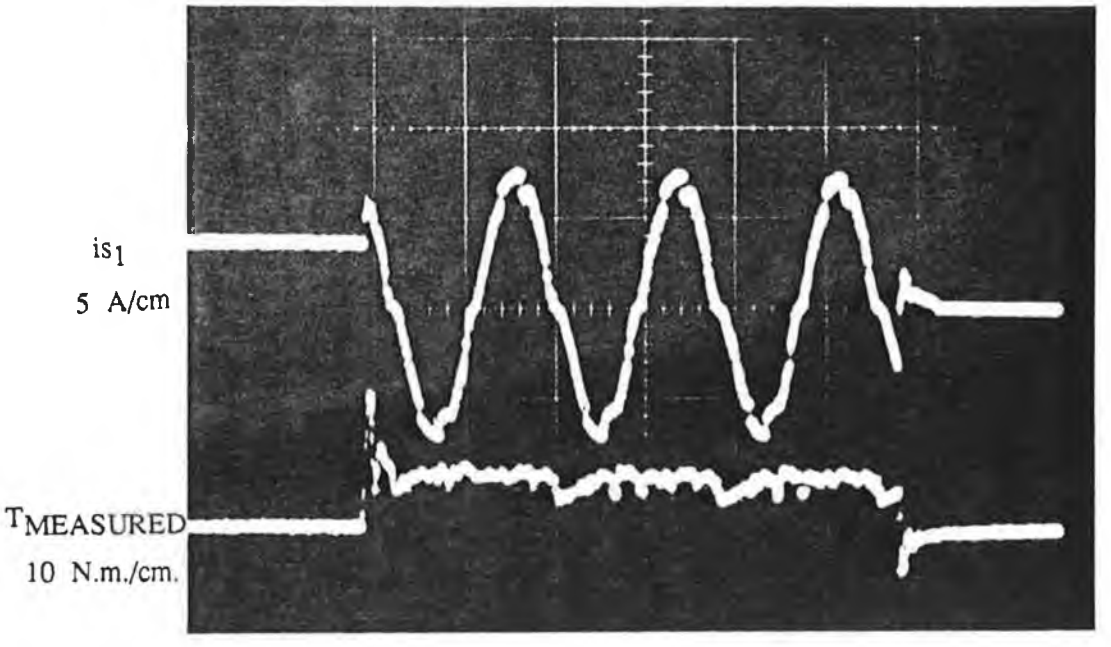

Oscillograph 5.10. 500 millisec./div.

Natural Response.

10 N.m./div.

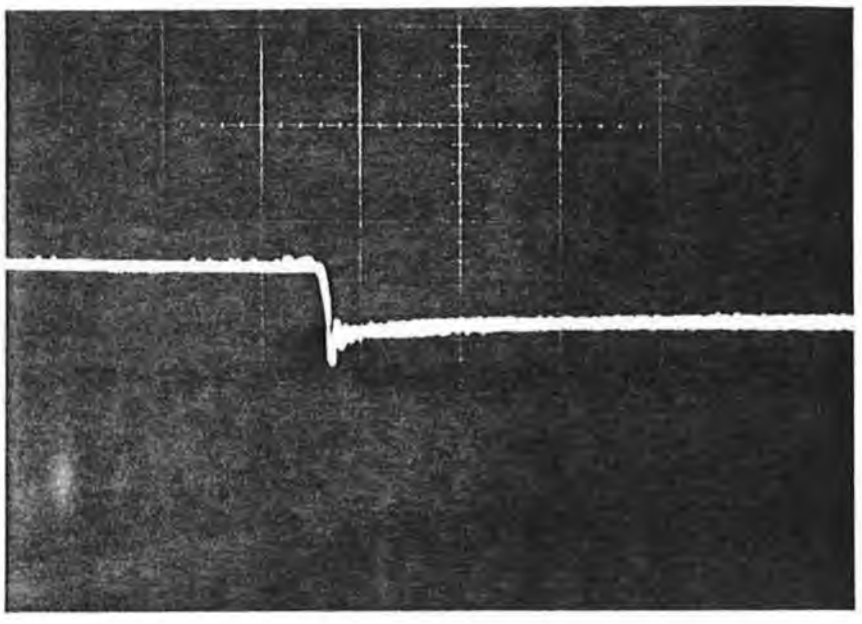

Oscillograph 5.11. 500 millisec./div.

EXPERIMENTAL AND THEORETICAL ANALYSIS OF ROTOR TIME CONSTANT VARIATION EFFECTS.

6.1 Introduction

To achieve accurate, decoupled control over both field flux and torque with the field oriented control strategy, an accurate estimate or measurement of both angle and magnitude of either the rotor flux vector or the air-gap flux vector is needed. For good servo performance the vector must be known at speeds ranging from far into the field weakening region right down to zero speed. Direct flux measurement schemes involve the use of either delicate sensing coils or temperature dependent Hall Effect devices and so are usually not feasible. Alternatively for any estimation scheme the problem is the identification of the rotor time constant, Tr, a parameter which varies widely (± 50% of a nominal value). Tr varies slowly with temperature due to variation in Rr and dynamically with variations in Lr caused by magnetic saturation, (especially with operation in the field weakening region). A difference between the controller time constant value and the actual time constant value will result in dynamic oscillations in the output torque and steady-state under or over excitation of the machine. The degree to which these effects will occur, is largely dependent on the specific controller design.

The problem of Tr variation has been regarded as the major obstacle to achieving high performance field oriented controllers for low speed and position control applications. Consequently, a variety of flux vector estimation schemes, involving techniques such as model reference adaption have been proposed, with a view to designing controllers more robust to parameter variations. No general consensus, however, as to the best flux vector estimation method has yet been achieved. Estimation techniques are briefly reviewed in the next section.

Several studies on the sensitivities of particular control schemes to variations in the

rotor time constant have arrived at expressions relating error in output torque to error in the time constant parameter but again these equations vary widely. Some of these equations, giving both steady state and dynamic torque errors are presented. Expressions relating the steady state errors in the d and q rotor flux linkages derived as part of this work are also presented.

In the remainder of this section the effects of rotor resistance variations on the field oriented controller for the voltage source inverter fed motor are investigated. Steady state and dynamic effects are qualitatively examined by simulation, and these results are verified by varying the controller time constant value in actual prototype servo systems and observing the changes in the developed torque.

It was thought that off-line identification of the time constant could be empirically achieved by varying the controller time constant until the smallest lag between a phase current and the corresponding phase voltage occurred. The least amount of lag between phase current and phase voltage for a change in demanded torque would indicate good decoupling of the torque producing current component from the field component. Investigation of this idea was conducted experimentally and by use of the simulations.

6.2 Analysis of Rotor Time Constant Variation Effects.

Many papers concerning controller design discuss the relative sensitivities of I-type and V-type control methods to parameter variation of the secondary resistance. Harashima et al., [14], presents an argument based on the steady state operation of each controller type to show that V-type control is less sensitive to secondary resistance variation than I-type control, when these methods are used with closed loop speed controllers. With constant current control a change in the secondary resistance will result in a change in the secondary current but this will be accompanied by a corresponding change, of the opposite sense, in the magnetising component of current. There will therefore be no change in output torque so that the speed controller will not command a change in i_{qes}, giving no change in the slip frequency so that the actual slip frequency will differ from the required slip frequency. With V-type control a change in the secondary resistance will not cause a change in the magnetising current thereby causing a change in the developed torque and so the speed controller will cause a change in $iqes_{ref.}$ The actual slip frequency will therefore follow the required slip frequency.

Verghese et al., [21], focuses attention on observers for flux estimation in Induction machines. Both Full and Reduced Order Observers with correction for the prediction error are treated. In dealing with Observers based on the rotor circuit he first looks at the errors associated with real time simulation (open loop estimation schemes), the subject of this chapter. The real time simulation estimation scheme for rotor flux is given as

$$\underline{\Psi r}_{ref}' = \left[\left[-\frac{1}{Tr} \right] I + \omega J \right] \underline{\Psi r}_{ref} + \left[\frac{1}{Tr} \right] M \underline{i_s}$$

..... (6.1.)

Where ω is the rotor speed (slip speed)
I is the identity matrix

$$J = \begin{bmatrix} 0 & -1 \\ 1 & 0 \end{bmatrix}$$

By defining the error as $\underline{\Psi r}_{ref} - \underline{\Psi r}$, the following state space equation governing the error dynamics is presented:

$$\underline{\varepsilon}' = \left[\left[-\frac{1}{Tr} \right] I + \omega J \right] \underline{\varepsilon}$$

..... (6.2.)

Each scalar component of **e** displays an oscillation at frequency, ω, that is damped with a time constant equal to the rotor time constant.

Ohnishi et al., [13] describes a Model Reference Adaptive System against rotor resistance variation. Again an analysis, using steady state models and neglecting leakage effects, is done to determine the sensitivities of both I type and V-type control schemes to variations in the rotor resistance. Again it is concluded that with V-type control the flux level will remain constant:

$$| I_m |^2 = \frac{R_{Rref}\, T_e}{3\, M^2\, w_{slipo}}$$

..... (6.3.)

w_{slipo} is the slip frequency that would occur if the controller time constant were to equal the actual time constant value. In the case of the controlled current source the total motor torque is derived to be

$$T_e = \frac{3\, Rr_{ref}\, Rr\, M\, i_{deso}\, i_{qeso}}{Rr_{ref}^2\, i_{qeso}^2 + Rr^2\, i_{deso}^2} \left[i_{deso}^2 + i_{qeso}^2 \right]$$

..... (6.4.)

The subscript $_o$ indicates the value which would occur with nominal Rr.

i_{qes} is given as an extremely complicated function of rotor resistance errors and values of stator currents which should occur.

Krishnan et al., [22], derive analytic expressions to evaluate the effects due to parameter sensitivity in a vector controlled induction motor drive. Parameter sensitivity effects on the response of the electromagnetic torque of the Induction motor drive with the speed loop open are investigated in depth. Analysis of effects on the Closed Loop speed controlled motor is confined to the steady-state. In open loop mode the command value for torque is written as a function of stator current magnitude and the torque angle to give:

$$Te^* = \frac{1}{Kit} \frac{Lm^{*2}}{Lr^*} i_s^{*2} \cos\theta^* \sin\theta^*$$

..... (6.5.)

θ is the angle between field and torque producing components of the stator current vector.

Asterisks refer to nominal or command values.

The actual electromagnetic torque is given to be:

$$T_e = \frac{1}{Kit} \frac{Lm^2}{Lr} i_s^2 \sin\theta \cos\theta$$

..... (6.6.)

These expresssions are combined subject to the following assumptions to give the ratio of actual torque to the commanded value of torque.

$$w_{sl}^* = w_{sl}.$$

$$i_s^* = i_s.$$

$$\frac{Te}{Te^*} = \left[\frac{Lm}{Lm^*}\right]^2 \left[\frac{Lr^*}{Lr}\right] \left[\frac{Tr}{Tr^*}\right] \left[\frac{1 + [\, w_{sl}{}^* Tr^* \,]^2}{1 + [\, w_{sl}{}^* Tr \,]^2}\right]$$

..... (6.7.)

Separate expressions are derived for errors in torque caused by rotor resistance errors due to temperature variation and for errors in the magnetising inductance caused by saturation. For a rotor resistance error the ratio of the torque to its command value is expressed as:

$$\frac{Te}{Te^*} = \left[\frac{1 + [\, w_{sl}{}^* Tr^* \,]^2}{1 + [\, \alpha\, w_{sl}{}^* Tr^* \,]^2}\right]$$

..... (6.8.)

with:

$$Tr = \alpha\, Tr^*$$

It is quoted that typically, $0.5 \lesssim \alpha \lesssim 1.5$. The error in d-axis rotor flux linkage is given as:

$$\frac{\Psi r}{\Psi r^*} = \frac{1 + [\, w_{sl}{}^* Tr^* \,]^2}{1 + [\, \alpha\, w_{sl}{}^* Tr^* \,]^2}$$

..... (6.9.)

Typical flux and torque error plots are given. In analysing transient characteristics it is given that the flux and torque have a time constant equal to the rotor time constant and a natural frequency of oscillation with a value equal to the slip speed.

Garcés, [23], develops a closed loop parameter adaption scheme by means of an identification function. In analysing the parameter influence a set of differential equations for the error functions $\Delta\Psi_{2x}$ and $\Delta\Psi_{2y}$ are written. The error systems damping factor and frequency are derived and steady state errors for a given value of slip frequency are presented:

$$\lim_{t \to \infty} \Delta \Psi_{qer} = \frac{\Delta Tr}{Tr} \Psi der_{ref} \frac{w_{sl} Tr}{1 + [w_{sl} Tr]^2} \quad \ldots\ldots (6.10.)$$

$$\lim_{t \to \infty} \Delta \Psi_{der} = \frac{-\Delta Tr}{Tr} \Psi der_{ref} \frac{[w_{sl} Tr]^2}{1 + [w_{sl} Tr]^2} \quad \ldots\ldots (6.12.)$$

These give a steady state error in the torque:

$$\lim_{t \to \infty} Te = \frac{\Psi der_{ref}^2}{Lr} [w_{sl} Tr] \frac{1 + [w_{sl} Tr_{ref}]^2}{1 + [w_{sl} Tr]^2} \quad \ldots\ldots (6.12.)$$

Sugimoto et al., [20], describes an algorithm based on Model Reference Adaptive System theory for on-line identification of the rotor time constant. To justify the motivation for this adaption scheme expressions are derived for the d-axis rotor flux and the open loop torque step response as functions of the error in the rotor resistance, a parameter which is quoted as typically varying, due to temperature changes, by ±25% of a nominal value.

$$\Psi_{der} = \frac{M\, i_{des} \left| 1 - \frac{Rr^*}{Rr} \right| \frac{Rr^*\, i_{qes}^2}{Rr\, i_{des}^2}}{1 + \left| \frac{Rr^*\, i_{qes}}{Rr\, i_{des}} \right|^2} \times h(t) + M\, i_{des} \qquad \ldots\ldots (6.13.)$$

$$\Psi_{qer} = \frac{M\, i_{qes} \left| \frac{1 - Rr^*}{Rr} \right|}{\left| 1 + \frac{Rr^*\, i_{qes}}{Rr\, i_{des}} \right|^2} \times h(t) \qquad \ldots\ldots (6.14.)$$

Where:

$$h(t) =$$

$$1 - e^{-\left[\frac{Rr}{Lr}\right]t} \left| 1 + \left| \frac{Rr\, i_{des}}{Rr^*\, i_{qes}} \right|^2 \right|^{\frac{1}{2}} \sin\left| \frac{Rr^*\, i_{qes}}{Lr\, i_{des}} t + \tan^{-1} \frac{Rr^*\, i_{qes}}{Rr\, i_{des}} \right|$$

and

$$Te = \frac{\frac{M^2 i_{des} i_{qes}}{Lr} \left| 1 - \frac{Rr^*}{Rr} \right| \left| \frac{Rr^* i_{qes}^2}{Rr i_{des}^2} - 1 \right|}{1 + \left| \frac{Rr^* i_{qes}}{Rr i_{des}} \right|^2 \times h(t) + \left| \frac{M^2 i_{des} i_{qes}}{Lr} \right|}$$

..... (6.15.)

These equations indicate that Ψder and T_e have transients which oscillate with the controller value for slip frequency and which decay exponentially subject to the actual rotor time constant when Rr_{ref} (Rr*) differs from the actual rotor resistance.

Matsuo et al, [24], developed a rotor parameter identification technique which involves injecting a negative sequence current perturbation signal and sensing the corresponding negative sequence voltage signal, which is resolved into d and q components. It is shown that these signals can be used to uniquely derive a value for the rotor resistance.

In examining the influence of rotor resistance change with open loop current control

the following expression is given to show the steady state error in rotor d-axis flux.

$$\Delta \Psi der = \frac{[\ Kr - 1\ ][\ ws1^{*}\ Lr\ ]^2}{[\ Kr\ Rr\ ]^2 + [\ w_{s1}^{*}\ Lr\ ]^2}\ \Psi der_{ref} \qquad \ldots\ldots\ (6.16.)$$

where $Kr\ Rr = Rr + \Delta Rr$

Sugimoto et al, [25], present differential equations describing the rotor flux error system and solve this system of equations to give expressions for the errors in the d and q rotor flux as

$$\Psi der - \Psi der_{ref} = c_2\ e^{-\left[\frac{Rr}{Lr}\right]t}\ \cos\left[-\int w_0\ dt\ \right] + c_3\ e^{-\left[\frac{Rr}{Lr}\right]t}\ \sin\left[-\int w_0\ dt\ \right] \qquad \ldots\ldots\ (6.17.)$$

$$\Psi qer = c_2\ e^{-\left[\frac{Rr}{Lr}\right]t}\ \sin\left[-\int w_0\ dt\ \right] - c_3\ e^{-\left[\frac{Rr}{Lr}\right]t}\ \cos\left[-\int w_0\ dt\ \right] \qquad \ldots\ldots\ (6.18.)$$

The expression for the d-rotor flux error here does not account for the steady state error in the rotor flux that is known to occur with a rotor resistance parameter mismatch.

Analysis of Parameter Sensitivity Effects with Open Loop Control over torque.

As part of this work equations were derived to predict the errors in rotor flux linkages due to parameter mismatch.Referring to the full model of the motor in d - q coordinates the following analysis gives expressions for the steady state errors in the d and q rotor flux linkages in terms of the stator currents and the error in the controller value for the rotor time constant. The coordinate reference frame is rotating at the stator current frequency, w_0 , which is assumed to equal the controller frequency value, w_0^*. The controller values, i_{des}^* and i_{qes}^* are therefore equal to i_{des} and i_{qes} in the model, regardless of the value taken for the rotor time constant. The Field Oriented Control method computes the slip - frequency input as:

$$w_{slip} = \frac{Rr_{ref}\, i_{qes}}{Lr\, i_{des}} \qquad \ldots\ldots (6.1).$$

(This equation assumes that $\Psi_{der} = M\, i_{des}$, which holds for the steady-state, when the field has stabilised at a constant value.)

From the model, the following relationships hold in the steady state:

$$\Psi_{der} = \left[\frac{i_{des}\, M\, Rr}{Lr} + \left[\frac{Rr_{ref}\, i_{qes}}{Lr\, i_{des}} \right] \Psi_{qer} \right]$$

$\ldots\ldots (6.20).$

$$\Psi_{qer} = \left[\frac{i_{qes}\, M\, Rr}{Lr} + \left[\frac{Rr_{ref}\, i_{qes}}{Lr\, i_{des}} \right] \Psi_{der} \right]$$

$\ldots\ldots (6.21)$

The expression for Ψ_{qer} is substituted into that for Ψ_{der} to yield an equation for Ψ_{der} in terms of i_{des}, i_{qes}, Rr and Rr_{ref}:

$$\Psi_{der} = \frac{i_{des}^3 M Rr^2 + Rr\, i_{des}\, Rr_{ref}\, i_{qes}^2 M}{Rr^2 i_{des}^2 + Rr_{ref}^2 i_{qes}^2}$$

..... (6.22).

The steady state error in the d rotor flux linkage is given by:

$$\Delta \Psi_{der} = \Psi_{der} - M i_{des}.$$

..... (6.23).

giving:

$$\Delta \Psi_{der} = \frac{(Rr\, Rr_{ref} - Rr_{ref}^2) M i_{des} i_{qes}^2}{Rr^2 i_{des}^2 + Rr_{ref}^2 i_{qes}^2}$$

..... (6.24).

A similar analysis gives the error in q axis rotor flux linkage.

$$\Delta \Psi_{qer} = \frac{(Rr - Rr_{ref}) M Rr\, i_{des}^2 i_{qes}}{Rr^2 i_{des}^2 + Rr_{ref}^2 i_{qes}^2}$$

..... (6.25).

The developed torque should be :

$$Te = \frac{3 M^2 i_{des} i_{qes}}{Lr}$$

..... (6.26).

To compute the steady state torque error due to rotor time constant mismatch this should be subtracted from the complete torque equation :

$$Te = 3 (i_{der} \Psi_{qer} - \Psi_{der} i_{qer}) \qquad \ldots\ldots (6.27).$$

with :

$$i_{der} = \frac{\Psi_{der}}{Lr} - \frac{M i_{des}}{Lr} \qquad \ldots\ldots (6.28).$$

&

$$i_{qer} = \frac{\Psi_{qer}}{Lr} - \frac{M i_{qes}}{Lr} \qquad \ldots\ldots (6.29)$$

6.3 Sensitivity of Forward Path to Tr Variation.

Both steady state and transient effects of rotor resistance variation on all the motor states are qualitatively assessed here by simulation, and by experiment on the prototype servo controller. Deviations of the nominal rotor resistance from the actual rotor resistance are possibly over exaggerated so that the effects can be regarded as worst case and also account for variations in secondary inductance caused by variations in the excitation level.

Plots (6.1) and (6.2) show the rotor q-axis flux linkage for R_{rref} = Rr and R_{rref} = 0.5 Rr. There is open loop control over iqes. The flux current loop is closed with

a PI controller with gain = 1.5 and integral time constant = 0.05. A torque current of 6 amps is commanded at t = 0.6 seconds, when the field has stabilised. Ψ_{qer} is the order of 5 mWb with no error in nominal resistance. This is accounted for by the assumptions made for the decoupling strategy which will not hold during each simulation time interval due to numerical error.

$$\frac{d\,\Psi_{der}}{dt} = 0 : \quad \Psi_{qer} = 0 : \quad \frac{d\,\Psi_{qer}}{dt} = 0$$

With $R_{ref} = 0.5\ R_R$ Ψ_{qer} is seen to ramp up linearly with time for a constant torque command. After 40 milliseconds it reaches 35 mWb. It will be seen later that this then settles at a constant value for a constant torque command.

Plots (6.3) and (6.4) show I_{des} for a similar open loop torque command at 0.6 seconds. Given that there is closed loop control over I_{des} these plots merely show that the closed loop controller is relatively insensitive to variations in Tr. In both cases the reference current of 3.0 amps is achieved with very little steady state error and transients due to change in torque demand decay after about 10 mSec.

Plot (6.5) - (6.8) show the torque reference voltage and corresponding stator q currents for perfect match in parameter values to actual values and for the case, $R_{Rref} = 0.5\ R_R$. There is virtually no difference between the current lags for the differences in nominal resistance values. The lag that is present is caused by motor leakage inductance. It was expected that with a mismatch in parameters, a decoupling in the coordinate d-axis from the rotor air-gap flux would occur, thereby indicating that a change in commanded i_{qes} would cause a change in the rotor flux and in doing so add a further lag to i_{qes} since i_{qes} would now be subject to some of the main field time constant of the machine.

Oscillographs (6.1) - (6.3) show the lag between phase current and phase voltage

reference for an open loop step change in torque demand for the cases where the controller rotor resistance value is less than, equal to and greater than the actual (nominal value). It is seen that when the controller value is equal to the nominal value the current lags the voltage by roughly 2 milliseconds. Although the lag is greater where mismatch between the controller value and the nominal value exists no conclusive statements can be made because of interaction with the currents of the other two phases.

Plots (6.9) - (6.14) predict the steady state values for the d and q-axis rotor flux linkages for a constant torque command at $iqes_{ref}$ = 6.0 amps between t = 1.0 and 3.5 seconds.

A number of steady state parameter mismatch effects are shown:

- When the nominal rotor resistance value is less than the actual value, (or when T_{rref} is greater than Tr acutal) over excitation occurs for a positive torque command. For a torque command of $iqes_{ref}$ = 6.0 amps Ψ_{der} = 0.33 Wb. whereas Ψ_{der} = 0.24 Wb. with perfect match of parameters.

- With no torque command no errors occur.

- An error in q-axis rotor flux linkage occurs. This increases to a significant steady state value of 0.12 Wb for the positive torque command.

- With perfect match no change in Ψ_{der} occurs for changing torque demands, and only small transient q-axis flux linkages arise for the reasons already outlined.

- With R_{rref} greater than the nominal (actual) value, Rr, (T_{rref} less than T_r Actual) under excitation of the machine occurs for a positive

torque command. With R_{rref} = 2 Rr: Ψ_{der} = 0.125 Wb as opposed to 0.24 Wb. for R_{rref} = Rr.

With R_{rref} greater than Rr transient oscillations in Ψ_{der} and Ψ_{qer} occur which are much greater in amplitude than those which occur when R_{rref} is less than Rr.

These oscillations have period 0.23 seconds and so are at 4.3 Hz.

Equations (6.13) and (6.14) give those oscillations as decaying subject to $e^{-(Rr/Lr)t}$ and at frequency:

$$\left| \frac{R_{Ref}\ I_{qes}}{L_R\ I_{des}} \right| \text{ rad.sec}^{-1}$$

$$\frac{1.60}{0.084.\ 3.0} = 23{\cdot}8 \text{ rad sec}^{-1}$$

$$= 3.78 \text{ Hz}$$

There is therefore reasonably good agreement with the predicted frequency of oscillation. The same equations, however, indicate that the amplitude of the oscillations should be lower for the case where R_{rref} is greater than Rr. The simulations do not show this to be the case. They predict the amplitude of the oscillations to be:

$$e^{-\left(\frac{Rr}{Lr}\right)} \checkmark \left[1 + \left| \frac{Rr\ i_{des}}{Rr_{ref}\ i_{qes}} \right|^2 \right]$$

Equations (6.24) and (6.25) were derived to give the steady state errors in flux

linkages due to parameter mismatch.

To analytically verify the Ψ_{der} deviation in Plot (6.9) eqn (6.24) is used:

$$\Delta\Psi_{der} = \frac{(0.5.0.25 - 0.25^2)\ 0.08\ .3.0\ .6.0^2}{0.5^2\ 3.0^2 + 0.25^2\ 6.0^2}$$

$$= 0.12 \text{ Wb}$$

From the plots $\Delta\Psi_{der}$ = 0.11 Wb.

To verify the Ψ_{qer} deviation in Plot (6.10) eqn (6.25) is used:

$$\Delta\Psi_{qer} = \frac{(0.5\ .0.25)\ 0.08\ .0.5\ .3.0^2\ .6.0}{0.5^2\ 3^2 + 0.25^2\ .6.0^2}$$

$$= 0.12 \text{ Wb}$$

Again there is perfect agreement with the error in the states given from the simulations.

Equation (6.25) gives an error in the rotor q-flux linkage as;

$$\Delta\Psi_{qer} = \frac{(0.5\ -1)\ 0.08\ .0.5\ .3^2\ .6}{0.5^2\ 3^2 + 1^2\ .6^2}$$

$$= -0.028 \text{ Wb}$$

The simulations show the error in this state to be -0.023 Wb.

Plots (6.15) - (6.20) show the developed torque (by forward path control over i_{qes})

and the corresponding phase 1 current. Stall torques are simulated so that frequencies are actual slip frequencies. The following observations can be made:

- If the reference value for rotor resistance is less than the actual value the slip frequency is decreased but the torque developed is increased. There are non symmetrical transients in the torque with undershoot on the rising edge.

- If the reference value is greater than the actual rotor resistance value the slip frequency is increased but the developed torque is lowered. Transient oscillations occur on the rising edge of the torque with none observed when the torque was commanded to be zero. The phase currents are at increased slip frequency but appear to be amplitude modulated.

For the case where Rr_{ref} = 2 * Rr: Te = 2.7 N.m. (Plot (6.15.)). From plot (6.17.), Te_{ref} = 4.1 N.m. when Rr_{ref} = Rr.

$$\Rightarrow \quad \frac{Te_{ref}}{Te} = 1.52.$$

Using equations (6.19) and (6.8) gives

$$\frac{Te_{ref}}{Te} = 2.0.$$

Using equations (6.27) - (6.29) predicts the developed torque to be 2.10 Nm when Rr_{ref} = 2Rr.

Sugimoto et al., [20] show experimental step responses in the torque where mismatches in the rotor resistance occur. These results give excellent agreement with

those predicted by plots (6.15.), (6.17.) and (6.19.).

Oscillographs (6.4) - (6.6) show the steady state operation of the prototype servo system in torque mode for discrepancies between the controller rotor resistance value and the nominal machine value. The results match those predicted by the simulation in Plots (6.15) - (6.20). Changes in transient torque effects (over/under shoot) due to parameter mismatch are not discernible due to the dominance of the bar rotor dynamics used in torque measurement. There are very significant oscillations in the steady state torque but these are not due to parameter mismatch effects. These oscillations are shown in the next chapter to result from distortions in the phase currents introduced by cross-over delays in the P.W.M. inverter. It is however important to note that with the controller resistance value greater than the machine value very significant torque oscillations occur, despite the fact that the slip frequency is higher and consequently there is less distortion in the current waveform.

6.4 Sensitivity of Closed Loop Controller to Rotor Time Constant Variation.

With closed loop control over speed or position the main motor states are not related by simple expressions as they are for forward path torque control. Analytic expressions for errors in these states due to parameter deviation from controller parameter values are not easily derivable (Krishnan et al, [22]). The simulations were used to qualitatively examine the robustness of the closed loop speed controller to mismatch between the controller parameter values and the machine values. No load speed responses are assessed along with the corresponding motor internal states. PI tuning values designed in Chapter three were used.

Plots (6.21) - (6.24) give the closed loop speed responses for various values of R_{Rref}. The desired speed is commanded to be 40 rpm at t = 0.6 seconds when the field has stabilised. From the plots it is seen that a halving or doubling of the controller value of resistance over the actual value has very little effect on the overall speed response. The following are the salient effects:

- An under estimated controller value marginally decreases the rise time and the speed settles faster but with slightly larger steady state error than when no mismatch occurs.

- An over estimated value marginally increases the rise time. Overshoot, settling time and steady state error are also increased.

Plots (6.31) - (6.33) give V_{qesref} for various values of Rr_{ref}. Plots (6.25) - (6.27) give the corresponding values of i_{qes}. From the v_{qesref} plots it is evident that stable performance would not be achieved if the controller time interval was much larger. The lags between i_{qes} and v_{qesref} do not vary noticably for varying R_{Rref}.

Plots (6.28) - (6.30) show Ψ_{qer} for various values of Rr_{ref}. In all cases the flux

linkage values are minimal, being of the order of millivebers. When the controller value for Rr_{ref} was twice the actual value the least error in Ψ_{qer} was observed. This effect is not expected since the corresponding torque component of current takes longer to settle at zero. The effect could possibly result from a cancellation of numerical errors.

6.5 Conclusions.

Very little work has been done to date on analysing the sensitivity of the field oriented control method to mismatches between controller parameter values and the actual values. Theoretical analysis has been done for the torque mode case, but there is still not complete agreement on equations for errors in developed torque or in rotor flux linkages. Equations derived in this work to give steady state deviations in the rotor flux linkages due to parameter mismatch were validated by the errors in these states given by the simulations. The assumptions made about the controller current values being equal to the actual currents and the controller frequency value equal to the actual frequency must also be valid. The simulations were in turn validated by results from the prototype system.

The concept of empirically identifying the rotor time constant, off line, by measuring the lag between a phase current and the corresponding phase voltage does not seem to be feasible. Firstly, if the method were to work, a nominal value for Tr only, would be achieved which would still vary substantially during operation because of temperature change and saturation. The interaction with the other phase currents also makes measurement of a lag difficult.

The simulations showed that greater transient oscillations occurred in all the states when the controller value for rotor resistance was over estimated. The results from the system itself also showed greater oscillations when Rr_{ref} was greater than Rr but in the actual system these oscillations did not decay as quickly as predicted by the simulations; the problem apparently being compounded by the oscillations resulting from the distortions in the phase currents. This is surprising given that current distortion effects are reduced with an over estimated value of resistance because of the increased slip frequency.

If no adaptive control scheme is to be used it can be concluded that under estimation

of the rotor resistance is more desirable.

- Transient oscillations will be minimised.

- Over-excitation will occur but this could be offset for by choosing a slightly lower flux reference value. The added advantage being that under excitation would then occur at low values of commanded torque, thereby minimising magnetising current losses.

- In a closed loop situation faster rise times and settling times would occur.

The closed loop speed controller structure has been found to be very robust to parameter variation from a control performance point of view. The main problem with rotor resistance deviation is the change in excitation level which occurs and which will then further vary according to torque command.

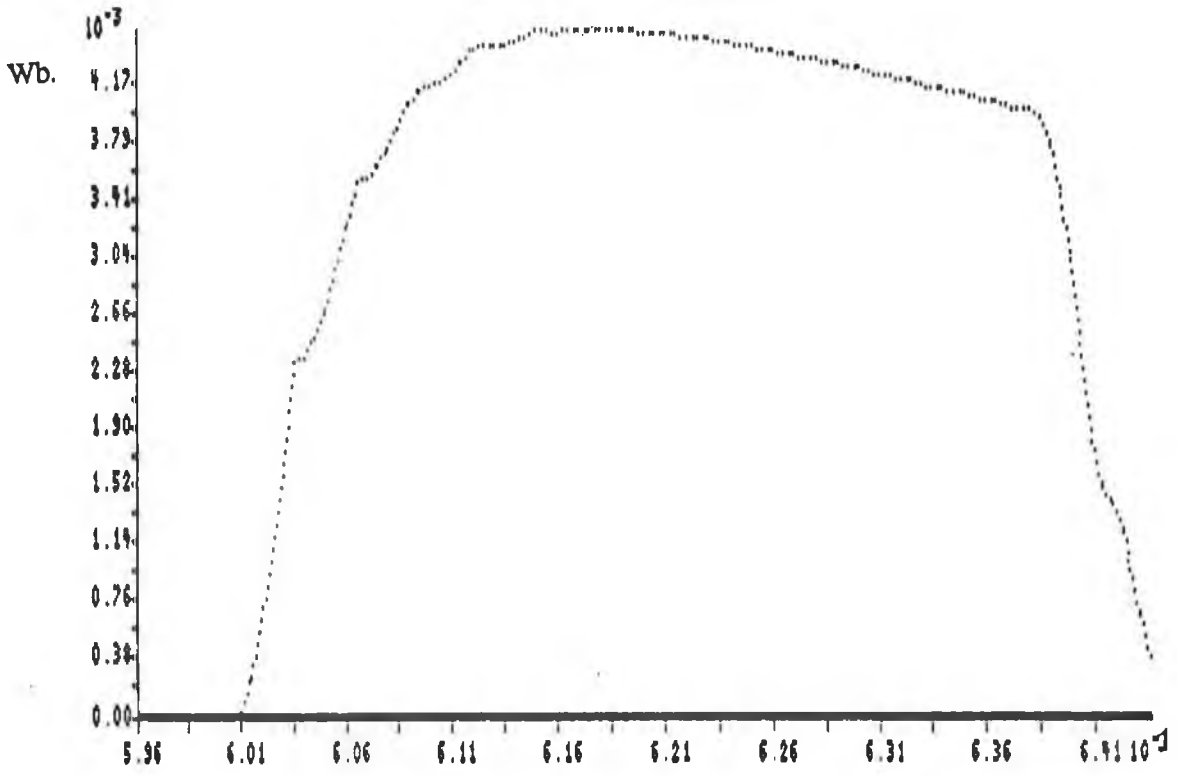

Plot (6.1) Ψqer Rr_{ref} = Rr. Seconds

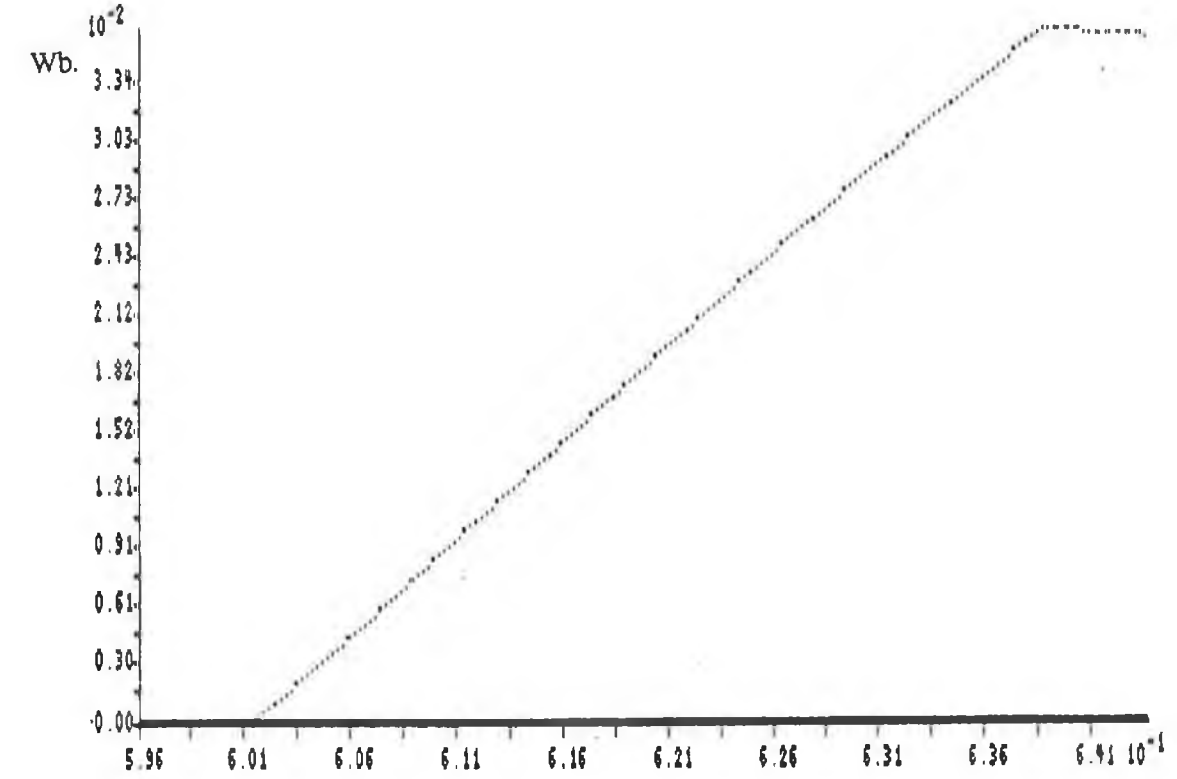

Plot (6.2) Ψqer Rr_{ref} = 0.5 * Rr Seconds

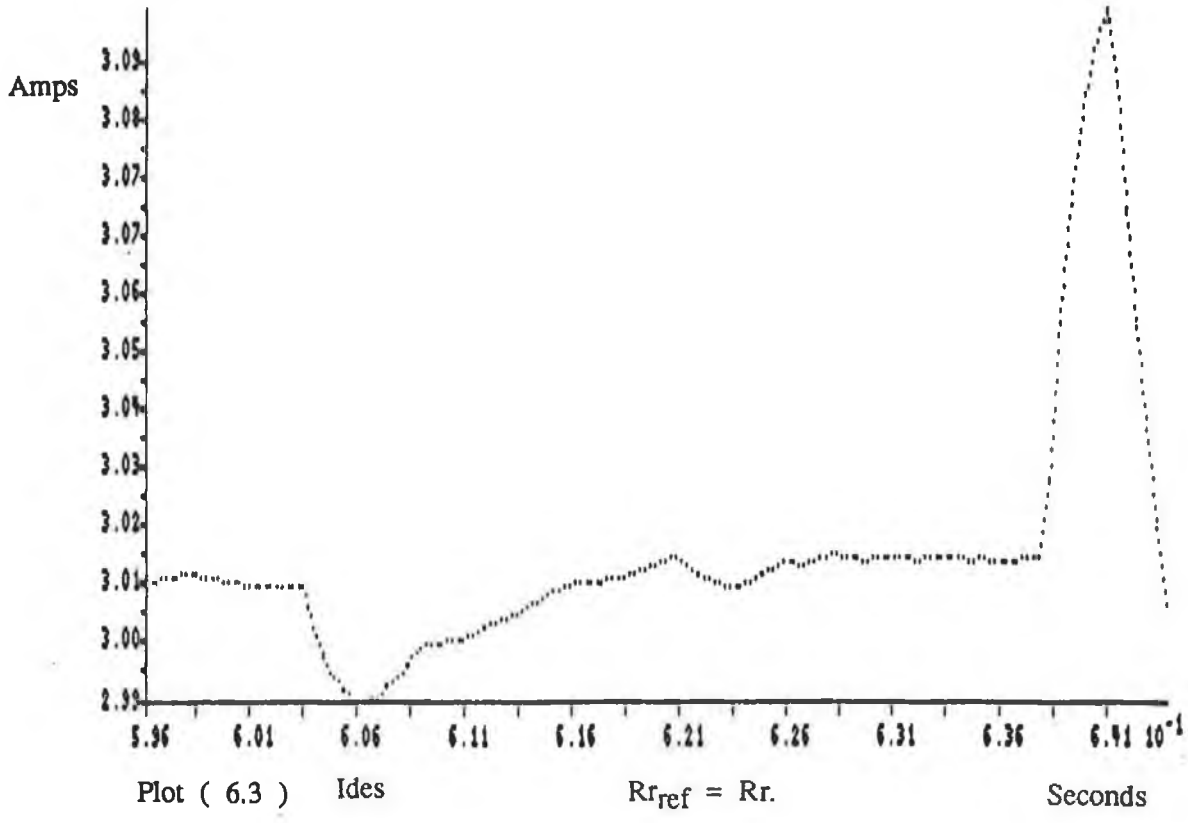

Plot (6.3) Ides Rr_{ref} = Rr. Seconds

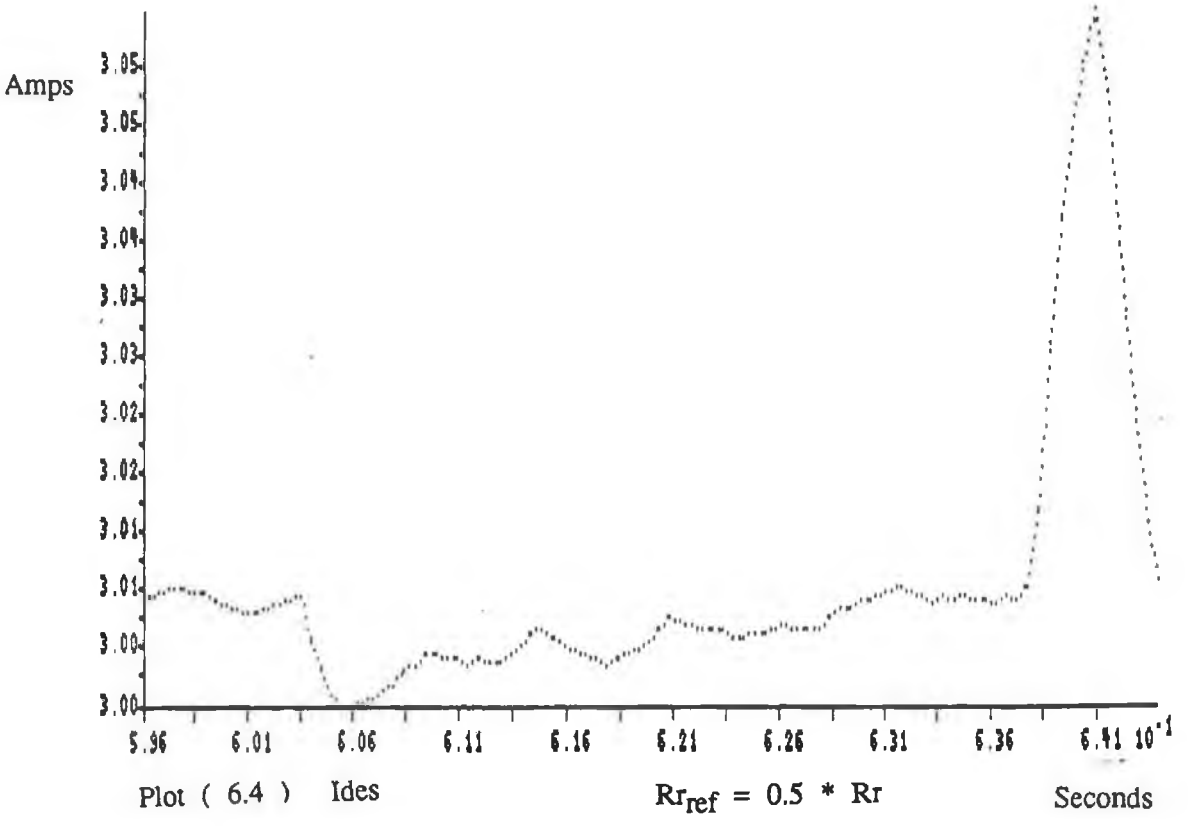

Plot (6.4) Ides Rr_{ref} = 0.5 * Rr Seconds

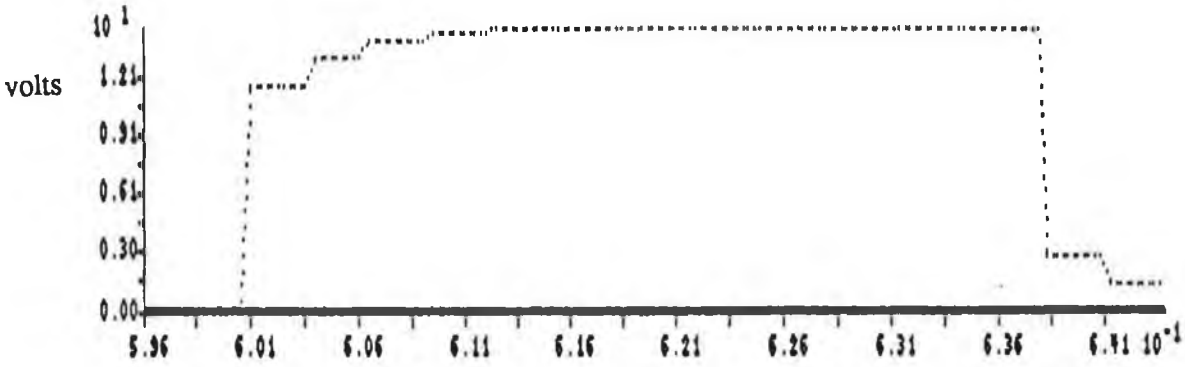

Plot (6.5) $Vqes_{ref}$ Rr_{ref} = Rr. Seconds

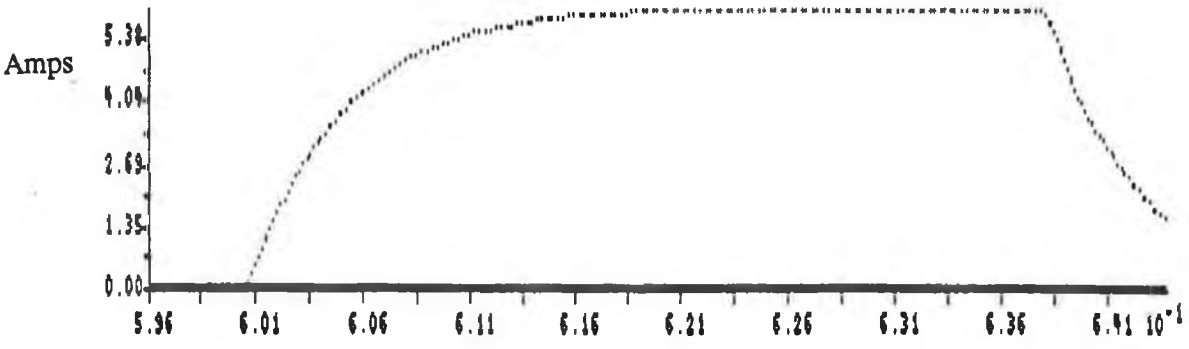

Plot (6.6) Iqes Rr_{ref} = Rr. Seconds

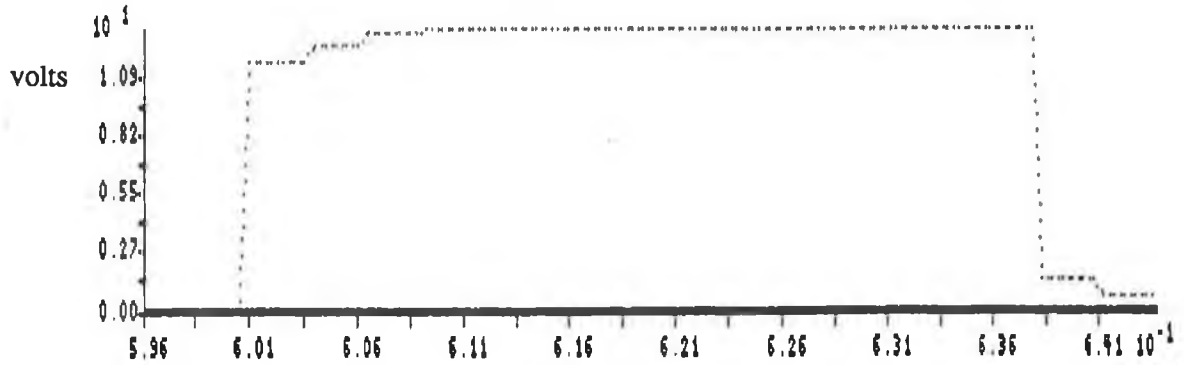

Plot (6.7) $Vqes_{ref}$ Rr_{ref} = 0.5 * Rr Seconds

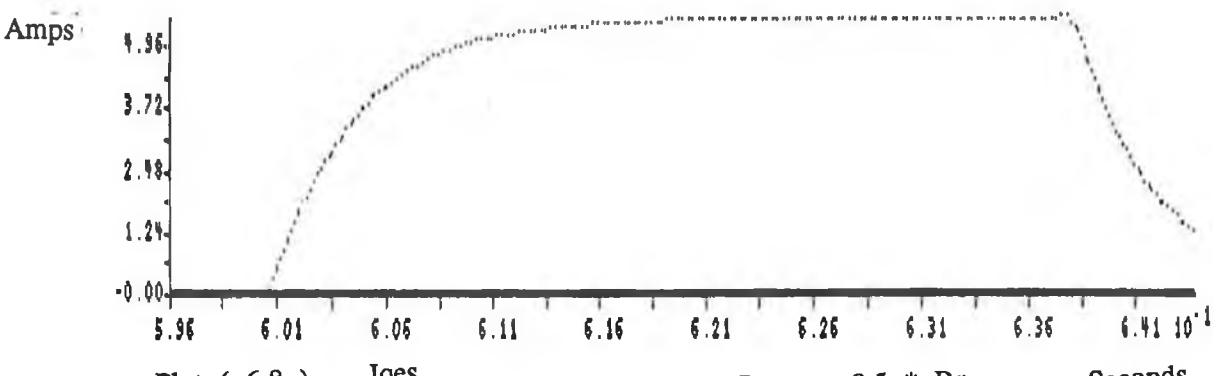

Plot (6.8) Iqes Rr_{ref} = 0.5 * Rr Seconds

Oscillograph (6.1)

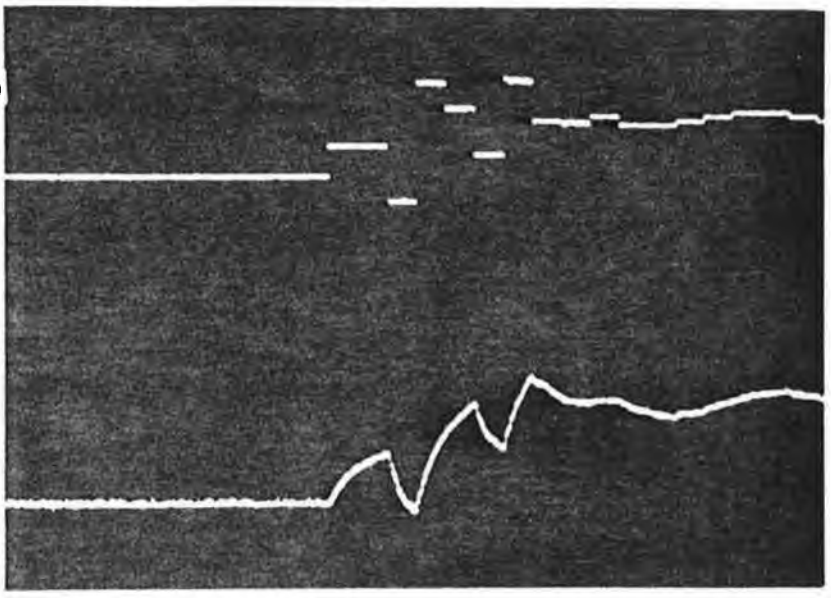

Vs_1

10 msec/div.

Is_1

10 A/div.

$Rr_{ref} = 2 * Rr$

Oscillograph (6.2)

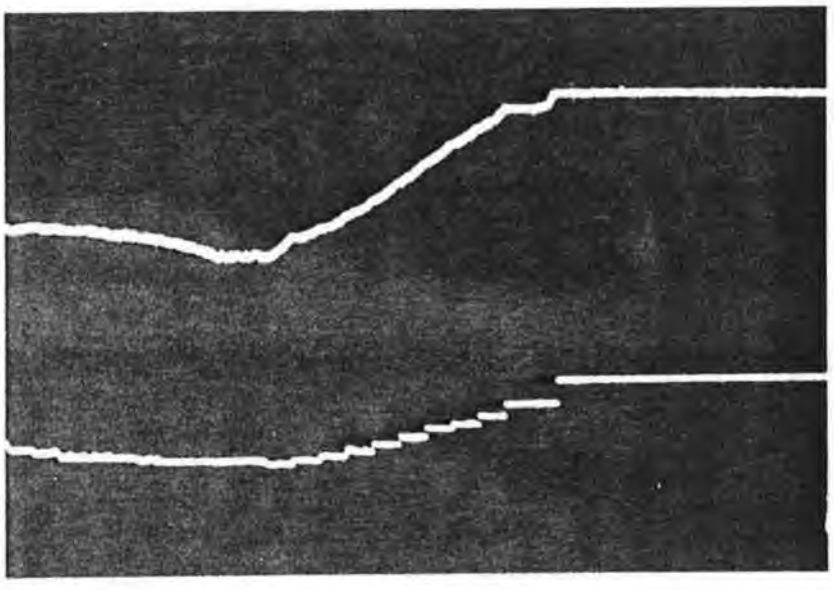

Is_1

10 A/div.

10 msec/div.

Vs_1

$Rr_{ref} = Rr.$

Oscillograph (6.3)

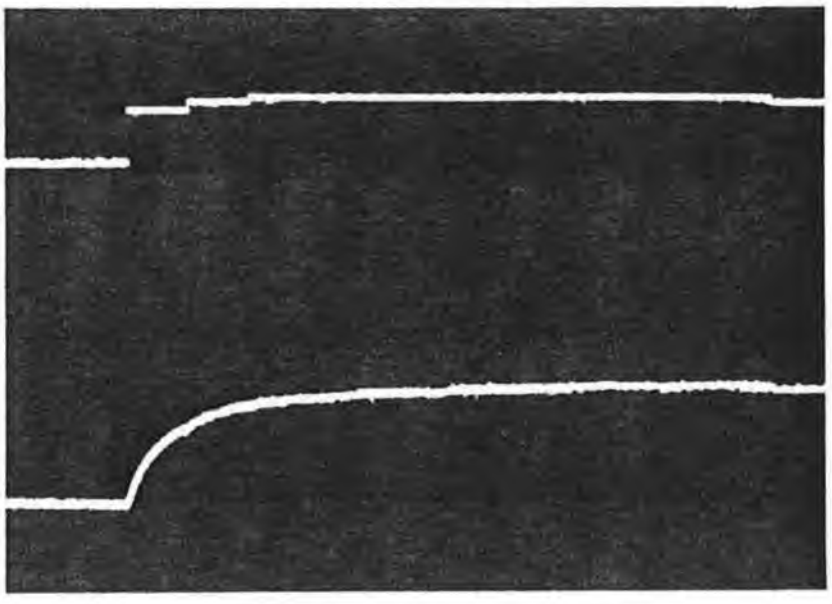

Vs_1

10 msec/div.

Is_1

10 A/div.

$Rr_{ref} = 0.5 * Rr$

Wb.

Ψder

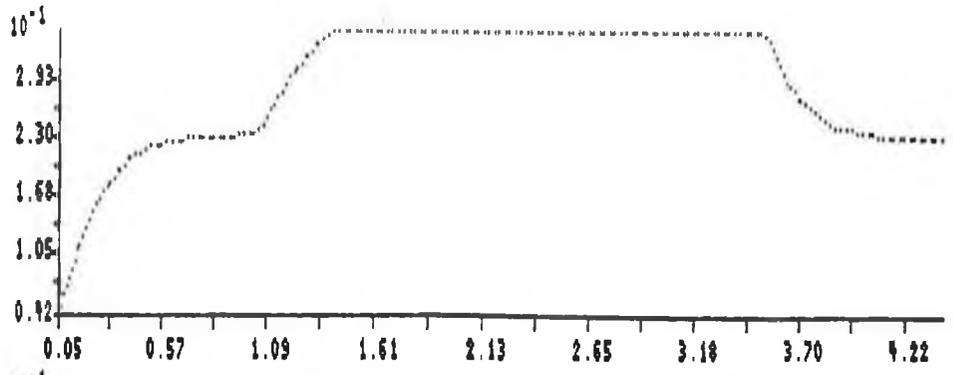

Rr_{ref} = 0.5 * Rr

Plot (6.9)

Wb.

Ψqer

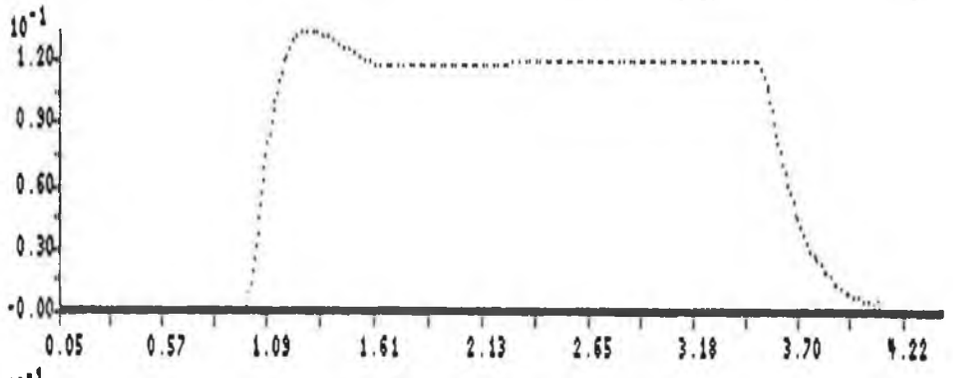

Rr_{ref} = 0.5 * Rr

Plot (6.10)

Wb.

Ψder

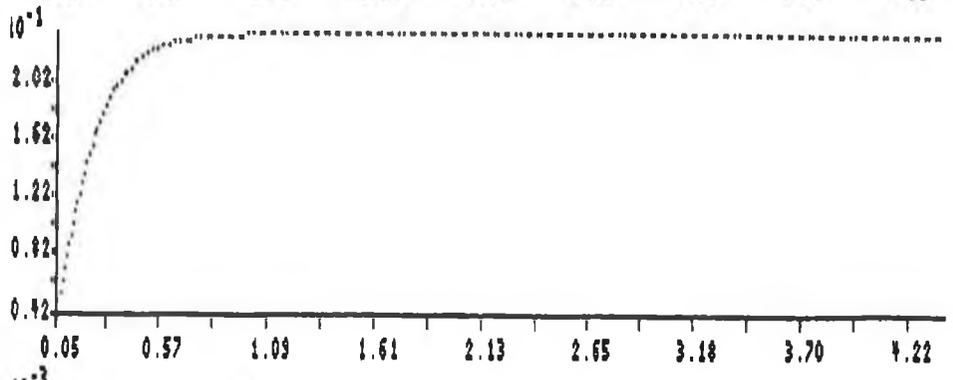

Rr_{ref} = Rr.

Plot (6.11)

Wb.

Ψqer

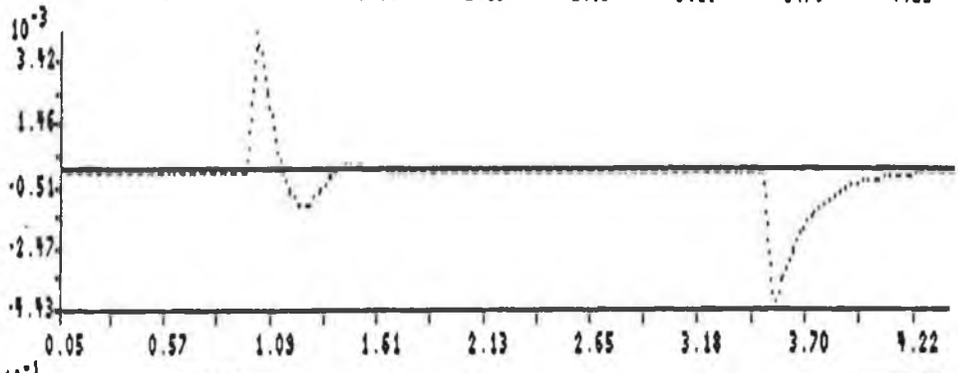

Rr_{ref} = Rr.

Plot (6.12)

Wb.

Ψder

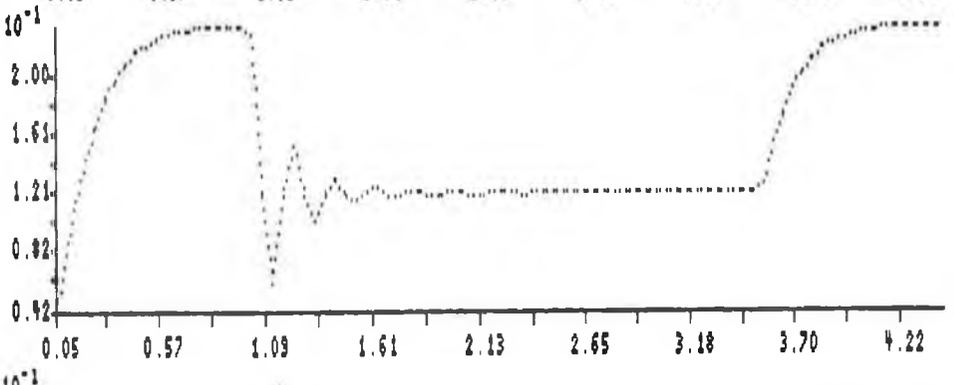

Rr_{ref} = 2 * Rr

Plot (6.13)

Wb.

Ψqer

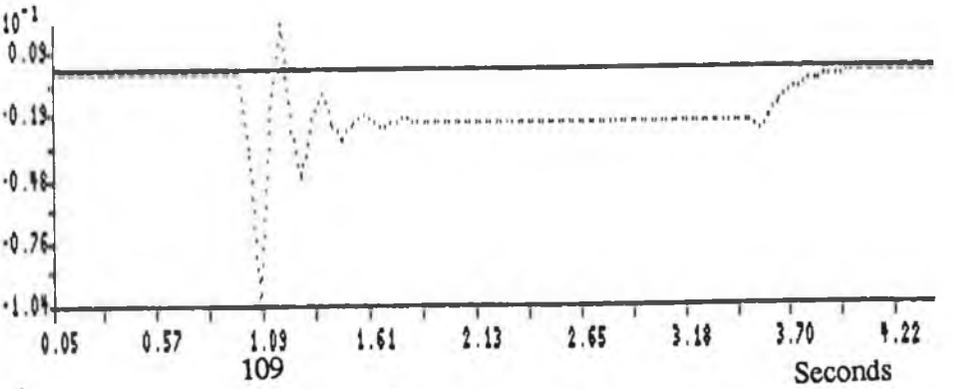

Rr_{ref} = 2 * Rr

Plot (6.14)

Seconds

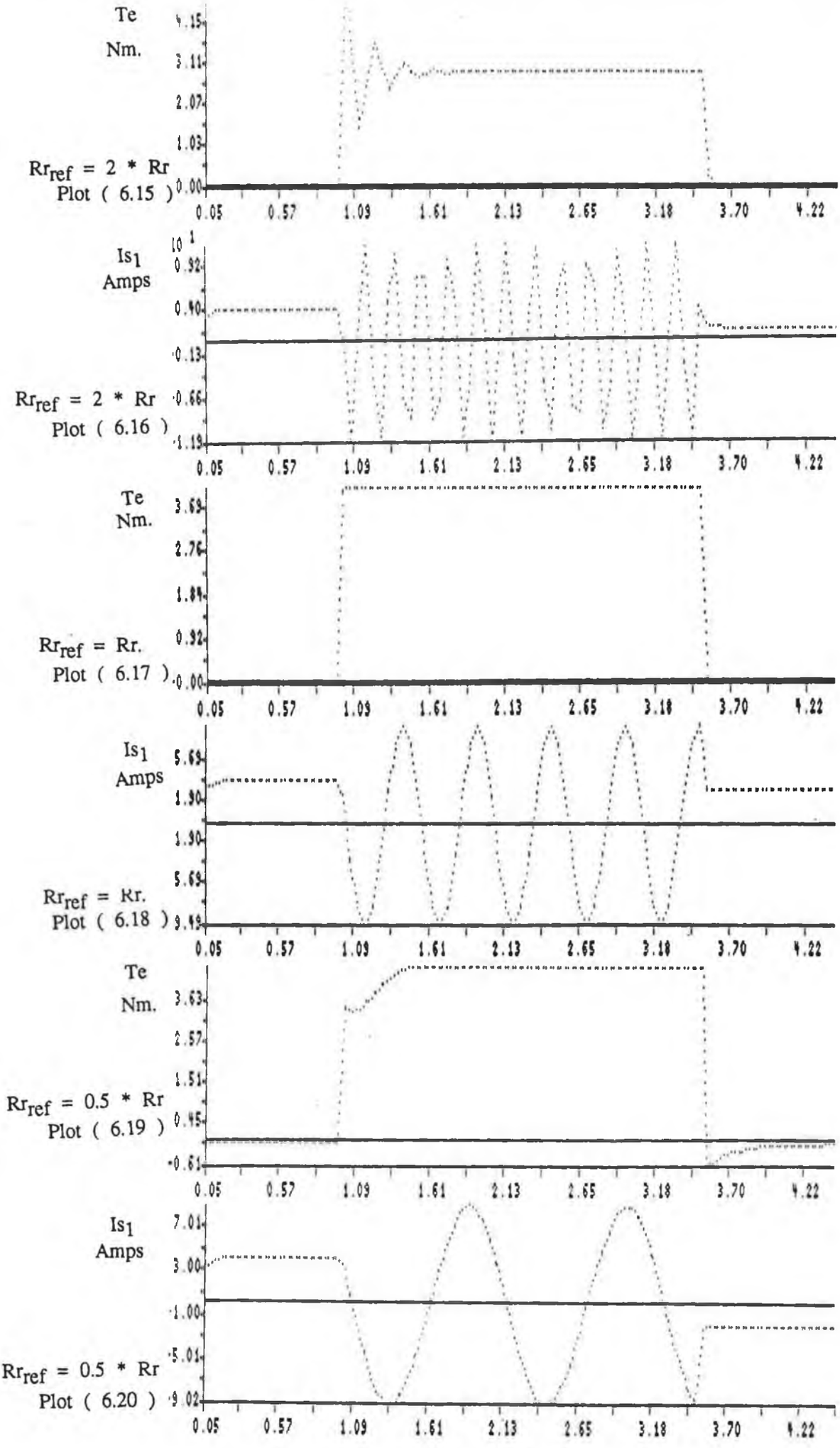
Te
Nm.
Rr_ref = 2 * Rr
Plot (6.15)
Is1
Amps
Rr_ref = 2 * Rr
Plot (6.16)
Te
Nm.
Rr_ref = Rr.
Plot (6.17)
Is1
Amps
Rr_ref = Rr.
Plot (6.18)
Te
Nm.
Rr_ref = 0.5 * Rr
Plot (6.19)
Is1
Amps
Rr_ref = 0.5 * Rr
Plot (6.20)
0.05
0.57
1.09
1.61
2.13
2.65
3.18
3.70
4.22
Seconds

Oscillograph (6.4)

Torque

500 msec/div.

Is_1

5 A/div.

Rr_{ref} = 0.5 * Rr

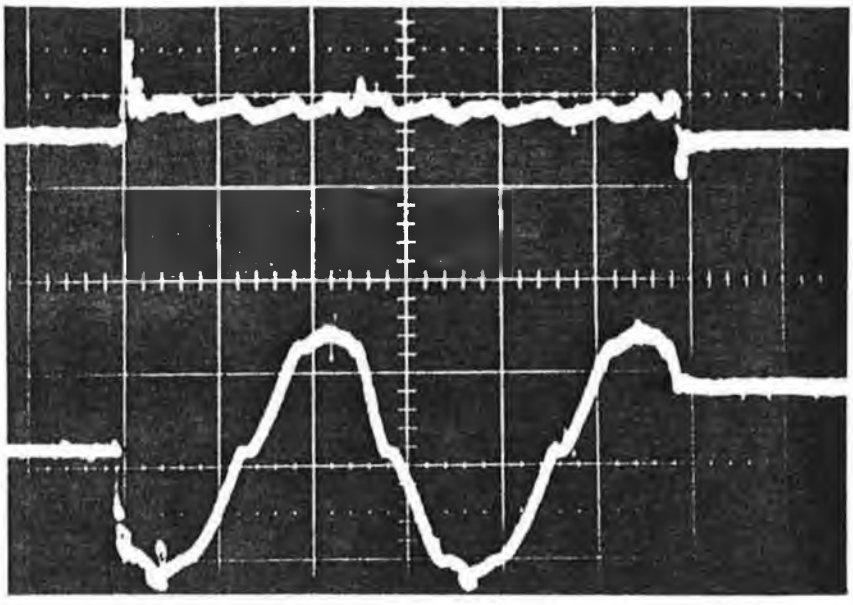

Oscillograph (6.5)

Torque

500 msec/div.

Is_1

5 A/div.

Rr_{ref} = Rr.

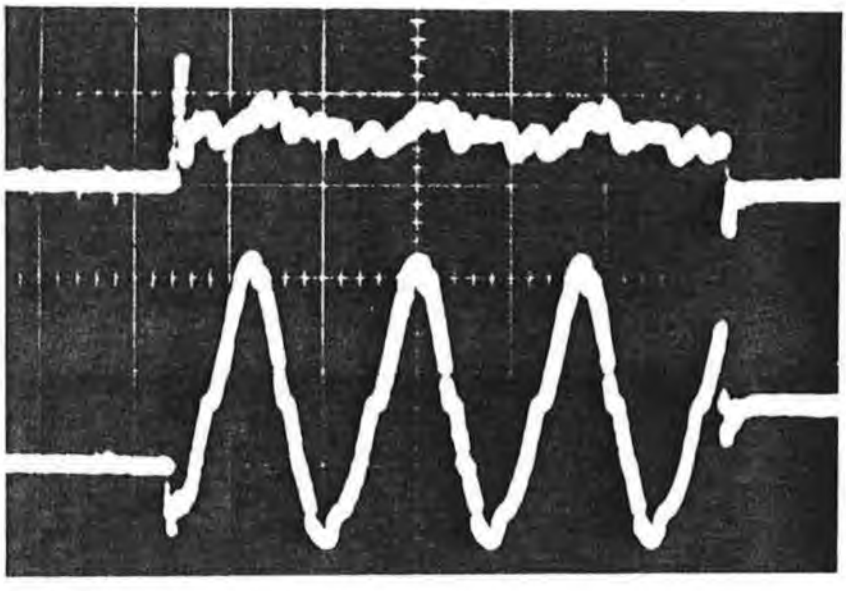

Oscillograph (6.6)

Torque

500 msec/div.

Is_1

5 A/div.

Rr_{ref} = 2 * Rr

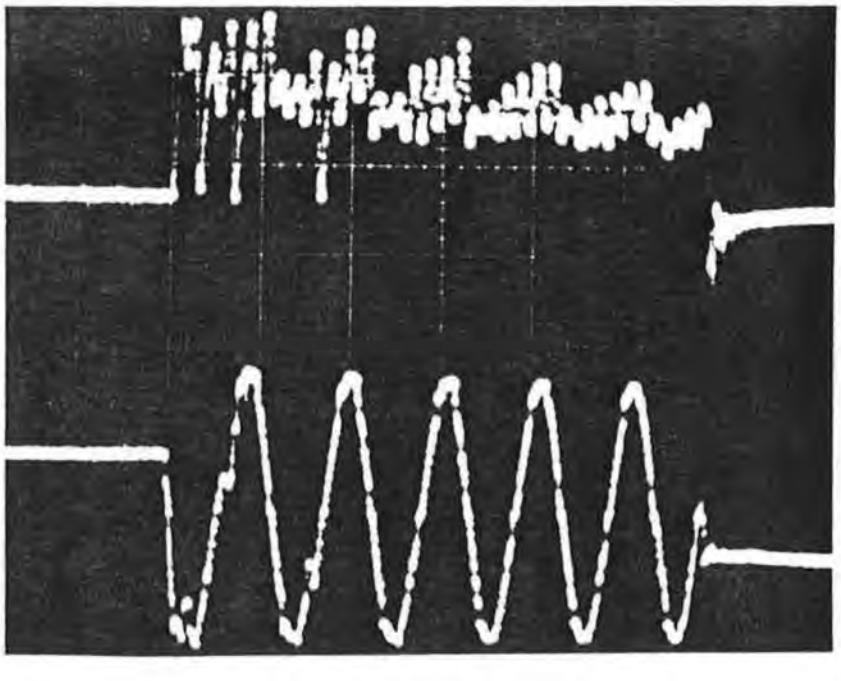

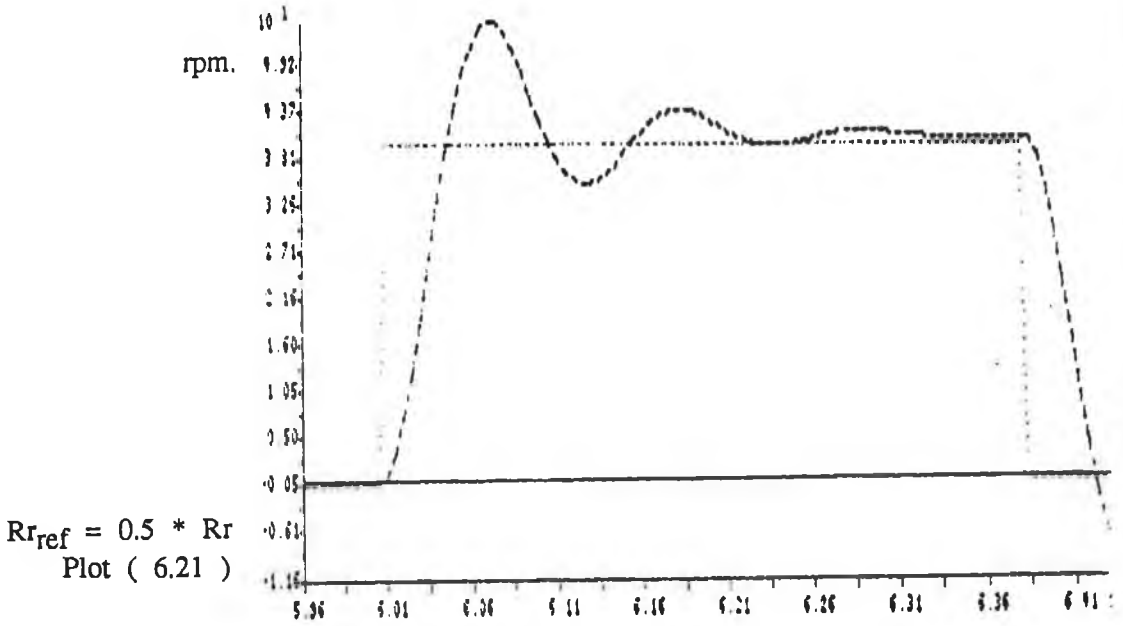

Closed Loop Speed Response.

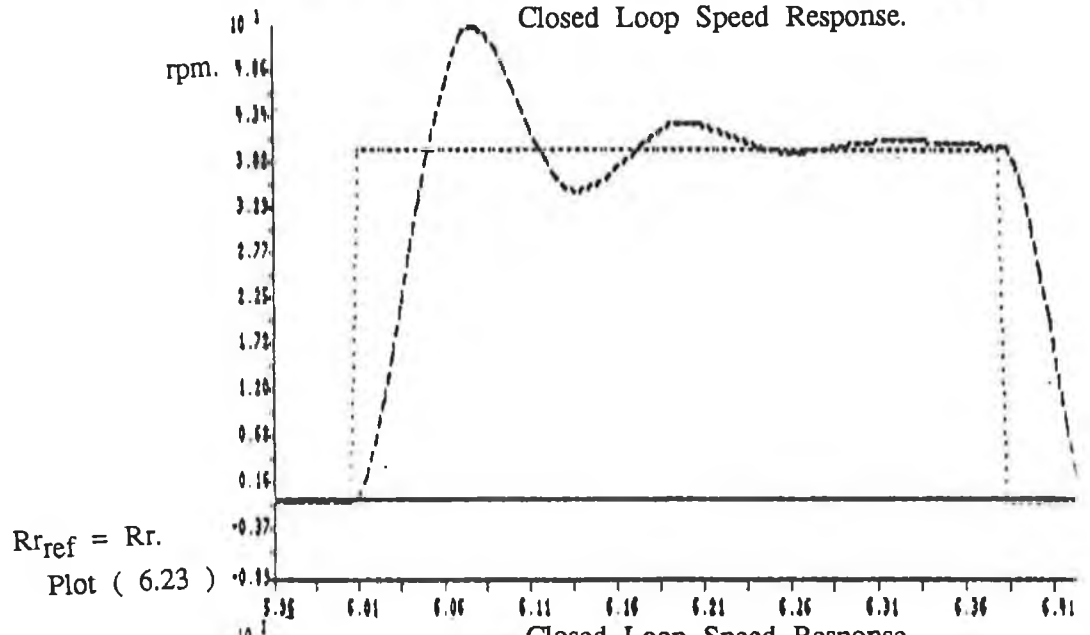

Closed Loop Speed Response.

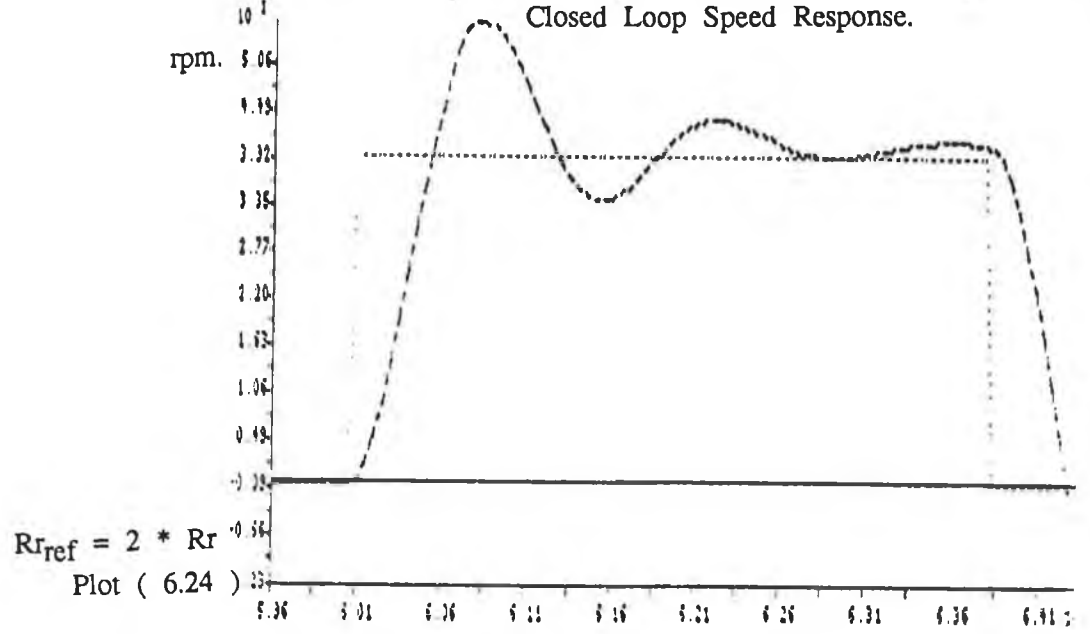

Closed Loop Speed Response.

Seconds

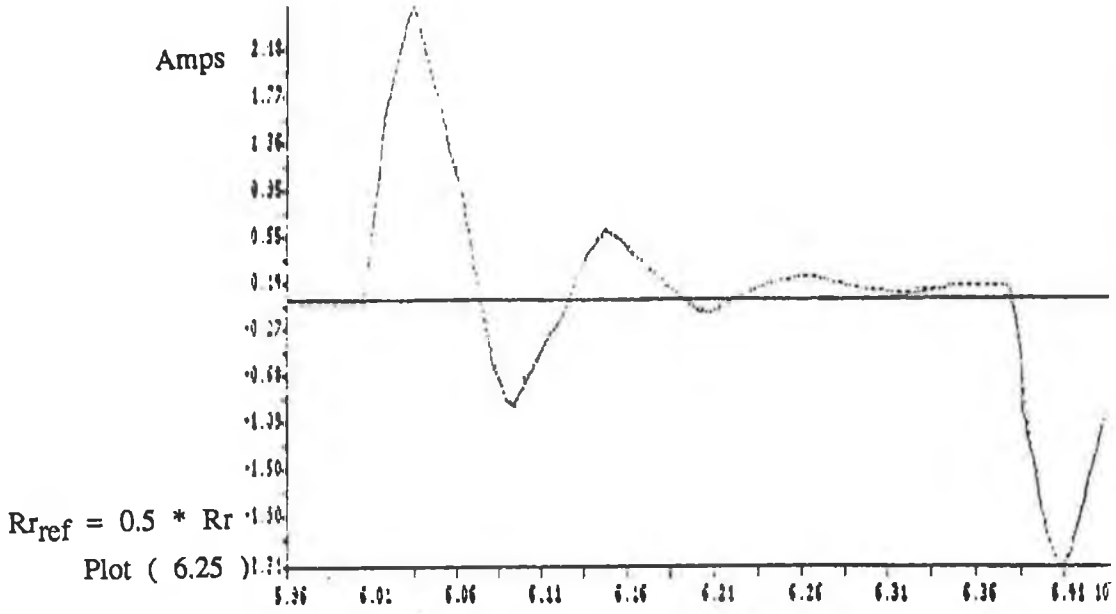

Rr_{ref} = 0.5 * Rr

Plot (6.25)

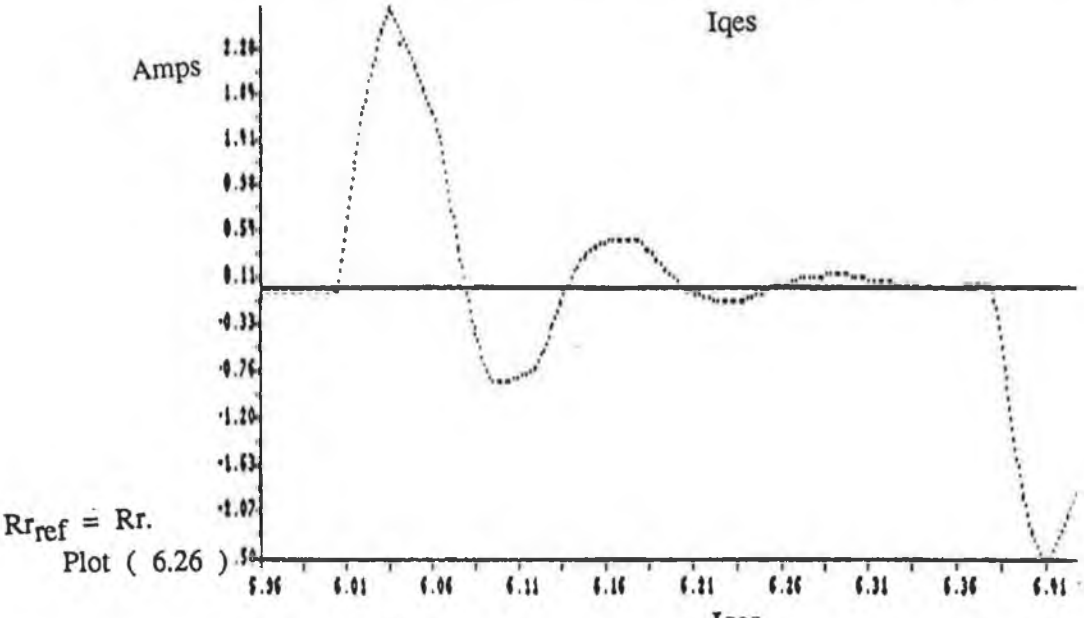

Rr_{ref} = Rr.

Plot (6.26)

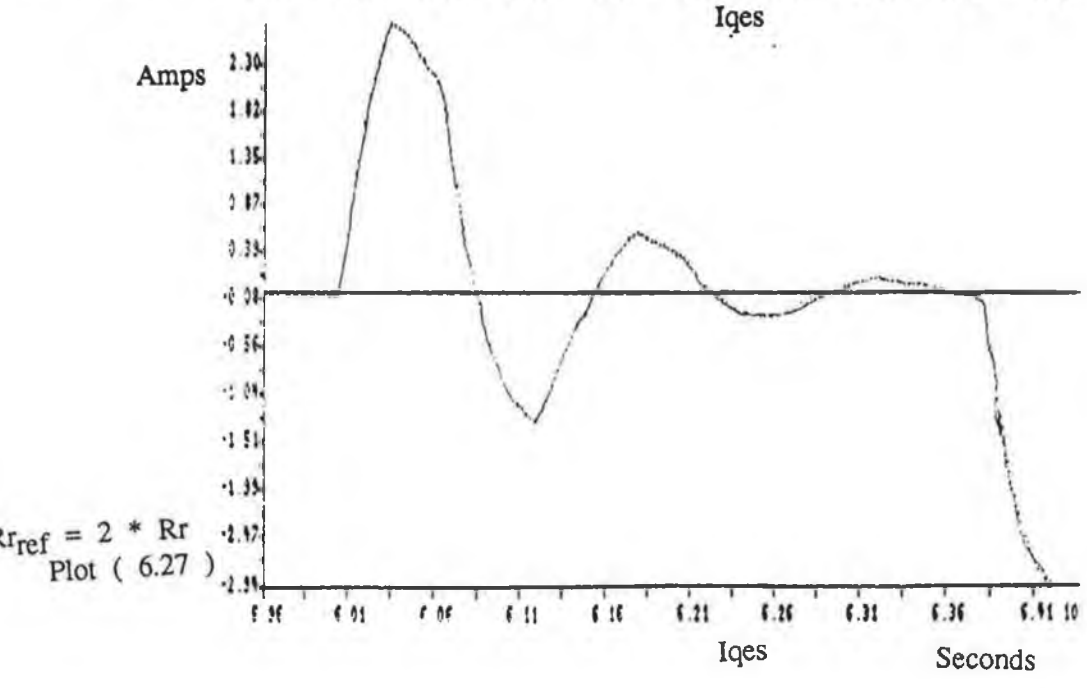

Rr_{ref} = 2 * Rr

Plot (6.27)

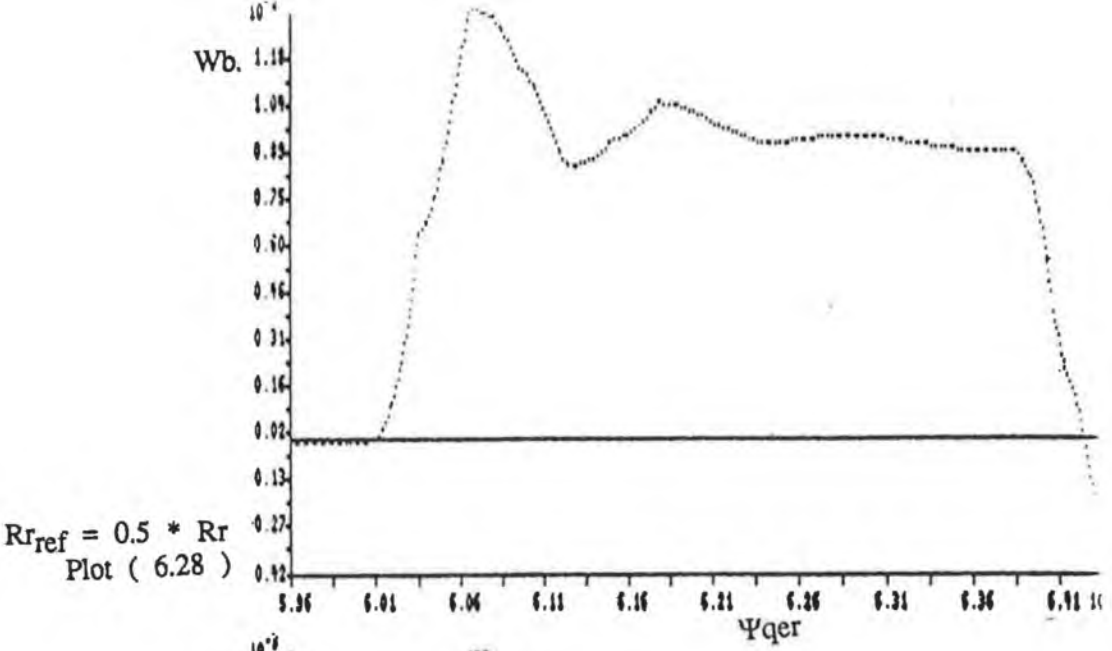

Rr_{ref} = 0.5 * Rr
Plot (6.28)

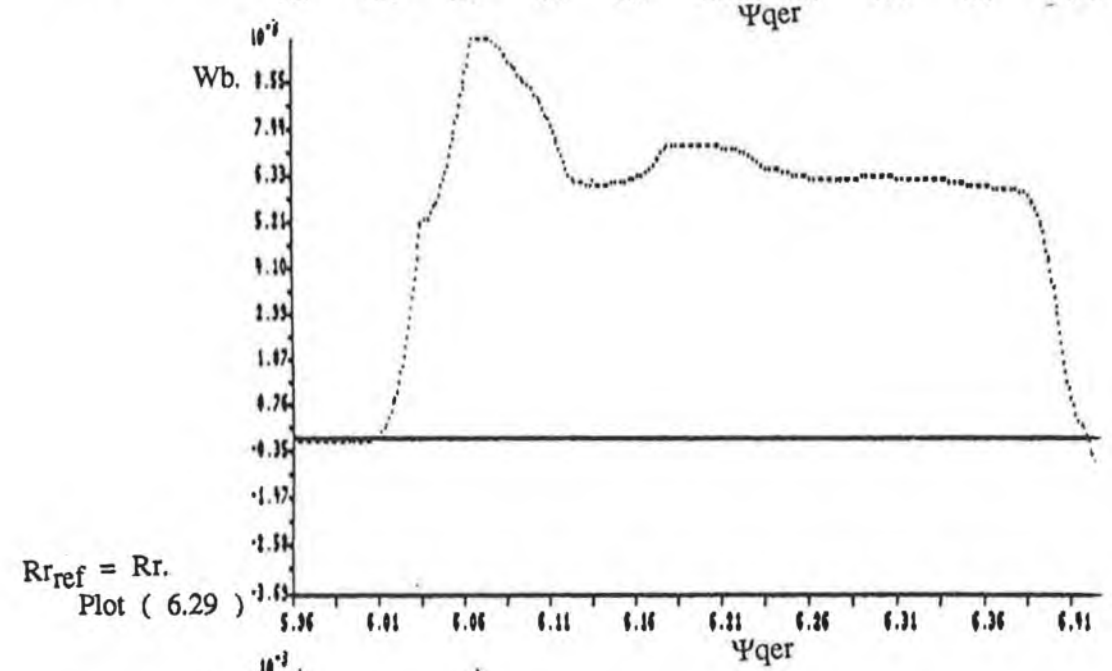

Rr_{ref} = Rr.
Plot (6.29)

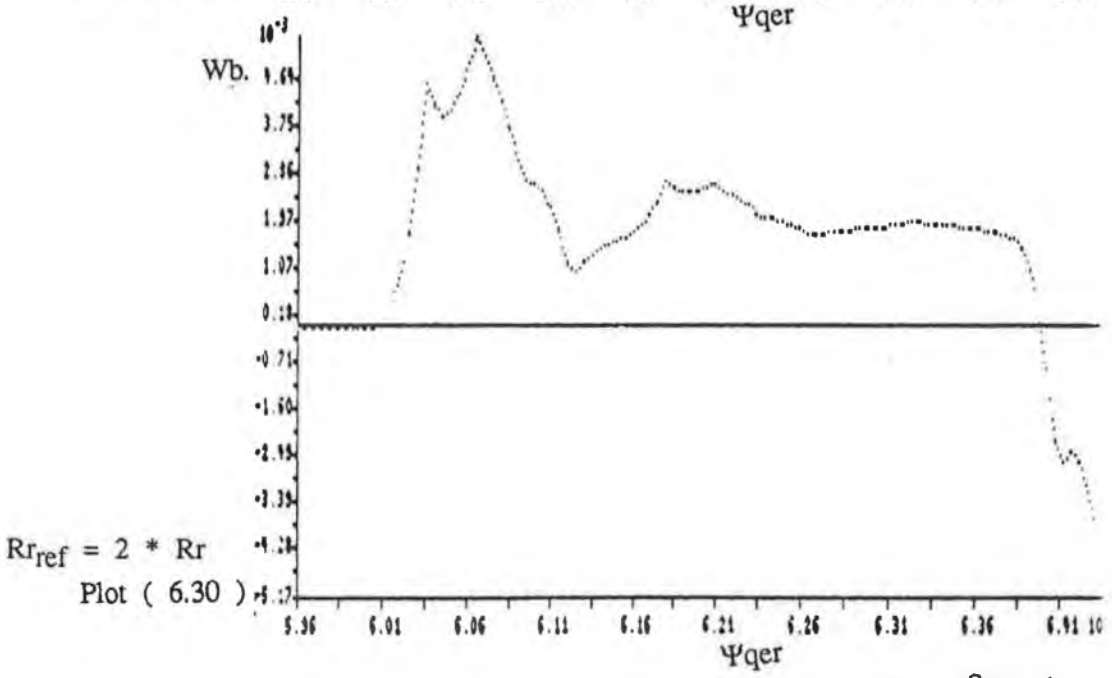

Rr_{ref} = 2 * Rr
Plot (6.30)

Seconds

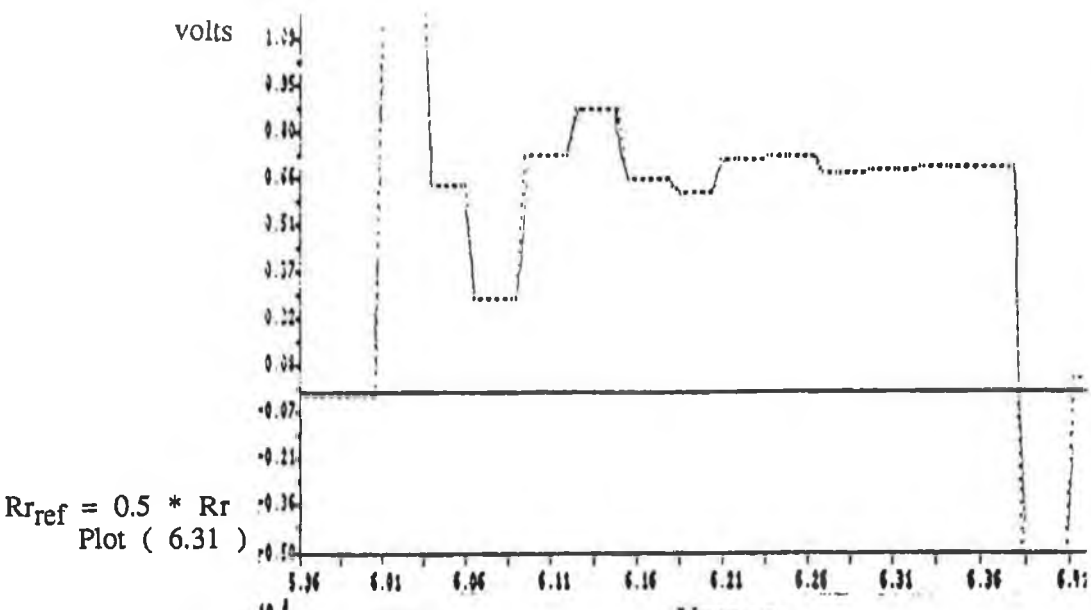
volts
Rr_{ref} = 0.5 * Rr
Plot (6.31)
$Vqes_{ref}$

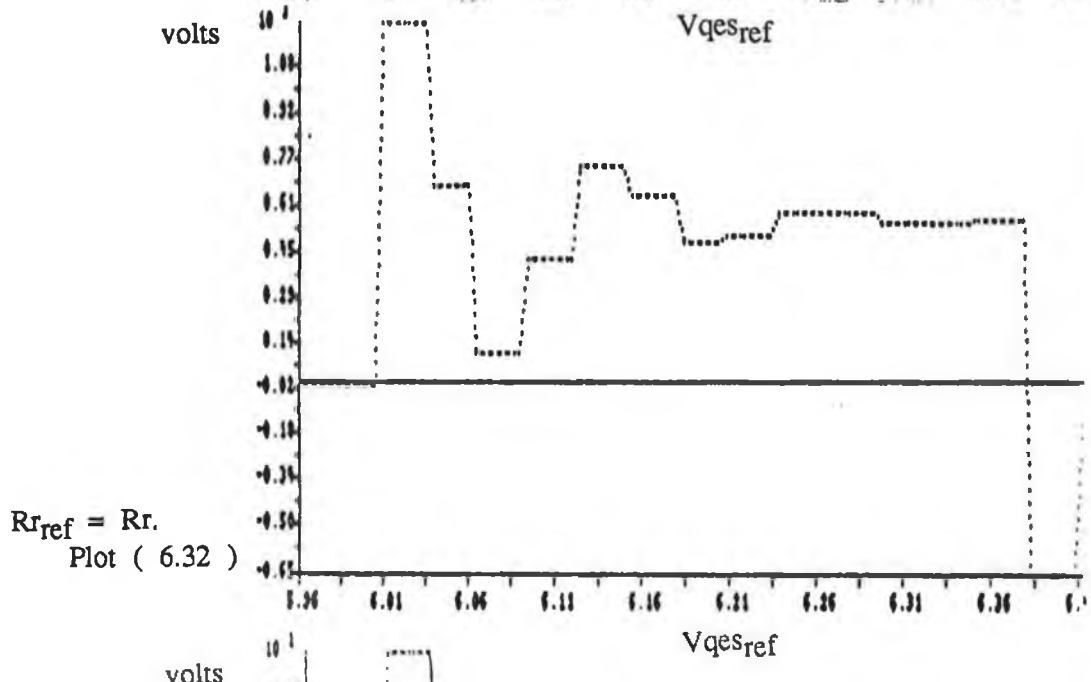
volts
Rr_{ref} = Rr.
Plot (6.32)
$Vqes_{ref}$

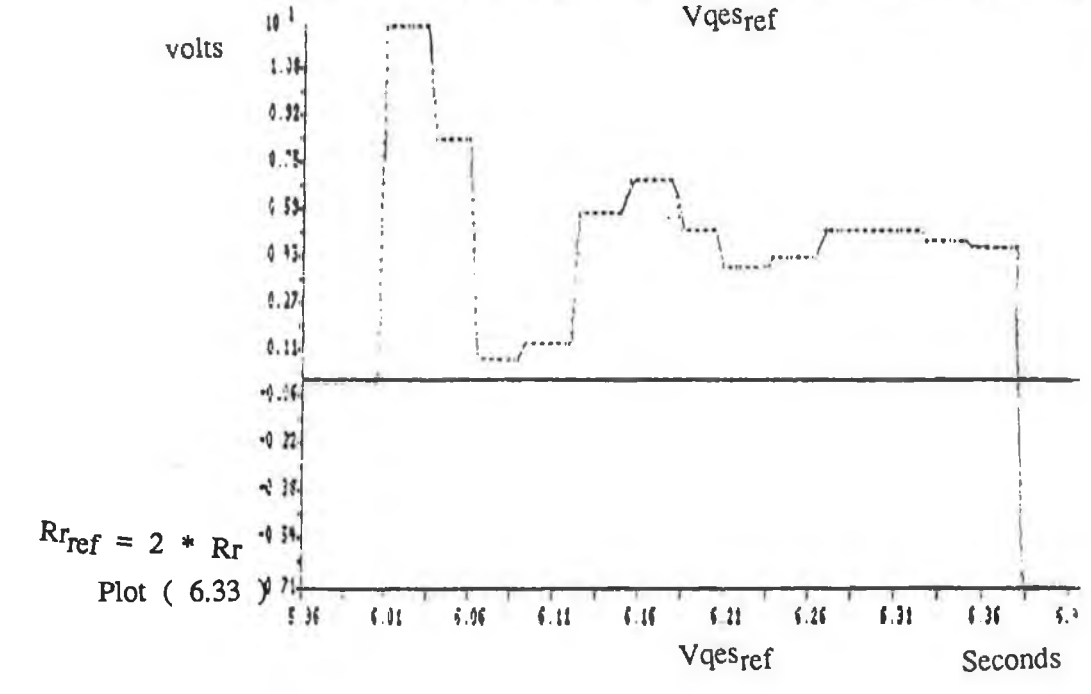
volts
Rr_{ref} = 2 * Rr
Plot (6.33)
$Vqes_{ref}$
Seconds

EXPERIMENTAL AND THEORETICAL ANALYSIS OF PWM DISTORTION EFFECTS

7.1 Introduction

While assessing the influences of controller rotor time constant mismatch on the developed stall torque of the prototype servo system, very significant steady state oscillations, which could not be attributed to the parameter mismatch, were found to exist. Ramp-type variations of ±50% of the mean developed torque were observed.

These distortion effects are shown to originate as a result of the delays inserted between the P.W.M. switching signals and the inverter power transistors. Although these delays are only a fraction of the period of the modulation carrier signal they are known to cause intervals of low gain, around the zero crossing points of inverter output current waveforms, lasting 10's of milliseconds, (Evans et al, [26], [27]).

In this chapter the distortion effects on the open loop torque are experimentally quantified. Spectrum analyses of phase currents, voltages and the A.C. coupled torque measurement are compared. The PWM distortion effects are modelled into the simulations to examine closed loop sensitivity to the effects. Controller design for robustness to the problem is examined and the effects are shown to have major implications on the stability of Field Oriented controllers with Voltage Source Inverter fed induction motors.

7.2 Experimental Observations

Oscillograph (7.1) shows steady state stall torque. There is closed loop control over the field flux linkage and forward path control over torque. The initial dynamics at the step command in torque are modified by the bar-rotor torque measurement system. Phase one current, at slip frequency, equal to 1.2 Hz is also shown. Regions of low

current are to be seen for 30 millisecond intervals at each side of every zero crossing. Glitches at 60° intervals from the zero crossings due to the interaction of the other phases can also be observed. At each glitch a change in slope can be seen in the developed torque. Oscillograph (7.2) shows Te and i_{s_1} with an expanded timescale. Ramp changes can easily be seen to occur, in the torque, with each distortion effect in the current. The effects of the other phase currents must also be considered.

Oscillograph (7.3) shows line-line voltage. To check that the current distortion effects were not driven by variations in reluctance around the air gap of the motor or by the non-sinusoidal nature of the windings the output voltages from the inverter were examined, in both the time and frequency domain. The high frequency switching has been filtered out by the motor. Glitches again occur at 60° intervals, indicating that the distortion effects are voltage driven.

Oscillograph (7.4) shows the harmonics in the current waveform from 0 to 25 Hz. The fundamental is at 1.2 Hz. A linear scale is used to show the relative amplitudes of the harmonics. The largest sub-harmonic occurs at 3.6 Hz and would cause distortions at 60° intervals.

Frequency	1.2	2.4	3.6	4.8	6.0	7.2	8.2
Amplitude, Amps	8.3	.56	.71	.24	.46	.23	.24

Oscillograph (7.5) shows the harmonics in the A.C. coupled torque. The voltages are those from the output of the strain gauge bridge amplifier.

Frequency	1.2	2.4	3.6	4.7	5.9	7.2	8.3
Amplitude, Amps	.56	.84	.46	.49	.36	.53	.07

Significant higher harmonics are visible. This is due to the fact that glitches occur at 60° intervals in each of the three phases.

Oscillograph (7.6) shows the torque harmonic spectrum and the current harmonic spectrum superimposed. The relative magnitudes of subharmonics to the fundamental are much greater in the torque spectrum than in the current spectrum.

Oscillograph (7.7) shows the voltage harmonics. The largest subharmonic occurs at 3.6 Hz. The relative amplitudes of harmonics at different frequencies are almost identical with those of the phase current, thereby proving that distortion effects arise in the power amplification stages.

7.3 Theoretical Validation of Distortion Effects.

To see if the distortions observed in the phase currents could be responsible for such significant deterioration of the torque response the regions of low gain around the zero crossing points of each phase current where modelled into the simulations to give a simple time domain study of the problem.

Plots (7.1) and (7.2) show the phase 1 current and the corresponding ideal torque. A

stall torque to give a phase 1 current of approximately 1 Hz was commanded.

Plots (7.3) and (7.4) show i_{s_1} and corresponding torque with simulated distortion effects in the motor voltages. For the 1 Hz i_{s_1} (actual phase current) in oscillograph (7.1) the current was assumed to be zero for an interval about each zero crossing. This time interval was measured to be 60 milliseconds. In the simulations the voltages in the stationary reference frame were to set to zero for a 60 millisecond interval about each zero crossing. A prior knowledge of the magnitude of the phase voltages was needed to do this. For the commanded torque the steady state sinusoidal voltages were 15 volts peak. These were simply set to zero whenever their absolute value was less than 15 Sin 2π (0.03) = 2.8 volts. A scheme for insertion of PWM delay distortion effects for any commanded torque, in the time domain would necessitate sampling of the waveform to detect its peak amplitude or its phase angle. Plot (7.3) shows the simulated i_{s_1} with distortion effects in evidence at the zero crossings and at 60° intervals. This waveform corresponds well with that in oscillograph (7.1). The developed torque Plot (7.4) is seen to have ramp type glitches at each instant of distortion in the currents, and correlates well with the actual measured torque in oscillograph (7.1).

Plot (7.5) the simulated line-line voltage is presented with the actual line-line voltage. Again there is good correspondence.

Plot (7.6) and (7.7) show the rotor flux linkages. Small ramp type errors occur in Ψ_{qer} but are only of the order of $\pm 0.5 \times 10^{-3}$ Wb in the steady state. Small variations can also be seen in Ψ_{der}. These virtually disappear when $iqes_{ref}$ is zero.

Plot (7.8) shows the distortion in Vqes. The distortion effects in the stationary reference frame voltages have been transformed to the rotating reference frame. The distortion effects in $Vqes_{ref}$ clearly model those in the developed torque waveform, indicating that the field flux linkage is reasonably insensitive to the influences of the

PWM inverter introduced delays.

7.4 Closed Loop Sensitivity to PWM Distortion Effects

In the cases of open loop commanded torques, good agreement was obtained between simulated and actual, for torque, current and voltage waveforms, thereby proving that the effects had been adequately modelled into the controller simulation. The closed loop effects can therefore be correctly predicted. A speed of 50 rpm was commanded in all cases, with no load on the motor so that torques required were similar to those commanded in the open loop investigations. The following proportional gains and integral time constants were chosen.

Flux Current Gain	=	1.5
Torque Current Gain	=	1.0
Flux Loop Gain	=	3.0
Speed Loop Gain	=	1.0

Flux Current Integral time constant	=	0.05
Torque Current Integral time constant	=	1.00

Plots (7.9) and (7.11) show the closed loop speed response and the corresponding torque current waveform. Plots (7.10) and (7.12) show the speed and torque current waveforms with the voltage distortion effects included. No robustness design against the cross-over distortion has been done. The motor is unloaded so that the total inertia of 0.035 Nm sec^2 rad^{-1} is due to the rotor alone. Ramp glitches in the speed of ±7 rpm are predicted. These would be further reduced if an inertial load was attached to the motor.

Plots (7.13) and (7.14) show the rotor field flux linkage for cases where voltage distortion is and is not present. The closed loop field controller is virtually

insensitive to voltage distortion, especially when commanded torques are small.

Plots (7.15) and (7.16) show the speed response and the developed torque. The torque plot is virtually identical to the torque current component, plot (7.12).

Plots (7.17) and (7.18) show the closed loop speed responses for the cases where there is virtually no integral action in the speed loop and where there is a high degree of integral action present. It was anticipated that the steady state speed responses were to be different for varying amounts of integral action if it would be possible to tune the controller to be robust to distortion effects. Plot (7.17) shows the speed response when the integral time constant is 100 (small amount of integral action). This is marginally more insensitive to the distortion than Plot (7.18) where the integral time constant is (0.05), (a large amount of Integral Action).

Plot (7.19) shows the predicted closed loop speed response when a lot of integral action is built into the speed loop and when the PWM voltage distortion effects are not accounted for. The integral time constant is 0.005 which is a valid design value (Chapter three) to ensure a very low steady state error. As is characteristic with a lot of integral action there is significant overshoot in the step response.

Plot (7.20) shows the same closed loop speed response when the distortion effects are accounted for. The system is shown to be unstable, especially for low values of commanded torque. Up to t = 1 second the field has stabilised and the commanded torque is zero, yet there are oscillations in the speed. The commanded 50 rpm is more or less achieved but with a step command to zero speed instability sets in again. The greater the amount of integral action the closer the system is to instability. With an integral time constant of 0.005 the delay effects in the voltage waveform lead to instability. Plots (7.19) and (7.20) prove that the P.W.M. delay distortion effects in the driving phase voltages must be accounted for when tuning Field Oriented Controllers for Induction motors.

7.5 Conclusions and Implications of PWM Distortion Effects.

While examining the stall torque responses of the prototype servo system very significant steady state ramp type distortion effects were observed. Both time domain and frequency domain analyses showed glitches in the inverter output voltage waveforms as being the cause of this problem which even overshadowed effects due to gross inaccuracy in the nominal value for the rotor time constant.

The effects of the cross over distortions in the driving voltage were successfully incorporated in the simulations and good correlation between predicted and experimental results for open loop control was achieved. The sensitivity of the closed loop speed controller was then examined and it was found that tuning of the speed loop for adequate robustness to PWM distortion effects was not possible.

Discrete design methods had been used to draw a locus of the system poles as the controller integral time constant varied. From this procedure an integral time constant was chosen for the speed loop to give desired rise time, overshoot and steady state error specifications. It has been shown however that the resulting system would actually prove to be unstable due to the influence of the cross over delays in the phase voltages introduced after the P.W.M. section. This effect, therefore, has major implications on the stability of Field Oriented controllers with P.W.M. Inverter fed Induction motor systems.

This effect is clearly very significant and is relatively undocumented in the context of Field Oriented controller design for Induction motors. Research papers to date have concentrated primarily on the losses associated with harmonic distortion in the motor (Kliman, [28]). Presently, research is being conducted ([27]) to study the effects of the turn on delays inserted on the switching signals of inverter transistors on the Inverter output voltage waveforms. This work indicates that the distortion effects will

pose problems in the use of Induction motors for low speed servo applications:

- One of the main difficulties at present with induction motor servo controllers is the achievement of good low speed and position control performance. For this type of operation the supply currents are at very low frequency. It is at low modulating frequencies that the distortion in the Inverter output voltages is at its worst. With modulating frequencies of less than 1 Hz cross over delays of up to 100 milliseconds can occur in the voltages despite the fact that the typical dead times on the switching waveforms may only be tens of micro seconds. This effect, therefore, will pose a serious problem to the achievement of low stall torques with Induction motor servos because the motor supply frequency is typically 0.5 Hz (slip frequency).

- When the controller value for rotor resistance is over estimated dynamic oscillations occur in the developed torque. It is suspected that the PWM distortion effect exacerbates this problem by sustaining the oscillations (c.f. oscillograph 6.6).

- For efficiency reasons (due to less higher harmonic heating effects) a low modulation index is often selected with P.W.M. systems. This results in increased distortion due to the turn on delays.

- As the carrier frequency is increased distortion due to the turn on delay is increased.

- There is a complicated relationship between the amount of distortion and the load time constant. For the induction motor this time constant is continually varying so that the exact amount of distortion for a specific dead time will not be known.

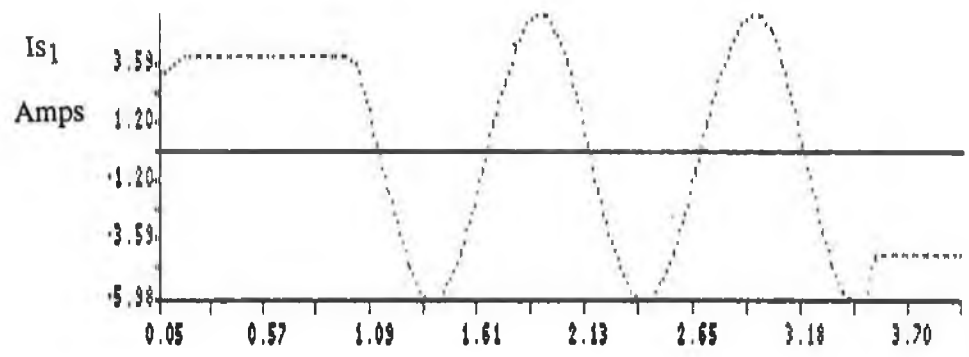

Plot 7.1. seconds.

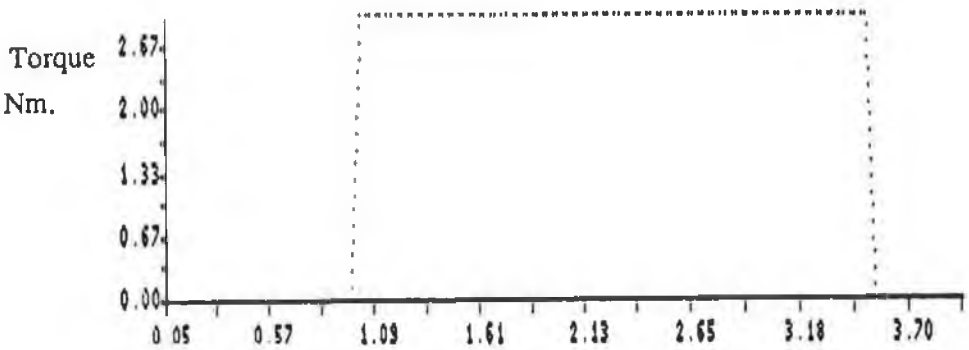

Plot 7.2. seconds.

Plot 7.3.

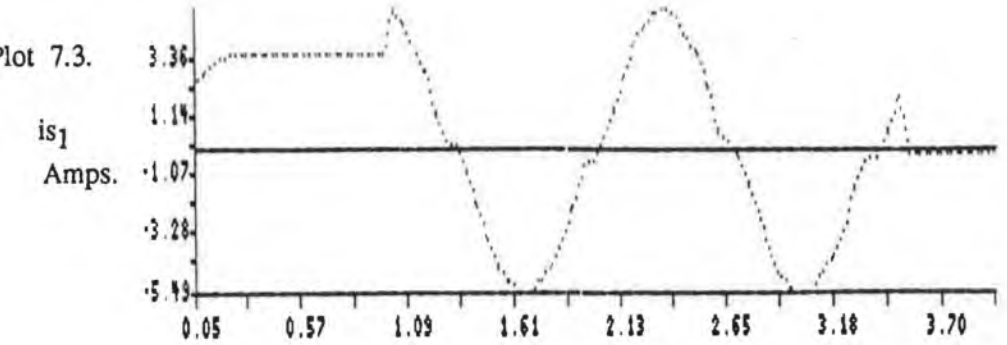

Plot 7.4.

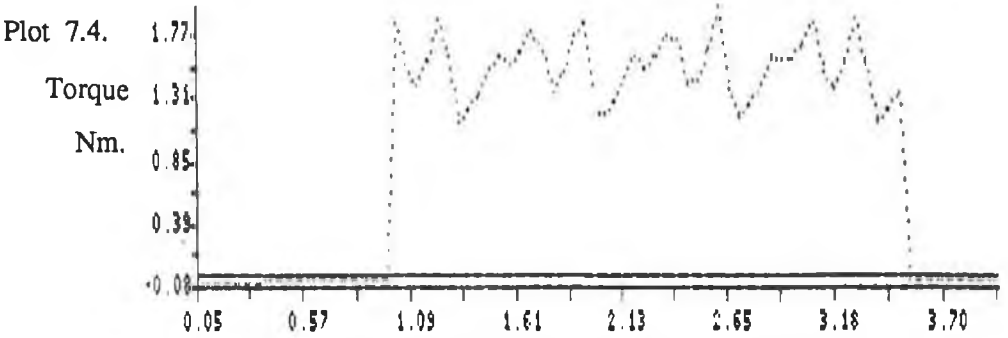

Oscillograph 7.1.

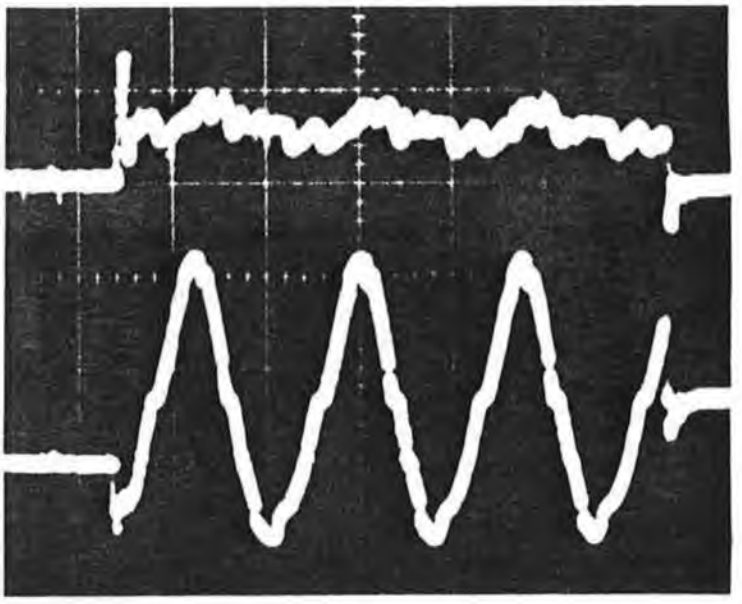

Oscillograph 7.2.

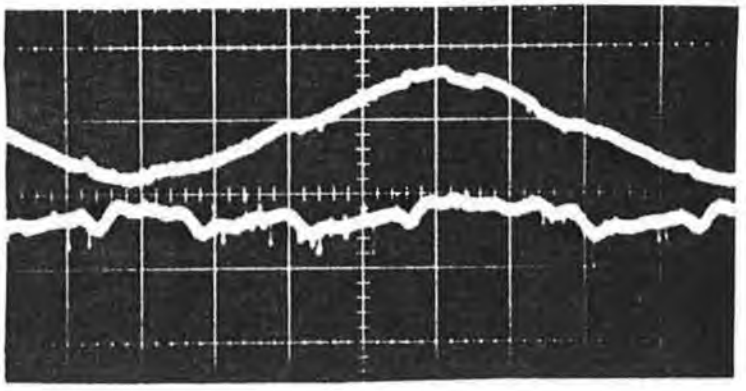

10 Volts/div.

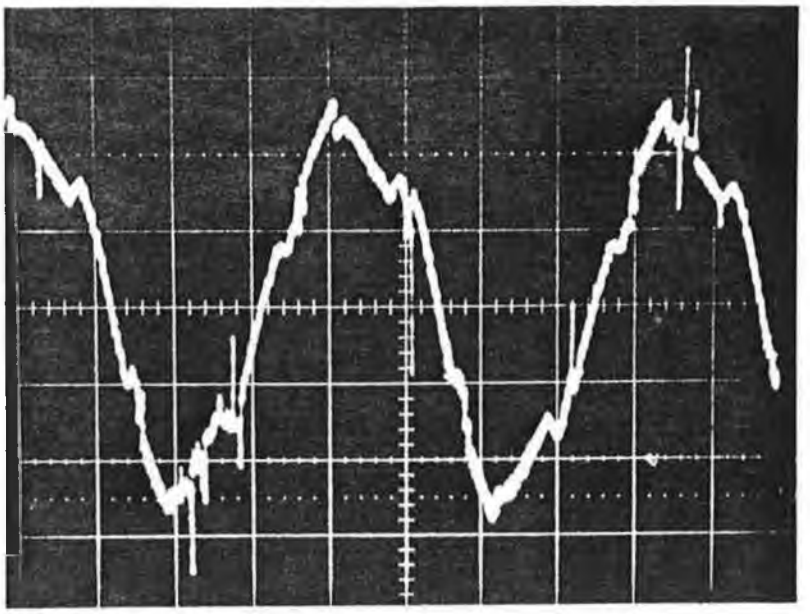

Oscillograph 7.3. Line - Line Voltage. 200 milliseconds/div.

Volts.

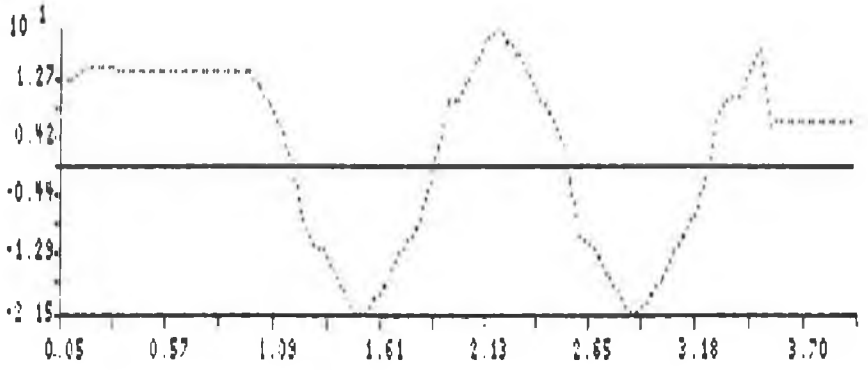

Plot 7.5. Line to Line Voltage.

Plot 7.6.

Wb.

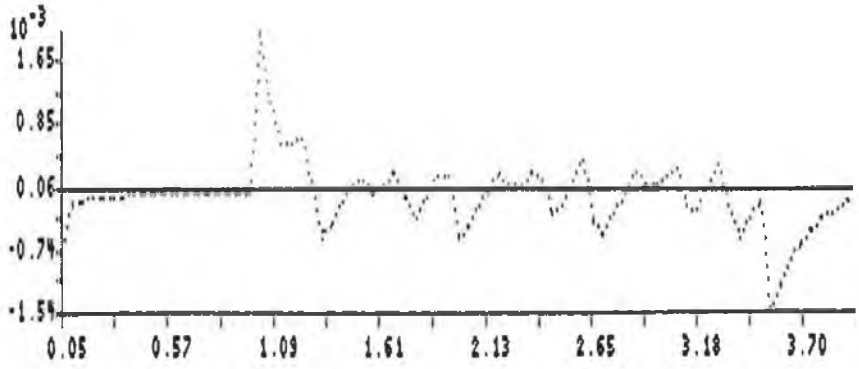

Ψqer. Distortion in Current.

Plot 7.7.

Wb.

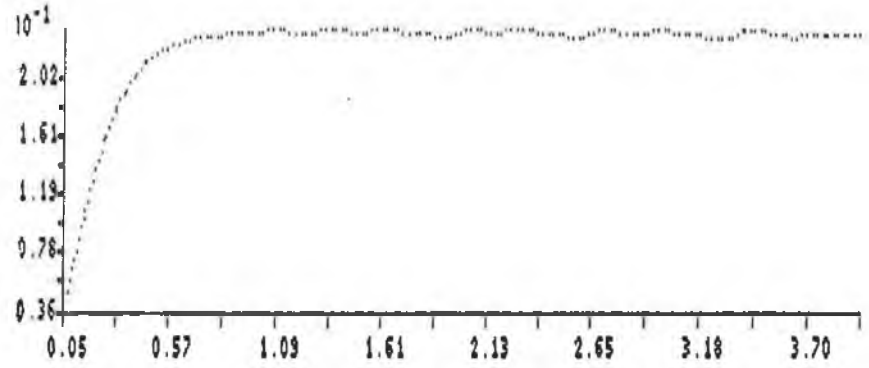

Ψder. Distortion in Current.

Plot 7.8.

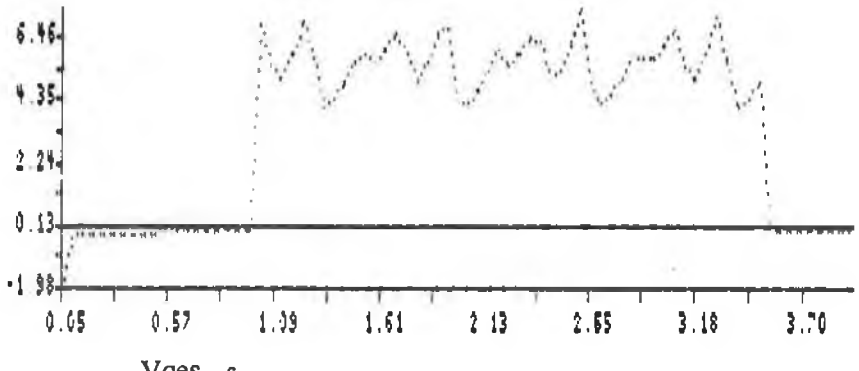

$Vqes_{ref}$. Distortion in Current.

Oscillograph 7.4.

Current Harmonics.

Linear Scale.

Peak at 8.3 amps.

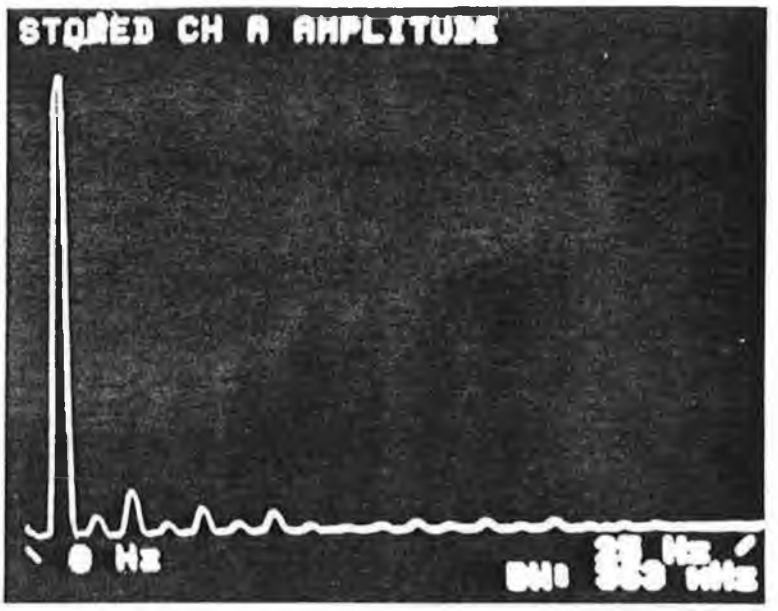

Peaks at 1.2 H_Z Intervals.

Oscillograph 7.5.

Harmonics in AC Coupled Torque.

Linear Scale.

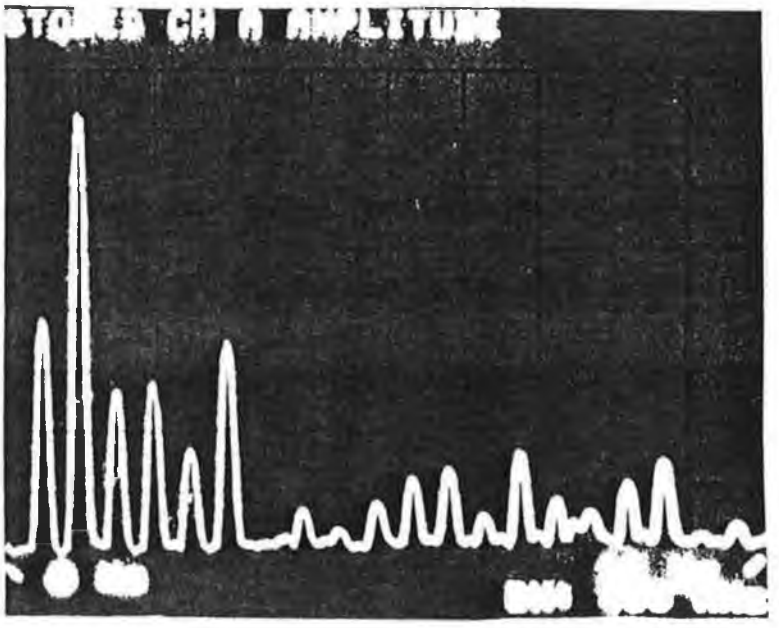

Peaks at 1.2 H_Z Intervals.

Oscillograph 7.6.

Current & Torque Harmonics Superimposed.

Linear Scale.

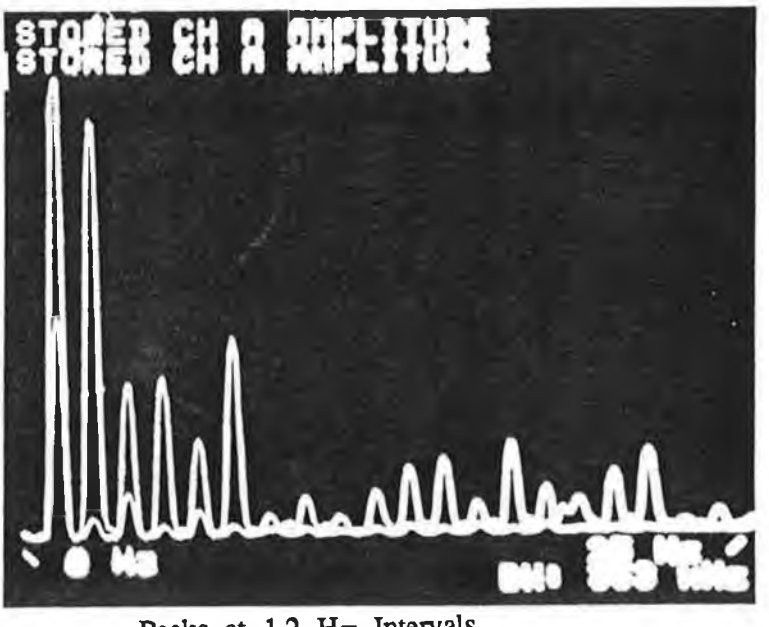

Peaks at 1.2 H_Z Intervals.

Linear Scale.

Peak at 9.7 volts.

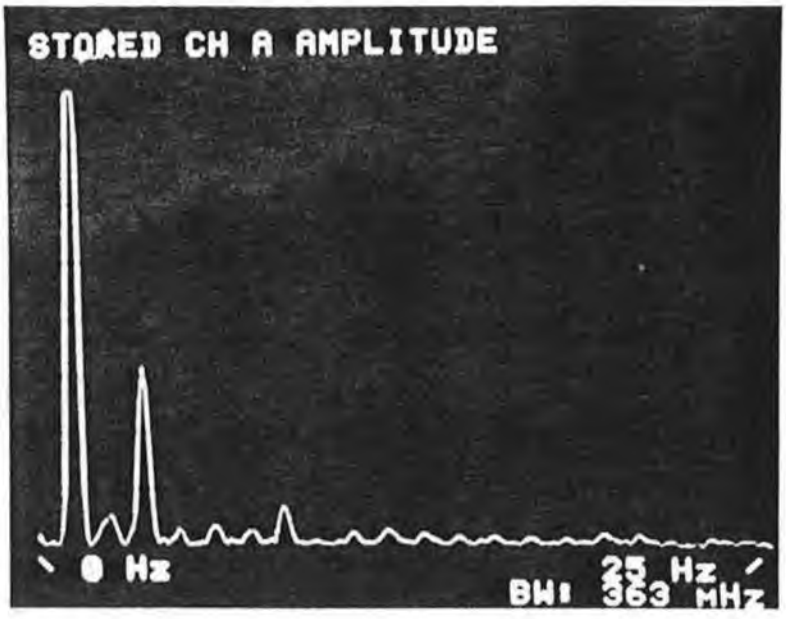

Oscillograph 7.7.

Peaks at 1.2 Hz Intervals.

Voltage
Harmonics

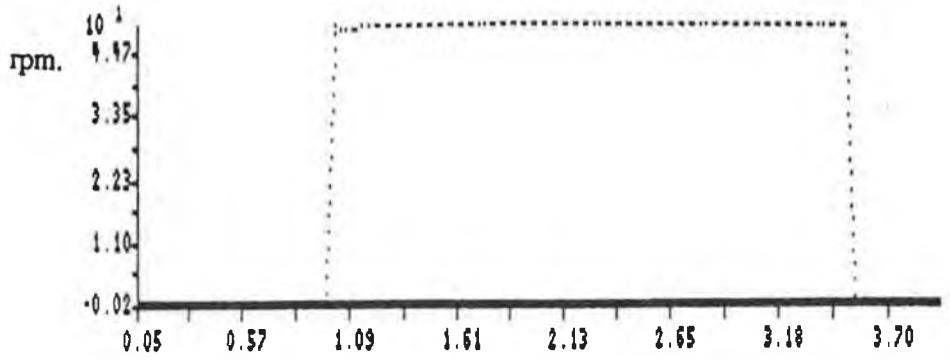

Plot 7.9. Speed No Distortion in Current.

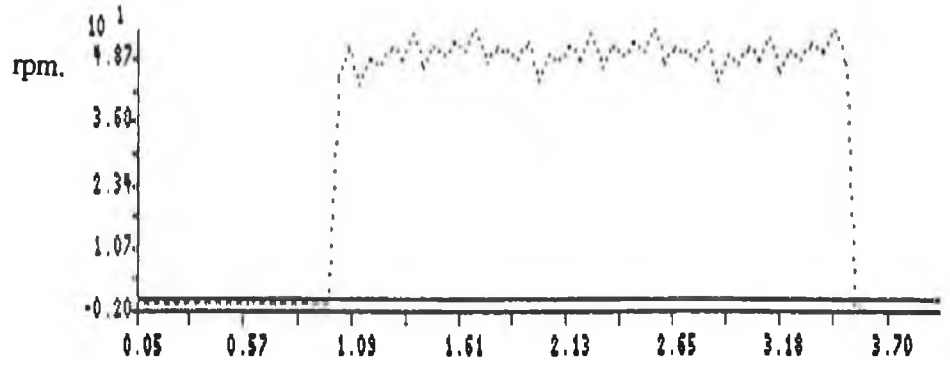

Plot 7.10. Speed Distortion in Current.

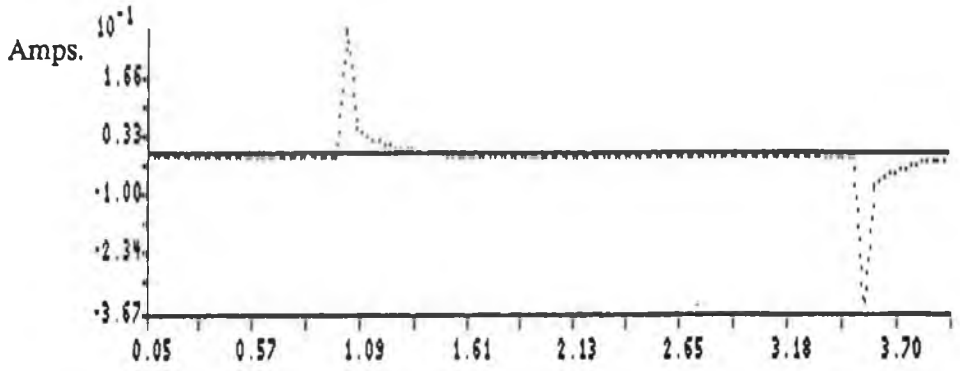

Plot 7.11. Iqes seconds.

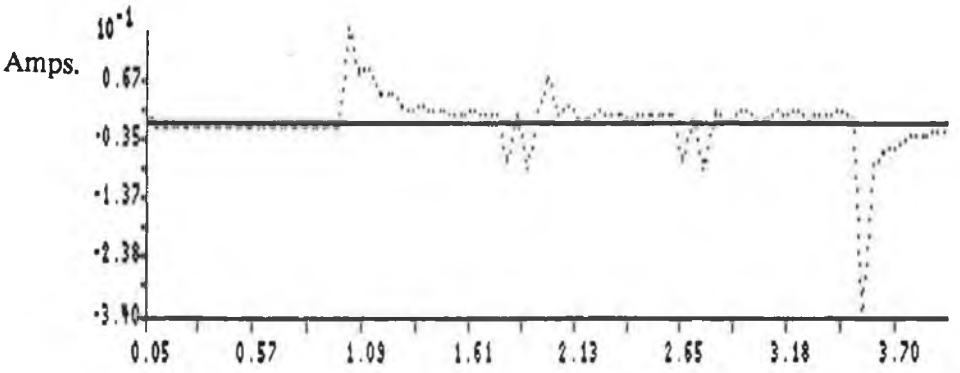

Plot 7.12. Iqes seconds.

Plot 7.13.

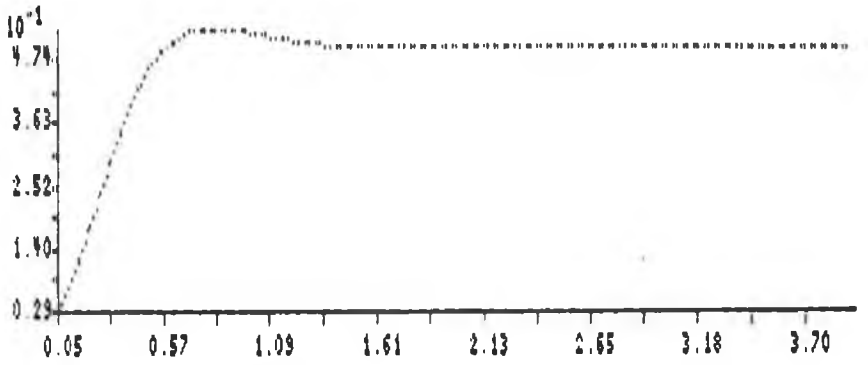

Wb.

Ψder. No Distortion in Current.

Plot 7.14.

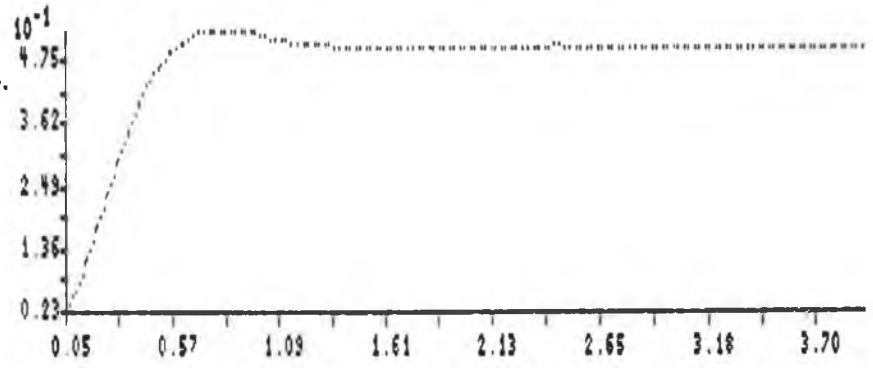

Wb.

Ψder. Distortion in Current.

Plot 7.15.

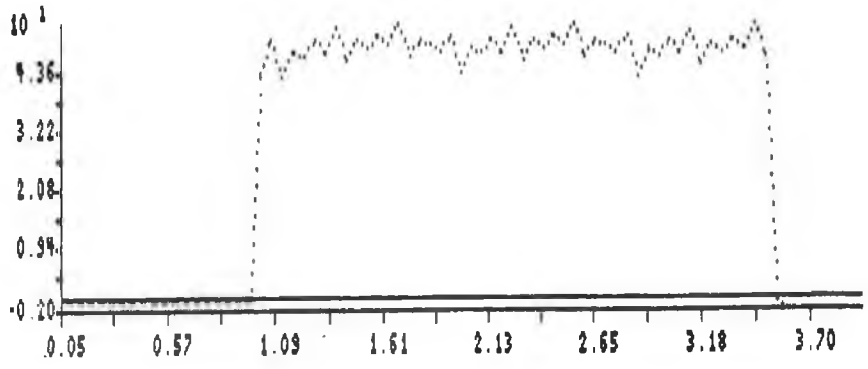

rpm.

Speed Distortion in Current.

Plot 7.16.

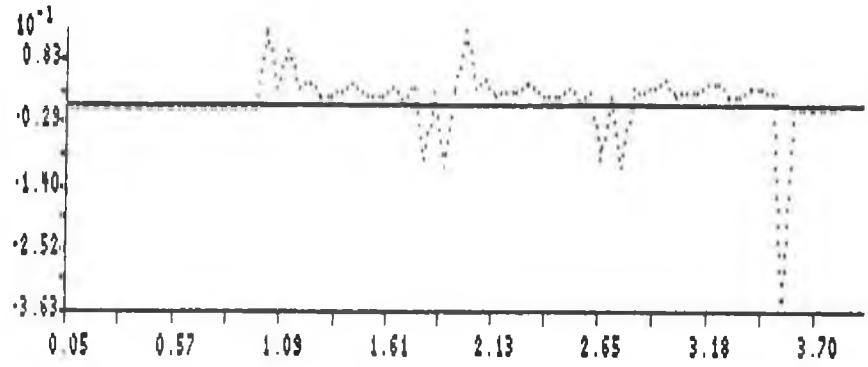

Nm.

Torque Distortion in Current.

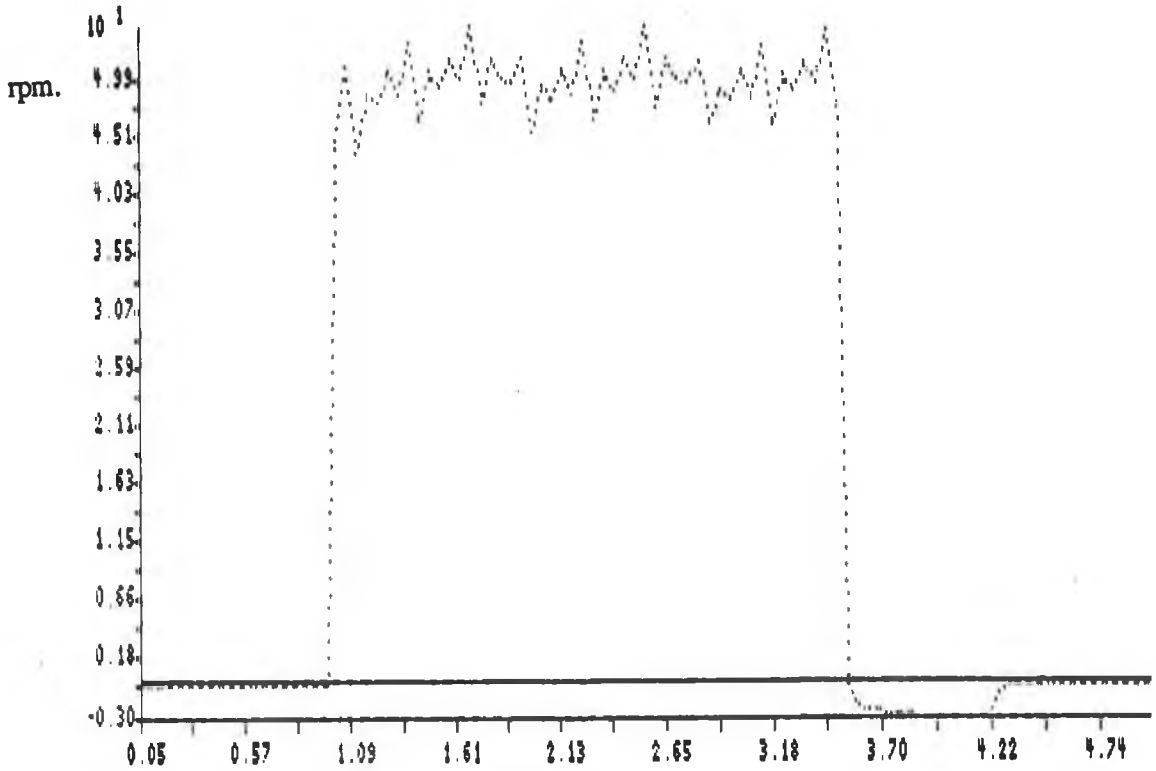

Plot 7.17. Speed. Integral Time Constant in Speed Loop = 100.

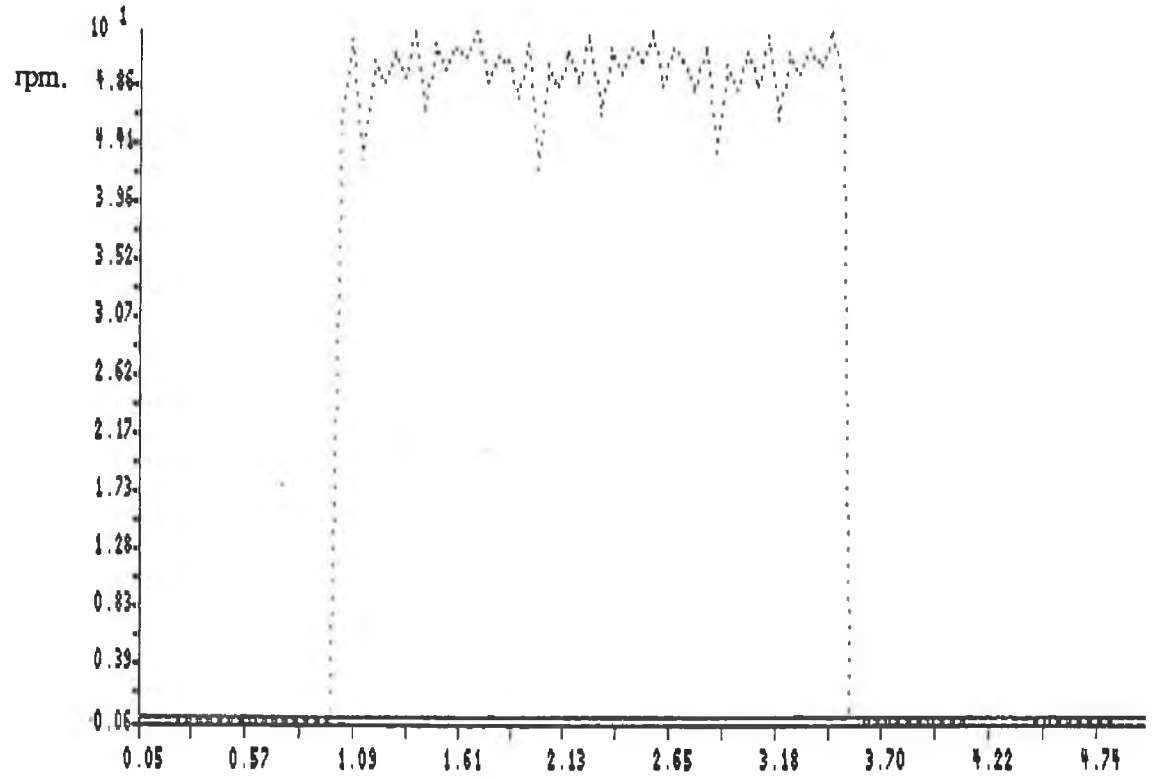

Plot 7.18. Speed. Integral Time Constant in Torque Loop = 0.05.

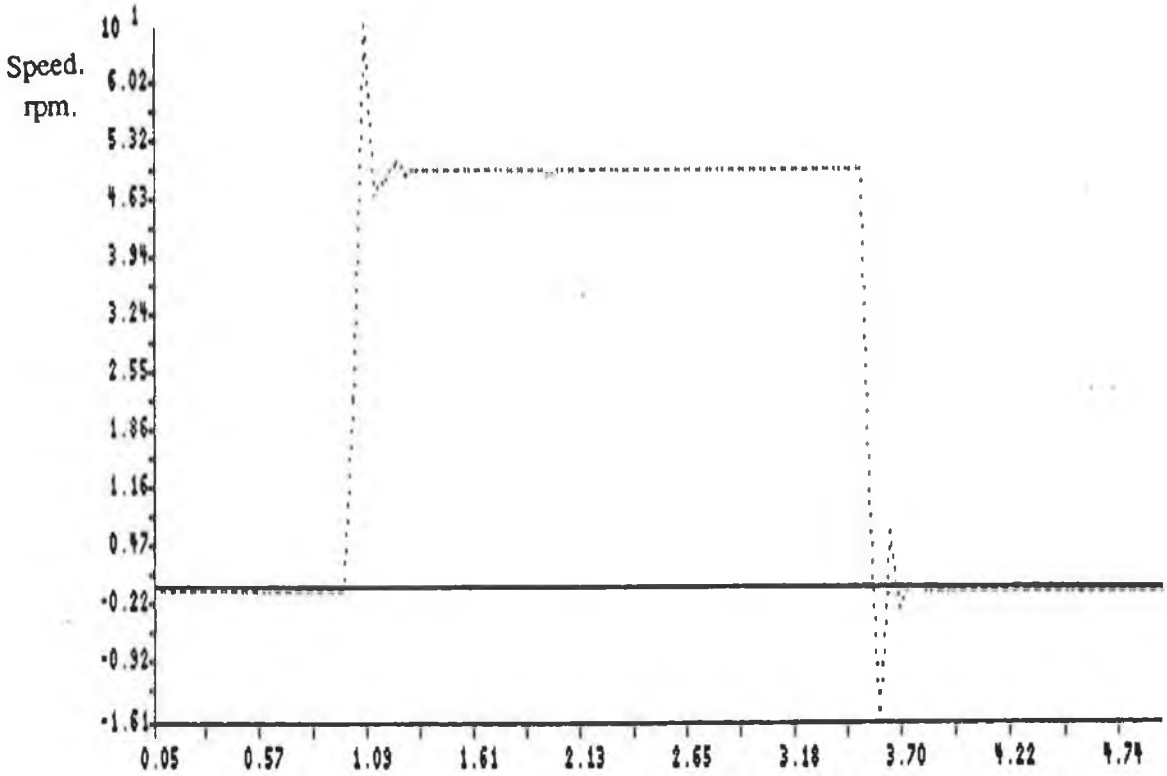

Plot 7.19. Integral Time Constant in Speed Loop = 0.005.
No Distortion in Current.

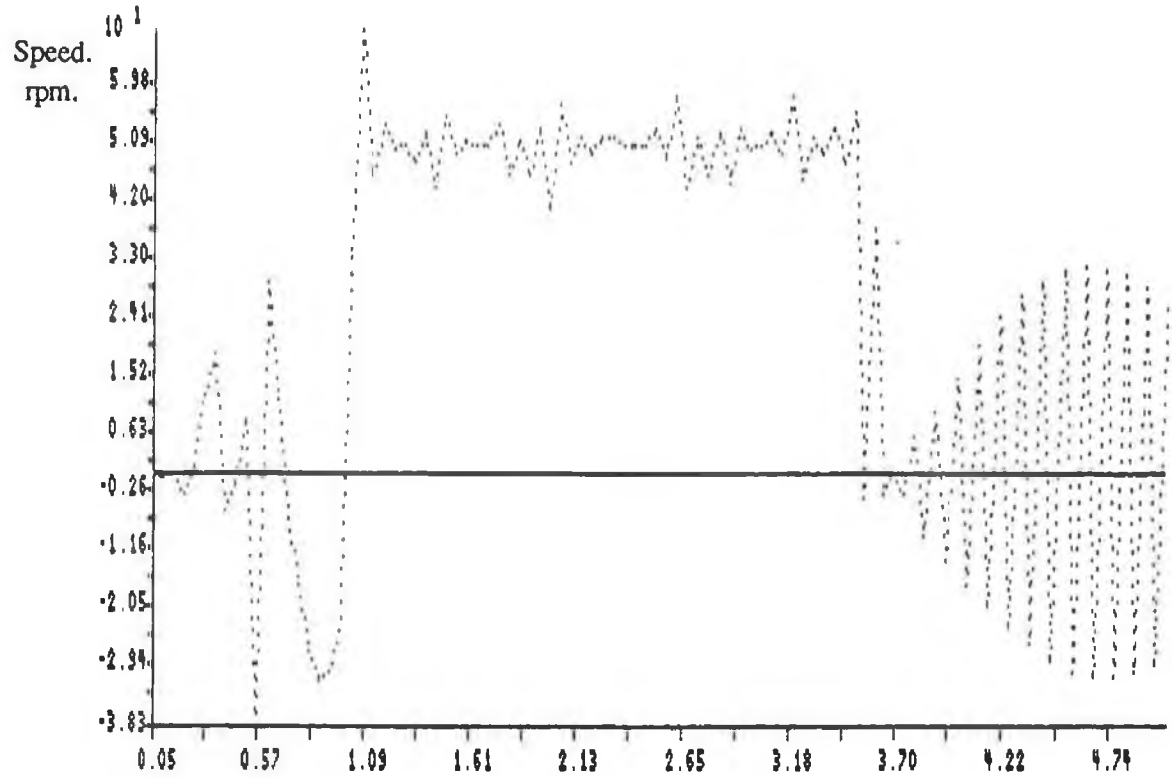

PLot 7.20. Integral Time Constant in Speed Loop = 0.005.
Distortion in Current.

CONCLUSIONS.

All the major issues of Field Oriented Controller design were addressed. A controller topology was selected and tuning values were designed. The action of this controller on the motor was simulated. Performance predictions for torque-mode operation correlated well with results from the actual prototype servo system. Indeed, on this system, any commanded stall torque, with forward path operation of the torque loop, was achieved within two sampling intervals.

To tune the controller, discrete-time controller design techniques were employed. Tuning values derived resulted in good performance in both the simulations and the actual system.

To simulate operation of the system the full D-Q model of the motor was used. Most simulations utilise the decoupled linear time invariant models for torque and flux generation. The full model was discretised and the resulting equations for the internal states were solved algebraicly to give expressions for the states at any time interval. The use of the full model enables analysis of parameter variation effects on Field Oriented controller operation.

Field weakening schemes in the controllers surveyed were reviewed. Equations were derived to show the conditions needed for adequate field weakening.

Studies on the sensitivities of controllers to rotor time constant variation were reviewed. It was found that discrepancies exist between equations derived by researchers to show the sensitivity of forward path torque control to error in the controller value for the rotor time constant. Equations were derived, as part of this work, to relate the steady state errors in the rotor flux linkages to error in the rotor resistance. These gave good agreement with simulated results, which were in turn

validated by experiemental results. It was concluded, from a controller performance point of view, that errors in the rotor time constant have very little affect on the closed loop controller. Machine excitation levels however, vary very substantially and dynamic oscillations will occur in developed torque and speed. A reduction in the flux loop gain is recommended to make the system less sensitive to rotor time constant variation. This would not adversely affect performance since the field flux is maintained constant except for operation in the field weakening region. If adaption to parameter variation is not being used it is recommended that the rotor resistance be slightly underestimated to minimise transient oscillations. Use of the simulation package suggests that tuning values for the PI controllers cannot be selected to build in significant robustness to rotor time constant variation effects.

While quantifying parameter variation effects experimentally, severe steady-state ramp type distortion effects were observed in the measured stall torque, developed by open loop control. These were shown to arise due to the turn on delays introduced on the transistor switching signals, introduced between the PWM circuitry and the base drives for the power inverter transistors. Although these delays, to prevent shorting in the inverter lags (due to relatively long turn off times with power transistors) are typically tens of microseconds long they were shown to cause cross over delays of up to one hundred milliseconds in the inverter output voltage waveforms. The effect is most severe at low frequencies. Induction motor currents will be at these frequencies in four speed and position control applications so that these distortion effects have major implications on the use of field oriented controllers with PWM and voltage source inverter fed induction motors in these applications. The effects would cause most distortion in the torque when low stall torques are being commanded since currents would be at low slip frequency, typically a fraction of a Hz.

To simulate these distortion effects on the developed torque, the cross-over delays in the phase voltages were measured and incorporated in the simulations. There was excellent correspondence between the simulated distortion effects in the developed

torque and in the actual measured torque, thereby showing that the effects had been adequately modelled into the simulations. Effects on the closed loop system could then be confidently predicted. For a closed loop speed controller tuned with a lot of integral action the speed responses were simulated for the cases where the distortion effects were and were not incorporated. When no account was taken of the distortion effects a speed response, as expected, with significant overshoot and very little steady state error, was predicted. With the cross-over delays inserted on the phase voltages, complete instability resulted proving that PWM/Inverter introduced distortion effects must be accounted for when theoretically deriving tuning values for field oriented controllers. No previous documentation on the closed loop stability implications of these cross over delay effects in the context of Field Oriented Controller design for the induction motor have been encountered.

The use of digital signal processors as opposed to floating point coprocessors is suggested. To implement a field oriented controller for a VSI fed motor a minimum of thirty eight multiplications are needed in conjunction with a considerable amount of conditional statements and trigonometric function evaluation. The controller algorithm arithmetic required is complex and will be floating point or extended integer. Many DSPs have single cycle multiplication times, trigonometric function evaluation algorithms and analog-digital conversion facilities. Selection of a slightly lower operating excitation level is recommended for position control applications. A lower field flux linkage will result in higher slip frequencies to develop the same torque. The higher slip frequencies will mean lower cross-over delays and give less distortion. More research into controller design to counteract the cross-over delays, which are modelled as the non-linear backlash effect, is suggested for cases where turn on delays on transistor switching signals must be inserted.

BIBLIOGRAPHY

[1] Lessmeier, R., Schumacher, W., Leonhard, W., "Microprocessor-Controlled AC-servo drives with synchronous or Induction Motors: Which is Preferable?", IEEE trans. on Ind. Appl. Vol IA-22, No. 5, pp 812-819 1986.

[2] Brown, J.W., "Induction Motor Servos: Where they apply in the Servo Market". Proc. Motorcon October 1985, pp 366-372.

[3] Blaschke, Felix, "The Principle of Field Orientation as applied to the new TRANSVEKTOR Closed-Loop control system for rotating field machines", Siemens Review, Vol. 34, pp 217-220, May 1972.

[4] Slemon, G.R., Straughen, A., "Electric Machines" Addison-Wesley, October 1982, ISBN 0-201-07730-2.

[5] Leonhard, W., "Control of Electrical Drives", Springer-Verlag, 1984, ISBN 3-540-13650-9.

[6] Bose, B.K., "Adjustable Speed AC Drives - A Technology Status Review", Proceedings of the IEEE, Vol. 70, No. 2, February 1982, pp 116-133.

[7] Blaschke, Felix, "The Principle of Field Orientation as applied to the new TRANSVEKTOR Closed-Loop control system for rotating field machines", Siemens Review, Vol. 34, pp 217-220, May 1972.

[8] Sathiakumar, S., Biswas, S.K., Vithayathil, J., "Microprocessor-Based Field-Oriented Control of a CSI-fed Induction Motor Drive", IEEE trans, on Ind. Electronics, Vol. JE-33, No. 1, February 1986, pp. 39-43.

[9] Bayer, K.H., Blaschke, F., "Stability Problems with the Control of Induction Machines using the Method of Field Orientation", Erlangen, Siemens A6,

Systemtechnische Entwicklung.

[10] Adkins, B., Harley, R.G., "The General Theory of Alternating Current Machines", Chapman and Hall, London, 1978. ISBN: 0 412 15560 5.

[11] Hindmarsh, J., "Electrical Machines and their Applications", 3rd Edition, Pergamon, ISBN: 0-08-021164-X.

[12] Ohnishi, K., Suzuki, H., Miyachi, K., Terashima, M., "Decoupling Control of Secondary Flux and Secondary Current in Induction Motor Drive with Controlled Voltage Source and its comparison with Volts/Hertz control", IEEE trans. on Ind. Appl., Vol. IA-21, No. 1, January/February 1985, pp. 241-247.

[13] Ohnishi, K., Ueda, Y., Miyachi, K., "Model Reference Adaptive System Against Rotor Resistance Variation in Induction Motor Drive", IEEE trans. on Ind. Electronics, Vol. IE-33, No. 3, August 1986, pp. 217-223.

[14] Harashima, F., Kondo, S., Ohnishi, K., "Multi-microprocessor Based control system for Quick Response Induction Motor Drive", CH2060-2/84/0000-0605 IEEE.

[15] Sathikumar, S., Vithayathil, J., "Digital Simulation of Field-Oriented Control of Induction Motor", IEEE trans. on Ind. Electronics, Vol IE.31, No. 2, May 1984.

[16] Nabae, A., Otsuka, K., Uchino, H., Kurosawa, R., "An Approach to Flux Control of Induction Motors Operated with Variable-Frequency Power Supply", IEEE trans. on Ind. Appl., Vol. IA-16, No. 3, pp. 342-349, 1980.

[17] Kumamoto, A., Tada, S., Hirane, V., "Speed regulation of an Induction Motor

Using Model Reference Adaptive Control", 0272-1708/86/1000-0025, October 1986.

[18] Koyama, M., Yano, M., Kamijama, I., Yano, S., "Microprocessor-Based Vector Control System for Induction Motor Drives with Rotor Time constant Identification Function", IEEE trans. on Ind. Appl., Vol IA-22, No. 3, May/June 1986, pp. 453-459.

[19] Leonhard, W., "Microcomputer Control of High Dynamic Performance ac-Drives - A Survey", Automatica, Vol. 22, No. 1, pp. 1-19, 1986.

[20] Sugimoto, M., Tamai, S., "Secondary Resistance Identification of an Induction - Motor Applied Model Reference Adaptive System and Its Characteristics", IEEE trans. on Ind. Appl., Vol IA-23, No. 2, March/April 1987.

[21] Verghese, G.C., Sanders, S.R., "Observers for Flux Estimation in Induction Machines", IEEE trans. on Ind. Elect., Vol. 35, No. 1, February 1988.

[22] Krishnan, R., Doran, F., "Study of Parmeter Sensitivity in High-Performance Inverter-Fed Induction Motor Drive Systems", IEEE trans. on Ind. Appl., Vol IA-23, No. 4, 1987, pp. 623-635.

[23] Garces, L.J., "Parameter-Adaption for the Speed-Controlled Static AC Drive with a Squirrel-Cage Induction Motor", IEEE trans, on Ind. Appl., Vol. IA-16, No. 2, 1980, pp. 173-178.

[24] Matsuo, T., Lipo, T.A., "A Rotor Parameter Identification Scheme for Vector Controlled Induction Motor Drives", CH2060-2/84/0000-0538, 1984 IEEE pp. 538-545.

[25] Sugimoto, H., Koyama, M., Yano, M., Ohno, E., "A New Transfer Function of an Induction Motor Driven by Variable Frequency Source", 0275-9306/83/0000-0102, 1983 IEEE.

[26] Evans, P.D., "Harmonic Distortion in PWM Inverter Output Waveforms", IEEE Proc., Vol. 134, Pt.B, No. 4, July 1987, pp. 224-232.

[27] Walsh, N., McCorkell, C., "Distortion in Pulse-width Modulated Power Inverter", Internal Research Report, Moog Ltd., Ringaskiddy, Co. Cork 1988.

[28] Kliman, G.B., "Harmonic Effects in Pulse Width Modulated Inverter Induction Motor Drives", IEEE/IAS 1972 Annual Meeting pp. 783-790.

APPENDIX

APPENDIX A.

Solutions of Simultaneous Equation Set 4.5. - 4.8.

$$\Psi der_k = \frac{k_{30}\, k_{25} - k_{27}\, k_{28}}{k_{29}\, k_{25} + k_{26}\, k_{28}}.$$

$$iqes_k = (k_{30} - \Psi der_k\, k_{29}) / k_{28}.$$

$$\Psi qer_k = \frac{iqes_k}{c_{21}} - \Psi der_k w_{sla}\, c_{27} + \frac{Yqer_{k-1}\, Lr}{T_2}.$$

$$ides_k = - \Psi der_{k-1}\, c_{28} + \Psi der_k\, c_{21} - \Psi qer_k\, c_{29}\, w_{sla}.$$

Where:

$$k_{25} = w_0^2\, w_{sla}\, c_{26} + w_{sla}\, c_{27} - w_0\, T + w_0 / c_{17}.$$

$$k_{26} = w_0^2\, c_{20} + c_{21} + w_{sla}^2\, w_0^2\, c_{22} + w_{sla}^2\, c_{23} + w_0^2\, c_{24} + c_{25}.$$

$$k_{27} = - c_{10}\, w_0^2\, \Psi der_{k-1} - c_{11}\, \Psi der_{k-1} - c_{12}\, w_0^2\, w_{sla}\, \Psi qer_{k-1} - c_{13}\, w_{sla}\, \Psi qer_{k-1} - c_{14}\, w_0\, f - c_{15}\, w_0\, iqes_{k-1} - c_{16}\, w_0\, \Psi qer_{k-1} - e\, T / T_1 - c_4\, ides_{k-1} - c_5\, \Psi der_{k-1}.$$

$$k_{28} = c_{17} / w_0 + c_{18}\, w_0 + c_{19} / w_0 + w_0 / c_{17}.$$

$$k_{29} = - c_6\, w_{sla}\, w_0 + c_7 - c_8\, w_{sla} / w_0 - c_9.$$

$$k_{30} = - w_0\, c_1\, \Psi qer_{k-1} - \Psi qer_{k-1}\, c_2 / w_0 + f / w_0\, L_\sigma + iqes_{k-1} / w_0\, T + c_3\, \Psi qer_{k-1} / w_0 - e\, T / T_1 - c_4\, ides_{k-1} - c_5\, \Psi der_{k-1}.$$

$$c_1 = \frac{M\ T}{T_2\ T_1} \qquad c_{12} = \frac{Lr^2\ L_\sigma\ T^2}{T_2\ T_1\ M\ Rr} \qquad c_{23} = \frac{T\ Lr^2}{T_2\ M\ Rr}$$

$$c_2 = \frac{M}{T_2\ L_\sigma\ T} \qquad c_{13} = \frac{Lr^2}{T_2\ M\ Rr} \qquad c_{24} = \frac{T^2\ M}{Lr\ T_1}$$

$$c_3 = \frac{M}{Lr\ L_\sigma\ T} \qquad c_{14} = \frac{T^2}{T_1} \qquad c_{25} = \frac{M}{Lr\ T_1}$$

$$c_4 = \frac{L_\sigma}{T_1} \qquad c_{15} = \frac{L_\sigma\ T}{T_1} \qquad c_{27} = \frac{T\ Lr}{T_2}$$

$$c_5 = \frac{M}{Lr\ T_1} \qquad c_{16} = \frac{M\ T}{Lr\ T} \qquad c_{26} = \frac{T^3\ Lr\ L_\sigma}{T_2\ T_1}$$

$$c_6 = \frac{M\ T^2}{T_2\ T_1} \qquad c_{17} = \frac{T_1}{L_\sigma\ T} \qquad c_{28} = \frac{Lr}{M\ Rr\ T}$$

$$c_7 = \frac{M}{Lr\ L_\sigma} \qquad c_{18} = \frac{M^2\ Rr\ T^2}{T_2\ Lr\ T_1} \qquad c_{29} = \frac{Lr}{M\ Rr}$$

$$c_8 = \frac{M}{T_2\ L_\sigma} \qquad c_{19} = \frac{M^2\ Rr}{T_2\ Lr\ L_\sigma}$$

$$c_9 = \frac{M}{Lr\ T_1} \qquad c_{20} = \frac{L_\sigma\ T\ T_2}{T_1\ M\ Rr}$$

$$c_{10} = \frac{Lr\ L_\sigma\ T}{T_1\ M\ Rr} \qquad c_{21} = \frac{T_2}{M\ Rr\ T}$$

$$c_{11} = \frac{Lr}{M\ Rr\ T} \qquad c_{22} = \frac{T^3\ Lr^2\ L_\sigma}{T_2\ T_1\ M\ Rr}$$